NATIONAL TECHNICAL UNIVERSITY OF ATHENS

SCHOOL OF NAVAL ARCHITECTURE & MARINE ENGINEERING

DIVISION OF MARINE ENGINEERING

DIPLOMA THESIS

A COMPARATIVE STUDY OF THE REYNOLDS EQUATION SOLUTION FOR SLIDER AND JOURNAL BEARINGS WITH STOCHASTIC ROUGHNESS ON THE STATOR AND THE ROTOR

DIMITRIOS SKALTSAS

Thesis Committee:

Supervisor: C. I. Papadopoulos, Associate Professor, NTUA

Members: L. Kaiktsis, Professor, NTUA

G. Papalamprou, Assistant Professor, NTUA

Athens, February 2021

ΕΘΝΙΚΟΜΕΤΣΟΒΙΟΠΟΛΥΤΕΧΝΕΙΟ

ΣΧΟΛΗΝΑΥΠΗΓΩΝΜΗΧΑΝΟΛΟΓΩΝΜΗΧΑΝΙΚΩΝ

ΤΟΜΕΑΣΝΑΥΤΙΚΗΣΜΗΧΑΝΟΛΟΓΙΑΣ

ΔΙΠΛΩΜΑΤΙΚΗ ΕΡΓΑΣΙΑ

ΣΥΓΚΡΙΤΙΚΗ ΜΕΛΕΤΗ ΤΗΣ ΕΠΙΛΥΣΗΣ ΤΗΣ ΕΞΙΣΩΣΗΣ REYNOLDS ΓΙΑ ΟΛΙΣΘΗΤΗΡΕΣ ΚΑΙ ΑΚΤΙΝΙΚΑ ΕΔΡΑΝΑ ΜΕ ΣΤΟΧΑΣΤΙΚΗ ΤΡΑΧΥΤΗΤΑ ΣΤΟΝ ΑΞΟΝΑ ΚΑΙ ΤΟ ΕΔΡΑΝΟ

ΔΗΜΗΤΡΙΟΣ ΣΚΑΛΤΣΑΣ

Εξεταστική Επιτροπή

Επιβλέπων: Χ. Ι. Παπαδόπουλος, Αναπληρωτής Καθηγητής ΕΜΠ

Μέλη: Λ. Καϊκτσής, Καθηγητής, ΕΜΠ

Γ. Παπαλάμπρου, Επίκουρος Καθηγητής, ΕΜΠ

Αθήνα, Φεβρουάριος 2021

Acknowledgements

The current thesis marks the end of my undergraduate studies in the School of Naval Architecture and Marine Engineering in the National Technical University of Athens, and thus I would like to express my gratitude to all the people that supported and inspired mε throughout my student life.

First of all, I would like to thank my family and friends for their support and trust. Their help and faith in me was indispensable to overcome the difficulties I faced in my journey towards the end of my studies.

Furthermore, I would like to express my deepest appreciation to my supervisor, Mr. Christos Papadopoulos, for being an excellent collaborator and professor. Without his guidance, inspiration and constant help, the completion of this thesis would not be possible.

Moreover, I am extremely grateful to Mr. George Rossopoulos, Ph.D. candidate, and Dr. Konstantinos Mamis for their continuous help, intuition and mentoring. Without their help it would be impossible to complete my undergraduate studies.

Last but not least, I would like to thank the professors of SNAME – SMH for the academic help they offered me, in pursuing and learning about the stochastic processes and their applications. Their help contributed in utilizing the core mathematics of this thesis.

Abstract in English

Friction is one of the most important causes of energy losses and wear in all mechanical systems. In ships, substantial friction losses are present in the propulsion system, both in the engine and in the shaft arrangement. Guided by the 2030 and 2050 environmental goals set by IMO, the maritime industry is challenged to utilize advanced technologies for optimal energy consumption and minimum power losses.

Journal bearings are mechanical components used to support the radial loads of rotating shafts. During operation, a thin lubricant film is generated and maintained hydrodynamically between the shaft and the bearing, preventing metal to metal contact and minimizing the friction losses. The performance of journal bearings is commonly quantified in terms of minimum film thickness, friction losses and maximum pressure of the lubricant. All of the above vary substantially at different operating conditions, such as radial load, shaft rotational speed and lubricant viscosity. Additionally, an important factor that needs to be taken into account is the micro differences in the surface geometry of the stator and the rotor (due to machining), which may significantly affect the performance of the bearing, its total load capacity and friction losses, as well as the subsequent wear rates of the bearing.

In the present work, a novel semi – stochastic solution of the Reynolds Equation for hydrodynamic lubricated journal bearings with stochastic surface roughness is presented. On the basis of stochastic theory, an advanced form of Reynolds Equation is derived. The mathematical formulation of this new equation yields the original deterministic Reynolds Equation for smooth surfaces, by removing the terms used to describe the roughness standard deviation

The derived differential equations are solved using the Finite Difference Method (FDM), developed as in house software. The obtained results are compared with (a) bearing performance results using the deterministic solution of the Reynolds Equation for smooth bearings, and (b) with results for bearings with surface roughness reported in the relevant literature, aiming at quantifying the extent of the roughness impact to different operational states of the bearing. Further, by assigning different values to the standard deviations of the roughness, we seek to optimize bearing performance by maximizing load carrying capacity and minimizing the total friction losses.

The proposed methodology has been validated against relevant results in other literature works, and a comparison of different numerical approaches for the treatment of the stochasticity of roughness profile and subsequent correlated bearing parameters has been performed. The effect on bearing performance of different roughness profiles for different bearing geometries and bearings operational parameters has been quantified. The ultimate goal of the present dissertation is to examine, evaluate and optimize bearings performance, by applying the optimum surface roughness during the manufacturing process of the bearing.

KEYWORDS:

Journal Bearings, Hydrodynamic Lubrication Theory, Reynolds Equation, Stochastic Roughness, Finite Difference Method

Abstract in Greek

Η τριβή αποτελεί την πιο συνήθη και σημαντική αιτία ενεργειακών απωλειών σε όλα τα μηχανικά συστήματα. Στο σύστημα πρόωσης ενός πλοίου, υψηλές απώλειες ενέργειας λόγω τριβής παρουσιάζονται τόσο στην κύρια μηχανή όσο και στο αξονικό σύστημα του πλοίου. Η ναυτιλία, καθοδηγούμενη από τους περιβαλλοντικούς στόχους του 2030 και 2050 που τέθηκαν από τον IMO, καλείται να χρησιμοποιήσει και να αξιοποιήσει προηγμένα τεχνολογικά συστήματα για τη βελτιστοποίηση της κατανάλωσης ενέργειας και την ελαχιστοποίηση των απωλειών ισχύος.

Τα ακτινικά έδρανα είναι μηχανολογικά κομμάτια που χρησιμοποιούνται για την παραλαβή των ακτινικών φορτίων των αξόνων. Κατά την λειτουργία τους, ένα λεπτό στρώμα λιπαντικού δημιουργείται και διατηρείται υδροδυναμικά μεταξύ του άξονα και του εδράνου, αποτρέποντας την επαφή μεταλλικών επιφανειών και ελαχιστοποιώντας τις ενεργειακές απώλειες λόγω τριβής. Ο βαθμός απόδοσης των ακτινικών εδράνων συνήθως ποσοτικοποιείται με βάση το ελάχιστο πάχος του λιπαντικού, τις ενεργειακές απώλειες λόγω τριβής και την μέγιστη πίεση λιπαντικού. Όλα τα παραπάνω, πρέπει να σημειωθεί, ότι αλλάζουν σε σημαντικό βαθμό αναλόγως την κατάσταση λειτουργίας, όπως είναι το ακτινικό φορτίο, η ταχύτητα περιστροφής του άξονα καθώς και το ιξώδες του λιπαντικού. Επιπροσθέτως στα προηγούμενα, ένας σημαντικός παράγοντας, ο οποίος πρέπει να λαμβάνεται υπ' όψιν, είναι αυτός των γεωμετρικών μικροδιαφορών στις επιφάνειες του άξονα και του εδράνου. Αυτές, μπορούν να επηρεάσουν σημαντικά την απόδοση, την χωρητικότητα φορτίου και τις ενεργειακές απώλειες λόγω τριβής του εδράνου, καθώς επίσης και τον ρυθμό φθοράς του.

Στην παρούσα εργασία, παρουσιάζεται μια νέα επίλυση της εξίσωσης Reynolds σε ακτινικά έδρανα υδροδυναμικής λίπανσης, τα οποία παρουσιάζουν στοχαστική τραχύτητα. Με βάση την θεωρία στοχαστικών μαθηματικών, εξάγεται μια καινούργια εξίσωση Reynolds. Ο μαθηματικός τύπος αυτής της νέας εξίσωσης παράγει της κλασική ντετερμινιστική εξίσωση Reynolds για λείες επιφάνειες, με τον μηδενισμό, και άρα απαλοιφή, της τυπικής απόκλισης των δύο τραχυτήτων.

Οι διαφορικές εξισώσεις που εμφανίζονται, λύνονται με την βοήθεια της μεθόδου πεπερασμένων διαφορών. Τα αποτελέσματα που προκύπτουν για την νέα εξίσωση Reynolds συγκρίνονται με αυτά της αρχικής εξίσωσης Reynolds καθώς και με άλλες προσεγγίσεις που έχουν υλοποιηθεί, στοχεύοντας την ποσοτικοποίηση και προσδιορισμό της επίδρασης της τραχύτητας σε διάφορες καταστάσεις λειτουργίας των ακτινικών εδράνων. Επίσης, με την ανάθεση διαφορετικών τυπικών αποκλίσεων στις τραχύτητες τόσο του άξονα όσο και του εδράνου, σκοπεύουμε να βελτιστοποιήσουμε την απόδοση του συστήματος. η οποία επιτυγχάνεται με την μεγιστοποίηση της αναπτυσσόμενης δύναμης καθώς και με την ελαχιστοποίηση των ενεργειακών απωλειών λόγω τριβής.

Η προτεινόμενη μεθοδολογία επαληθεύεται μέσω των αποτελεσμάτων σε βιβλιογραφικές πηγές, καθώς επίσης τίθενται σε σύγκριση διαφορετικές προσεγγίσεις για την μεταχείριση και θεώρηση της επιφανειακής τραχύτητας, καθώς και άλλων ακολούθων παραμέτρων του εδράνου, ως στοχαστικών ποσοτήτων. Έτσι, στοχεύουμε στην ποσοτικοποίηση της επίδρασης που έχουν τόσο η τραχύτητα όσο και η γεωμετρία της εγκατάστασης στις παραμέτρους λειτουργίας του εδράνου. Απώτερος σκοπός της παρούσας διπλωματικής είναι η διερεύνηση, εκτίμηση και βελτιστοποίηση της απόδοσης των εδράνων, μέσω της απόδοσης της πλέον κατάλληλης τραχύτητας κατά την διάρκεια της παραγωγής των υλικών και

μέσω της κατηγοριοποίησης των εδράνων σε ομάδες, οι οποίες υπό την ίδια επιφανειακή τραχύτητα αποδίδουν ίδιες συνθήκες λειτουργίας.

ΛΈΞΕΙΣ ΚΛΕΙΔΙΑ:

Ακτινικά Έδρανα, Θεωρία Υδροδυναμικής Λίπανσης, Εξίσωση Reynolds, Στοχαστική Τραχύτητα, Μέθοδος Πεπερασμένων Διαφορών

Table Of Contents

Table Of Figures

Nomenclature

B: bearing width

c: Bearing clearance

$\mathsf{C}_{(\bullet)}$: Covariance of $(\bullet)$ variable

D_B: Bearing diameter

D_S: Shaft diameter

e: Eccentricity

$\mathbb{E}^{\beta}[\bullet]$: Average operator

$\mathbb{F}_0(h)$: Correlation coefficient of mean pressure and mean film thickness

$\mathbb{F}_1(h)$: First negative power coefficient

$\mathbb{F}_2(h)$: Second negative power coefficient

F: Friction force

F^*: Dimensionless friction force

$f_{(\bullet)}$: Probability distribution function of $(\bullet)$ variable

$g(t)$: Relative rotation of shaft and bearing

h_T: Stochastic film thickness

h: Deterministic film thickness

h^*: Dimensionless film thickness

$h_{\min}$: Minimum film thickness

$h_{\max}$: Maximum film thickness

k: Convergence ratio

L: Bearing length

$\mathsf{m}_{(\bullet)}$: Mean value of $(\bullet)$ variable

N : Shaft rotational speed

O_S : Shaft center

O_B : Bearing center

P : External force

P_x : x - axis external force component

P_z : y - axis external force component

p : Pressure

$p_{\max}$: Maximum pressure

Q_{in} : Inlet flow rate

Q_{out} : Outlet flow rate

r : Roughness ratio

$r_B(\beta)$: Bearing roughness

$r_s(\beta)$: Shaft roughness

q_x : Lubricant inlet flow rate per unit length

q_y : Lubricant outlet flow rate per unit length

R_B : Bearing radius

R_S : Shaft radius

S : Sommerfeld number

t : Time variable

U : Shaft linear velocity

U_1 : x - axis bearing speed

U_2 : x - axis shaft speed

u : x - axis fluid velocity

V_1: y - axis bearing speed

V_2: y - axis shaft speed

v: y - axis fluid velocity

W: Total hydrodynamic force

W^*: Dimensionless hydrodynamic force

W_x: x - axis hydrodynamic force component

W_z: z - axis hydrodynamic force component

w: z - axis fluid velocity

x: x - axis coordinate

y: y - axis coordinate

z: z - axis coordinate

α_1: Standard deviation ratio for bearing

α_2: Standard deviation ratio for shaft

β: Stochastic Variable

ε: Eccentricity Ratio

η: Fluid dynamic viscosity

θ: Hydrodynamic film angle

μ: Friction Coefficient

ρ: Lubricant density

σ: Standard deviation

σ_B: Standard deviation of bearing

σ_S: Standard deviation of shaft

τ_x: Shear stress in x direction

τ_y: Shear stress in y direction

τ_z: Shear stress in z direction

φ: Attitude angle

ψ_y: Lateral misalignment

ψ_x: Vertical misalignment

1. Introduction

Tribology, the collective name given to the science and technology of interacting surfaces in relative motion, is a relatively new diverse science branch that studies the phenomena of friction, lubrication and wear. The application area of tribology is quite extensive, including, among others, the understanding and modeling of phenomena in lubrication, the optimization of tribological elements such as journal and thrust bearings, piston rings, mechanical seals, etc., the development of novel lubricants and methods of surface treatment and modeling, as well as the minimization of power losses, wear and associated maintenance and replacement costs of mechanical components.

The term tribology, apart from its conveniently collective character describing the field of friction, lubrication and wear, could also be used to coin a new word – Tribodesign[1]. It is, thus, obvious that the practical aim of tribology lies in its successful application to machine design. From the beginning of the 20th century, extended research and experiments have been performed to better understand the mechanisms of tribology.

The frictional and wear behavior of materials is greatly dependent upon the surface material used, as well as its topography. Since the early 1930s scientists had come to the conclusion that they need to better understand the surface topography, so to be able to grasp the way materials interact [2]; thus the assumption of smooth surfaces in the analysis of engineering surfaces was gradually replaced by rough surfaces. Evident of roughness is that engineering surfaces are created in various ways, typically by machining, surface treatment and coating, which produce surface topographies that deviate from smooth surfaces.

A considerable amount of research effort has gone into studying the true topography of solid surfaces. A surface profile was found to be composed of a range of frequency components. The high frequency components correspond to those that are perceived to be rough and hence called "roughness" or "asperities". The low frequency components correspond to more gradual changes in the profile and are often associated with the terms "waviness" or "form". The waviness component of a surface is periodic in nature, while the roughness has a random distribution in the surface.

Initially discreet roughness profiles were analyzed by Michell [3] and others [4], [5], [6], but in due course it became evident that statistical treatments were necessary to take account of the influence of real surface topography upon lubricating film performance. Greenwood &Williamson[7] using information obtained by digital analysis of profile meter outputs have shown that for many surfaces the distribution of height and the distribution of height peaks is very close to Gaussian; enabling the use of stochastic mathematical simulations. In 1981, volume (5) of the Tribology Series[8] was published, and was entirely devoted in the surface effects in adhesion, friction, wear and lubrication.

1.1. Literature Overview

Basedon[9],[10] and [11]

Tribology research has been extensive during the last decades, focusing on several mechanical components that have an interesting frictional behavior. One of the oldest and most important ways to reduce friction and its associated wear is to separate the two surfaces in relative motion by a thin fluid film. To this end, lubricating oils and other liquids, such as water, emulsions or even gases, can be utilized. It is therefore very important that models which can simulate accurately the tribological behavior of mechanical components such as bearings, piston rings and seals during hydrodynamic lubrication are developed in order to utilize the components in terms of friction losses and wear.

The basis of hydrodynamic lubrication is the theory introduced in 1886 by Osborne Reynolds. According to the theory, pressure can be transferred through a thin lubricating layer located between two sliding surfaces, which should not be parallel in order to create the necessary geometry of a hydrodynamic wedge. In journal bearings, which are the main subject of the present study, the shaft is supported by a cylindrical bearing. The shaft has by construction a diameter slightly smaller than that of the bearing. During operation, the shaft is eccentric with respect to the bearing; therefore wedge geometry is generated between the bearing and the shaft, leading to lubricant pressure build up and load support.

Since Osborne Reynolds introduced the theory of hydrodynamic lubrication, numerous studies have been performed, aiming to further explain the tribological characteristics of lubricated bearings. Several books and papers, concerned with the operational characteristics of journal bearings under a variety of running conditions, were published through the last century. One of the early papers to deal specifically with the effects of surface roughness on hydrodynamic lubrication was that of Tzeng and Saibel[12], who solved the problem for the case of a finite slider bearing and then averaged the corresponding solution. However, the difficulty of solving analytically the Reynolds Equation restricts the usage of the previous attempt to the case of transverse roughness in infinitely long bearings. Another approach, that is to make some heuristic assumptions concerning the pressure gradient and the flow rates and obtain an averaged equation, was followed by Christensen[13] and Tønder[14], who proposed three averaged equations for longitudinal, transverse and isotropic roughness. Following a similar approach, Patir and Cheng[15] and [16] deducted a Reynolds type equation, which used "flow factors".

However, these results have given rise to many controversies both in view of the numerical results and for the heuristic assumptions on which they are based on, i.e. [17] and [18], and it is claimed that the physical justification of these assumptions bring the applicability of the Reynolds Equation itself in question, i.e. [19].

1.2. Goals of the present study

The main goal of the current dissertation is to derive a novel solution of the Reynolds Equation for hydrodynamic lubricated bearings with stochastic surface roughness on both the stator and the rotor component of the bearing. To this end, an advanced form of the Reynolds Equation is derived.

In Chapter 2, the basics of the hydrodynamic lubrication theory are presented, followed by the derivation of the Reynolds Equation for journal bearings with surface roughness. Also, an analysis on the nature of the stochastic surface roughness is presented, alongside with its implications on the stochasticity of the film thickness.

In Chapter 3, the finite difference method and the adopted solution algorithm is developed and presented. Also, the solution matrices for a smooth and a rough bearing are calculated, both for the proposed approach and other approaches found in literature.

In Chapter 4, the validation of the proposed model is presented for both slider and journal bearings. The results for the operational parameters of the bearing, i.e. film thickness geometry, mean pressure distribution, load carrying capacity, friction force and coefficient of friction, are compared with literature findings and verified.

In Chapter 5, simulations of a journal bearing in various realistic operational conditions are presented. Using the proposed algorithm, the bearing performance parameters are calculated and discussed.

In Chapter 6 and 7, the main results of the present work are summarized, and conclusions and future work are drawn. Finally, the main mathematical analysis needed for the derivation of the proposed approach is summarized in the Appendixes (A) ~ (C).

2. Journal Bearings

2.1. Introduction

Journal bearings, based on [20], are the most common type of radial bearings with extended use in the maritime industry. They are used in a variety of applications and are extensively used for the support of the propulsion shaft of a vessel, to support radial loads and to guide a smooth transmission of torque from the engine to the propeller. A journal bearing consists of two parts; the stator or bushing, which is a stationary sleeve, and the rotor, which is the propulsion shaft in our case. The shaft rotates inside the bushing and between them a thin film of lubricant fills the gap. The lubricant is supplied to the system from arrangements such as inlet holes and grooves.

As the shaft is rotating, it drags lubricant which is forced to fill the converging (wedge- shaped) geometry between the shaft and the stator. The incompressible lubricant develops the desired pressure to preserve the hard metal shaft separated from the soft metal bushing. This is essential in order to avoid "dry friction" which is disastrous for the lifespan of the bearing. At the initiation of a rotary motion the shaft is forced, due to friction, to roll at the opposite direction within the bearing sleeve. This motion, accompanied with adequate lubricant supply, helps to immediately form a lubricant film and lift the shaft into steady state position. Lubrication starts taking effect at any relative rotational velocity greater than zero and is also very steady in sudden impulses or vibrations. A common instability that journal bearings face over the years, also known as self-excited oil whirl, is constrained using tilting- pads, elliptical, pressure dam and offset split bearings.

Once the shaft is operating in "steady state", it is located at a position within the bearing clearance and at some angle along the circumference. This position can be defined by the eccentricity e and the attitude angle φ, as shown in Figure (2.1). Attitude angle is the angle between the centers of the bore and the shaft and eccentricity is the distance between these points.

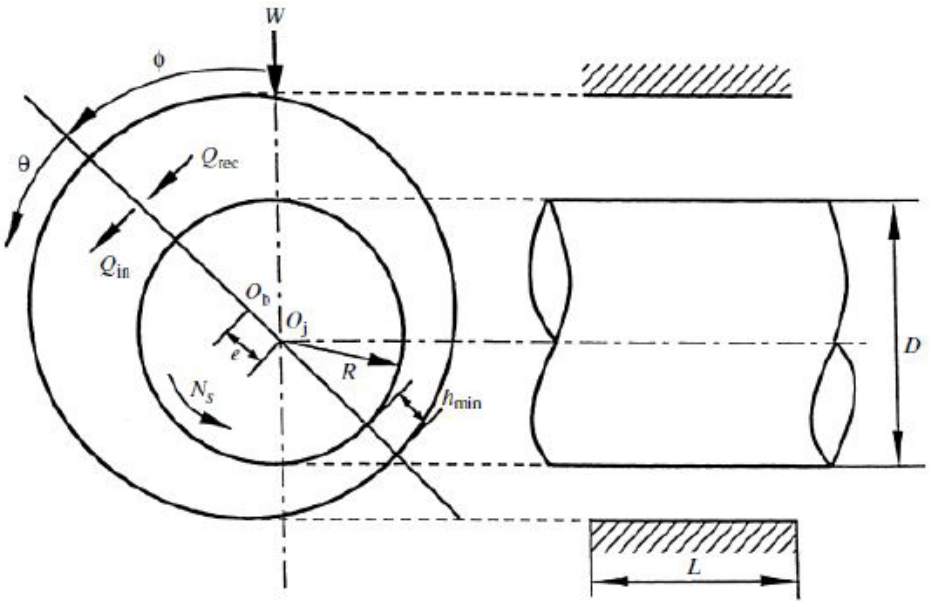

Figure 2.1: Cross Section of a typical Journal Bearing[9]

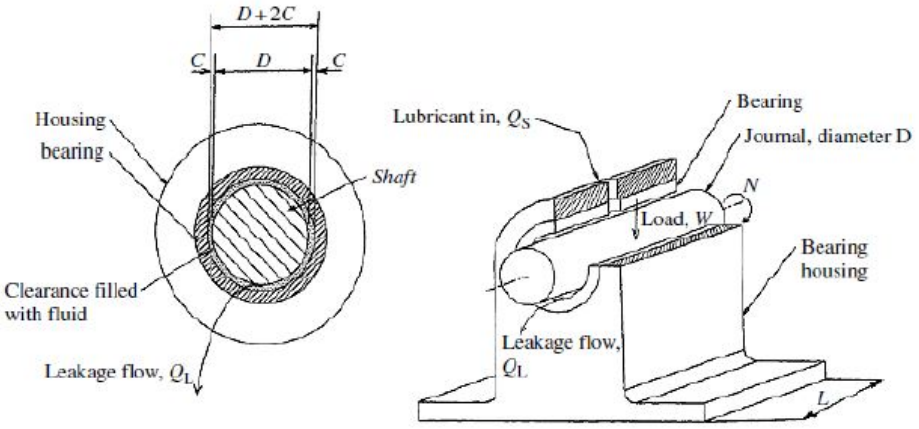

Figure 2.2: Typical Journal Bearing Geometry[20]

Journal bearings can be constructed quite simply and with very small tolerances, therefore they are used for high precision projects that also demand minimum wear and increased lifespan. Such bearings are quite economical, especially when they are produced massively. Additionally they have high capacity in sense of absorbing and damping vibrations, impulses or sudden force variation. On the other hand, journal bearings require frequent maintenance and special care against dust in the lubricant area. Furthermore they require a significant amount of lubricant and the friction coefficient during the startup process is inevitably high. According to[20], journal bearings can be subjected to six different ways of lubrication. Those categories are the below:

Hydrodynamic Lubrication: When the relative rotation speed surpasses a certain margin, a hydrodynamic pressure film is developed separating the two surfaces. A constant supply of lubricant is necessary, but there is no requirement for a certain inlet pressure.

Hydrostatic Lubrication: High pressure lubricant is fed to the system in order to separate the facing edges. There is no need for relative motion.

Elastohydrodynamic Lubrication: This is an extension of hydrodynamic lubrication, taking into account the elastic deformations of the shaft and the bore during operation.

Thermoelastohydrodynamic Lubrication: This is an extension of elastohydrodynamic lubrication, taking into account the thermal deformations of the shaft and the bore during operation.

Boundary Lubrication: This type takes place when the lubricant thickness is inadequate, due to small bearing surface, low rotational speed, inadequate amount of lubricant or high applied load. The transition between boundary and hydrodynamic lubrication occurs gradually and the intermediate condition is called mixed lubrication.

Solid- film Lubrication: A solid type of lubricant is used in applications where mineral oils cannot be used, or in cases of excessive heating of the interacting components.

In the present thesis, only the hydrodynamic lubrication of journal bearings will be treated. The fundamentals of hydrodynamic lubrication will be further analyzed in the current chapter.

2.1.1. Bearing Materials

Based on[21], [22], [23] and [24]

Materials used in tribological applications are, for the most part, common materials used generally in engineering applications, though there are some materials designed specifically for bearings. The selection of journal bearing material should be a careful process, since the chosen material should possess a combination of properties from compatibility, conformability, embeddability, fatigue strength, cavitation erosion resistance and corrosion resistance. In general, bearing materials can be either metallic or non-metallic materials.

Metallic material bearings are based on powder - metallurgy, and are made of white metal (tin and lead based), copper or aluminum based bronzes, porous metals and coated metals. They are relatively economical, suitable for high production rates and can be manufactured to precision tolerances. Nonmetallic material bearings are made of polymers, elastomers, ceramics and composites. Some significant characteristics of non-metallic materials are they are characterized by low wear rates, relatively high performance rating and the ability to conform under load. The non-metallic materials have been increasingly used as self-lubricating bearing. Their composition has been over refined so as to obtain favorable bearing characteristics, such as low friction and corrosion resistance.

The overlay selection process depends on the conformability required for the application. Conformability, in bearing materials, is the ability of the material to adapt to any geometry misalignments that might exist in the bearing. Depending on its nature, materials have different conformabilities, and thus are susceptible to different finishing works. This results in different surface roughness topography, yielding divergent standard deviations.

2.1.2. Bearing Lubricants

Based on[9] and[22]

The function of a lubricant is to control friction and wear in a given system. The basic requirements therefore relate to the performance of the lubricant, i.e. its influence upon friction and wear characteristics of a system. In journal bearings, the shaft rotates at sufficient speed to force the lubricant to move between the conforming surfaces of the shaft and the bearing, creating an oil wedge and a hydrodynamic oil film. This film is responsible for the support of extremely heavy loads and the operation of the system in high rotational speeds.

The parameter which plays a fundamental role in lubrication is oil viscosity. Different oils exhibit different viscosities. In addition, oil viscosity changes with temperature, shear rate and pressure;for engineering applications the oil viscosity is usually chosen to give optimum performance at the required temperature. Since the 1950s, additives began to be widely used in varying quantities, targeting the improvement of the oil properties and its life extension. Those additives can be listed in the following categories

- Antioxidants: Antioxidant additives are used in order to delay the severe oxidation of the oil. They can be classified into
  - ✓ Metal deactivators
  - ✓ Radical inhibitors
  - ✓ Peroxide decomposers
- Corrosion Control Additives: Those are additives that protect surfaces and components from corrosion. They are split into two categories
  - ✓ Corrosion inhibitors
  - ✓ Rust inhibitors
- Contamination Control Additives: Those additives are used to control the acidity of the products of sulfurous combustion and to prevent agglomeration of the soot. There exist two types of these additives
  - ✓ Mild dispersants
  - ✓ Over - based dispersants
- Foam Inhibitors: The main task of these additives is to destabilize the foam generation during machinery operations.
- Pour Point Depressants: Those additives help prevent the formation of wax structures at low temperatures.
- Viscosity Improvers: These additives are used to arrest the decline in oil viscosity with temperature.
- Wear & Friction Improvers: Probably the most important of all the additives, these chemicals control the lubricating performance of the oil. They can be divided into
  - ✓ Adsorption or boundary additives
  - ✓ Anti - wear additives
  - ✓ Extreme pressure additives

2.1.3. Common Bearing Damages

The most common bearing damages found in engines are the following

- Abrasion: It's the most common type of damage in bearings. Abrasion is caused by debris and foreign materials rotating alongside with the oil in the lubricant film. These substances include dirt, abrasive grit or dirt.
- Fatigue: Fatigue, or spalling, is often the result of overloading, an excessive preload, tight inner ring fits and using the bearing beyond its calculated fatigue life. In general, fatigue can be indicated by the fracture of running surfaces and subsequent removal of small discrete particles of material, and is always accompanied by a noticeable increase in vibrations and noises. Fatigue can be avoided if stronger bearing linings are used and a more cautious design is set.
- Corrosion: Corrosion depends on both the bearing material and the operating conditions of the bearing. Moisture, acid, low – quality or broken down grease, poor wrappings and condensation from excessive temperature reversals can cause corrosion that is abrasive to the surfaces of the bearing.
- Wiping: Wiping occurs in any kind of lining material if insufficient lubrication or cooling of the oil takes place. Wiping results in melting of the lowest melting point phase of lining alloys.
- Cavitation: Cavitation risk increases with rising bearing speeds and loads.
- Fretting: Fretting occurs due to insufficient contact pressure, local welding and tearing having taken place between the bearing back and housing bore.
- Static fretting: Fretting can take place whenever low amplitude vibratory sliding takes place between two surfaces. Fretting is common because most of the machinery is subject to vibrations, both in transit and in operation conditions.
- Incorrect assembly: This factor is associated with locating devices. Incorrect positioning results in oil feed connections being misplaced, which can block it off. Excessive care needs to be taken when locating the shaft correctly into the housing. Fretting of the bearing may occur if there is insufficient bolt load, while on the other hand, excessive dynamic stressing in the bolts can cause fatigue fractures.
- Misalignment: Misalignment in bearings consists of bent shafts, out of square shaft shoulders, clamping nuts that are not positioned in order and improper installation due to loose fits. Those factors may result in overheating and separator failure.
- Smearing: When two inadequately lubricated surfaces slide against each other, material is transferred from one surface to the other. This mechanism is commonly known as smearing. When smearing occurs, the material is generally heated to such temperatures that rehardening takes place. This process produces localized stress concentrations that may cause cracking of flaking to the bearing materials.
- Geometric factors: Geometric factors of bearings, if not properly selected, can lead to many damages. Such factors are the radial or axial clearance, bearing diameters or fits.

2.2. Journal Bearing Geometry

The geometry of a journal bearing is depicted in Figure (2.3). The journal bearing radius is R_1 and the shaft radius is R_2, while O_B and O_S are the bearings and shafts center respectively. The distance between these centers is called eccentricity, denoted by ε and the angle between the $y'y$ axis and the line defined by the centers is called attitude angle, φ. At this specific angle we can calculate the maximum and minimum of the film thickness.

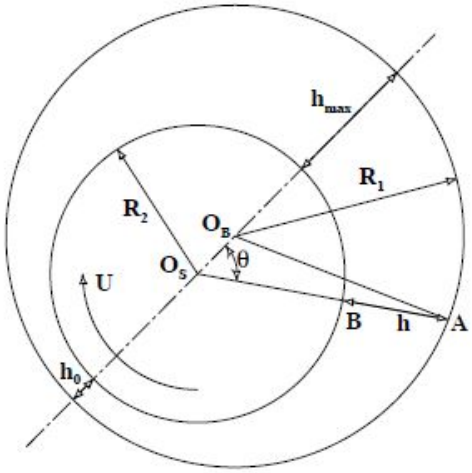

Figure 2.3: Typical journal bearing geometry[9]

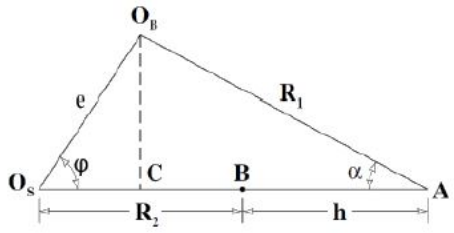

Figure 2.4: Details of geometry for the evaluation of film shape in journal bearing[9]

The film thickness geometry can be derived by basic geometric calculations presented in Figure (2.4). According to this figure the mathematical expression of the film thickness is given by the equation (2.1).

$$\left(O_S A\right) = \left(O_S C\right) + \left(CA\right) = \left(O_S B\right) + \left(BA\right) \tag{2.1}$$

$$R_2 + h = e\cdot\cos\left(\theta\right) + R_1\cdot\cos\left(\alpha\right)$$

Thus

$$h = e\cdot\cos\left(\theta\right) + R_1\cdot\cos\left(\alpha\right) - R_2 \tag{2.2}$$

Applying the sine rule in the triangles ACO_B and O_SCO_B we get that $\sin(\alpha) = \frac{e}{R}\cdot\sin(\theta)$. Using that $\sin^2(\alpha) + \cos^2(\alpha) = 1$ we get that

$$\cos(\alpha) = \sqrt{1 - \left(\frac{e}{R}\right)^2 \cdot \sin^2(\theta)}$$

Since $e \ll R$ we know that $\frac{e}{R} \cong 0$ and thus we get that $\cos(\alpha) = 1$. Substituting into equation (2.2) yields

$$h = e\cdot\cos(\theta) + R_1 - R_2 \qquad \textbf{(2.3)}$$

Substituting $c = R_1 - R_2$, the clearance of the bearing, and $\varepsilon = \frac{e}{c}$, the eccentricity ratio, we get equation (2.4).

$$h = c\cdot(1 + \varepsilon\cdot\cos(\theta)) \qquad \textbf{(2.4)}$$

Equation (2.4) gives a description for the film thickness in journal bearings to within 0.1 % accuracy.

2.3. Hydrodynamic Lubrication

According to [9] Hydrodynamic lubrication is the phenomenon in which two relative moving surfaces are separated by a pressurized thin lubricating fluid film. The upper surface is called the stator while the bottom surface is the rotor. This lubricating film allows the transfer of forces without direct metal to metal contact of the surfaces, reducing the friction coefficient at very low levels. Depending on the relative velocity of the surfaces and the lubricant properties, no additional agency is required to create and maintain a load - carrying film, provided that adequate lubricant is made available. The mathematical expression of hydrodynamic lubrication in the form of an equation has been first derived by simplifying the Navier-Stokes momentum and continuity equations, and is commonly known as the Reynolds Equation. Another, typical approach is by considering the equilibrium of an element of liquid subjected to viscous shear, and applying the continuity of flow. According to Osborne Reynolds, the conditions necessary for the hydrodynamic lubrication to occur are the below

(C1). The two surfaces must move relatively to each other with sufficient speed in order to generate a lubricating film that can carry the normal load

(C2). Surfaces must be inclined at some small angle, so that a hydrodynamic wedge is generated, and a pressure field is developed in the lubricating domain. A pressure field can be also generated between moving parallel stepped surfaces, as well as between surfaces that move towards each other

In figure (2.5) a sketch of a simple slider with inclined surfaces is presented. The motion of the top surface drags lubricant into the converging geometry, generating a pressure field. If pressure was not generated there would be more lubricant entering the wedge than leaving it. Therefore, pressure increases at the beginning of the wedge, restricting inflow, while it decreases near the end of the wedge boosting outflow. The existence of a pressure gradient causes the fluid velocity profile to bend inwards at the entrance and to bend outwards at the exit. The pressure generated is able to separate the two surfaces and support a certain load in the z direction

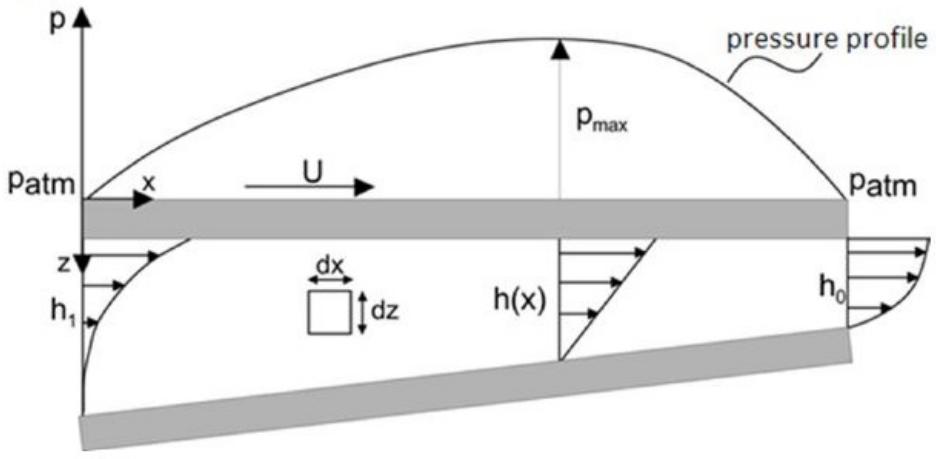

Figure 2.5: Hydrodynamic pressure generation between the non-parallel surfaces of a simple slider

Before starting to analyze the theory of hydrodynamic lubrication, there are some simplifying assumptions that need to be made:

(A1). Body forces acting on the fluid are neglected
(A2). Pressure is constant throughout the film thickness
(A3). No - slip condition is assumed at the slider surfaces
(A4). Oil lubricant behaves as a Newtonian fluid
(A5). Fluid flow is laminar
(A6). Fluid inertia is neglected
(A7). Viscosity is constant throughout the fluid film

2.3.1. Equilibrium of an element

For simplicity we assume that the forces of the element are only acting in the $x'x$ axis. Since the element of figure (2.6) is in equilibrium, then we know that

$$pdydz + \left(\tau_x + \frac{\partial \tau_x}{\partial z} dz\right) dxdy = \left(p + \frac{\partial p}{\partial x} dx\right) dydz + \tau_x dxdy \qquad \textbf{(2.5)}$$

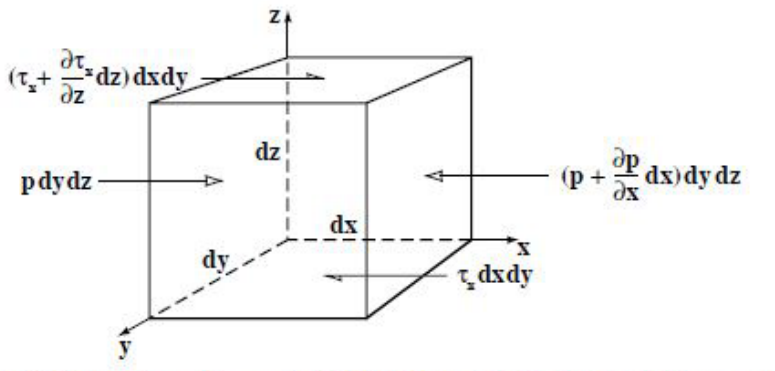

Figure 2.6: Equilibrium Of An Element Of Fluid From a Hydrodynamic Film

After simplifying the terms in equation (2.5) we get

$$\frac{\partial \tau_x}{\partial z} = \frac{\partial \mathbf{p}}{\partial x}$$

In the previous equations we know that **p** is the pressure and τ_x is the shear stress acting in the $x'x$ axis. The factor *dxdydz* is obviously positive, because the element has a volume, and thus we can neglect it. A similar expression can be obtain for forces acting in the $y'y$ axis, while in the $z'z$ axis we get that $\frac{\partial p}{\partial z} = 0$ because of the assumption (A2). Thus for the equilibrium of the element we get the system of equations (2.6).

$$\begin{cases} \dfrac{\partial p}{\partial x} = \dfrac{\partial \tau_x}{\partial z} \\ \dfrac{\partial p}{\partial y} = \dfrac{\partial \tau_y}{\partial z} \\ \dfrac{\partial p}{\partial z} = 0 \end{cases} \tag{2.6}$$

By using that $\tau_{(\cdot)} = \eta \cdot \dfrac{\partial u_{(\cdot)}}{\partial z}$, where $u_{(\cdot)}$ is the velocity in direction $(\cdot)$, we get that

$$\begin{cases} \dfrac{\partial p}{\partial x} = \dfrac{\partial}{\partial z}\left(\eta \cdot \dfrac{\partial u}{\partial z}\right) \\ \dfrac{\partial p}{\partial y} = \dfrac{\partial}{\partial z}\left(\eta \cdot \dfrac{\partial v}{\partial z}\right) \\ \dfrac{\partial p}{\partial z} = 0 \end{cases} \tag{2.7}$$

By integrating equations (2.7) we get that

$$\begin{cases} \dfrac{\partial p}{\partial x}\dfrac{z^2}{2} + C_1 z + C_2 = \eta u \\ \dfrac{\partial p}{\partial y}\dfrac{z^2}{2} + C_3 z + C_4 = \eta v \\ \dfrac{\partial p}{\partial z} = 0 \end{cases} \tag{2.8}$$

2.3.2. Continuity of Flow

Let us consider a column of lubricant as shown in figure (2.7). The principle of continuity of flow requires that the influx of a liquid must be equal to its efflux from a control volume under steady condition. Thus we get equation (2.9)

$$\begin{aligned} \rho u dydz + \rho v dxdz + \rho w dxdy = &\left(\rho u + \frac{\partial \rho u}{\partial x}dx\right)dydz + \left(\rho v + \frac{\partial \rho v}{\partial y}dy\right)dxdz \\ &+ \left(\rho w + \frac{\partial \rho w}{\partial z}dz\right)dxdy + \frac{\partial \rho}{\partial t}dxdydz \end{aligned} \tag{2.9}$$

After simplifying the terms in equation (2.9) we get

$$\frac{\partial \rho u}{\partial x} + \frac{\partial \rho v}{\partial y} + \frac{\partial \rho w}{\partial z} + \frac{\partial \rho}{\partial t} = 0 \tag{2.10}$$

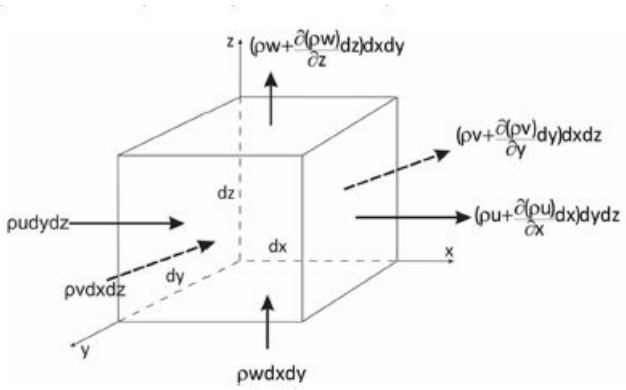

Figure 2.7: Continuity Of Flow In A Column

By using the Leibniz's rule for differentiation we get that

$$\int_0^h \frac{\partial \rho u}{\partial x} dz = -\rho u|_{z=h} \frac{\partial h}{\partial x} + \frac{\partial}{\partial x}\left(\int_0^h \rho u dz\right) \quad \textbf{(2.11)}$$

$$\int_0^h \frac{\partial \rho v}{\partial y} dz = -\rho v|_{z=h} \frac{\partial h}{\partial y} + \frac{\partial}{\partial y}\left(\int_0^h \rho v dz\right) \quad \textbf{(2.12)}$$

$$\int_0^h \frac{\partial \rho w}{\partial z} dz = \rho w|_{z=h} - \rho w|_{z=0} \quad \textbf{(2.13)}$$

$$\int_0^h \frac{\partial \rho}{\partial t} dz = -\rho|_{z=h} \frac{\partial h}{\partial t} + \frac{\partial}{\partial t}\left(\int_0^h \rho dz\right) \quad \textbf{(2.14)}$$

By differentiating equation (2.10) in respect to z we get that

$$\int_0^h \left(\frac{\partial \rho u}{\partial x} + \frac{\partial \rho v}{\partial y} + \frac{\partial \rho w}{\partial z} + \frac{\partial \rho}{\partial t}\right) dz = 0 \quad \textbf{(2.15)}$$

Or else, by using equations (2.11), (2.12), (2.13) and (2.14)

$$\frac{\partial}{\partial x}\left(\int_0^h \rho u dz\right) + \frac{\partial}{\partial y}\left(\int_0^h \rho v dz\right) + \frac{\partial}{\partial t}\left(\int_0^h \rho dz\right) = \rho u|_{z=h} \frac{\partial h}{\partial x} + \rho v|_{z=h} \frac{\partial h}{\partial y} + \rho|_{z=h} \frac{\partial h}{\partial t} - \rho w|_0^h \quad \textbf{(2.16)}$$

By using equations (2.8) we get that

$$\begin{pmatrix} \frac{\partial}{\partial x}\left(\int_0^h \frac{1}{\eta}\rho\left(\frac{\partial p}{\partial x}\frac{z^2}{2} + C_1 z + C_2\right) dz\right) \\ + \frac{\partial}{\partial y}\left(\int_0^h \frac{1}{\eta}\rho\left(\frac{\partial p}{\partial y}\frac{z^2}{2} + C_1 z + C_2\right) dz\right) \\ + \frac{\partial}{\partial t}\left(\int_0^h \rho dz\right) \end{pmatrix} = \rho u|_{z=h} \frac{\partial h}{\partial x} + \rho v|_{z=h} \frac{\partial h}{\partial y} + \rho|_{z=h} \frac{\partial h}{\partial t} - \rho w|_0^h \quad \textbf{(2.17)}$$

2.3.3. Initial Values

Equation (2.17) yields the Reynolds Equation. Before reaching the final form of Reynolds Equation we have to find the values of C_i, $i \in \{1,2,3,4\}$. Those values will be calculated by the system of equations (2.8). Since there is no slip or velocity discontinuity between liquid and solid at the boundaries of the wedge, according to (A3), for that system of equations we know that

for $z = 0$, $u = U_2$ for $z = 0$, $v = V_1$

for $z = h$, $u = U_1$ for $z = h$, $u = V_2$

Thus the system of equations (2.8) results in system (2.18)

$$\begin{cases} C_2 = \eta U_2 \\ \dfrac{\partial p}{\partial x}\dfrac{h^2}{2} + C_1 h + C_2 = \eta U_1 \\ C_4 = \eta V_2 \\ \dfrac{\partial p}{\partial y}\dfrac{h^2}{2} + C_3 h + C_4 = \eta V_1 \end{cases} \tag{2.18}$$

or else

$$\begin{cases} C_1 = \dfrac{\eta}{h}\left(U_1 - U_2\right) - \dfrac{\partial p}{\partial x}\dfrac{h}{2} \\ C_2 = \eta U_2 \\ C_3 = \dfrac{\eta}{h}\left(V_1 - V_2\right) - \dfrac{\partial p}{\partial x}\dfrac{h}{2} \\ C_4 = \eta V_2 \end{cases} \tag{2.19}$$

If we assume that $U_1 = 0, U_2 = U$, $V_1 = 0, V_2 = 0$, $w|_0 = 0$ and $w|_h = \dfrac{\partial h}{\partial t}$, then equation (2.17) turns into equation (2.20).

$$-\frac{\partial}{\partial x}\left(\frac{\rho h^3}{12\eta}\frac{\partial p}{\partial x}\right) - \frac{\partial}{\partial y}\left(\frac{\rho h^3}{12\eta}\frac{\partial p}{\partial y}\right) + \frac{U}{2}\frac{\partial}{\partial x}(\rho h) + \frac{V}{2}\frac{\partial}{\partial y}(\rho h) + \rho\frac{\partial h}{\partial t} = 0 \tag{2.20}$$

Further rearranging and simplifying yields equation (2.21), which is the Reynolds Equation that is going to be treated accordingly in the current thesis.

$$\frac{\partial}{\partial x}\left(\frac{\rho h^3}{12\eta}\frac{\partial p}{\partial x}\right) + \frac{\partial}{\partial y}\left(\frac{\rho h^3}{12\eta}\frac{\partial p}{\partial y}\right) = \frac{U}{2}\frac{\partial}{\partial x}(\rho h) + \rho\frac{\partial h}{\partial t} \tag{2.21}$$

2.4. The Stochastic Film Thickness

The current thesis applies the concept of stochastic process to the problem of the surface roughness in hydrodynamic lubricated bearings. Under this scope, the geometry of the lubricant film in the bearing is considered to be made up of two parts, which are demonstrated in equation (I)

$$h_T(x,y,t;\beta) = \underbrace{h(x,y,t)}_{(1)} + \underbrace{r_B(\beta)g(t) + r_S(\beta)g(t)}_{(2)} \qquad \textbf{(2.22)}$$

In equation (I), $h(x,y,t)$ is the nominal film thickness, measuring the large scale part of the film thickness geometry. This part is equivalent to the deterministic film thickness present in hydrodynamic lubrication if there was no surface roughness. The variables $r_B(\beta)$ and $r_S(\beta)$ are the stochastic variables that represent the surface roughness in the bearing and the shaft respectively, while $g(t)$ is a deterministic function of time representing the relative motion of the two surfaces.

The two surface roughness random variables are considered to be of such form that the application of the Reynolds Equation is still valid. Meaning, the surface roughness is a Reynolds type roughness; the heights of the two surface roughness should not be of the same order as h. For the two random variables we know that $r_B(\beta) \sim \mathcal{N}(0, \sigma_B^2)$ and $r_S(\beta) \sim \mathcal{N}(0, \sigma_S^2)$, having the following distribution probability function.

$$\mathsf{f}_{r(\beta)}(w) = \frac{1}{\sqrt{2\pi}\sigma^2}\exp\left\{-\frac{1}{2}\left(\frac{w}{\sigma}\right)^2\right\}$$

For the two random variables we can normalize their standard deviations by using $\sigma^2 = \sigma_S^2 + \sigma_B^2$, meaning that $\sigma_B = \alpha_1 \cdot \sigma$, $\sigma_S = \alpha_2 \cdot \sigma$; with $\alpha_1^2 + \alpha_2^2 = 1$. This normalization is taken into account to quantify the effect of each one of the two surface roughness components in the performance parameters of the bearing; load carrying capacity, friction force, friction coefficient and flow rates.

2.5. The Stochastic Reynolds Equation for constant viscosity & density

2.5.1. Averaging the Reynolds Equation

The current approach is considering an incompressible fluid of constant viscosity, thus we denote that $\eta(x,y,z,t) \equiv \eta$ and $\rho(x,y,z,t) \equiv \rho$. We also assume that $g(t) = const$, to simplify the calculations. Inserting the above assumptions in equation (2.21) we derive the Stochastic Reynolds Equation that will be treated in the current thesis, given by equation (2.23).

$$\nabla\left(h_T^3 \nabla p\right) = 12\eta \frac{\partial h_T}{\partial t} + 6U\eta \frac{\partial h_T}{\partial x} \tag{2.23}$$

The film thickness is given as $h_T(x,y,t;\beta) = h(x,y,t) + r_S(\beta)g(t) + r_B(\beta)g(t)$ and thus we know that

$$\frac{\partial h_T}{\partial x} = \frac{\partial}{\partial x}\left(h(x,y,t) + r_S(\beta)g(t) + r_B(\beta)g(t)\right) = \frac{\partial h}{\partial x}$$

$$\frac{\partial h_T}{\partial y} = \frac{\partial}{\partial y}\left(h(x,y,t) + r_S(\beta)g(t) + r_B(\beta)g(t)\right) = \frac{\partial h}{\partial y}$$

$$\frac{\partial h_T}{\partial t} = \frac{\partial}{\partial t}\left(h(x,y,t) + r_S(\beta)g(t) + r_B(\beta)g(t)\right) = \frac{\partial h}{\partial t}$$

Expanding the film thickness h_T in its terms and substituting the previous into equation (2.23) yields equation (2.24).

$$\begin{pmatrix} \nabla\left(h^3\nabla p\right) + g^3(t)r_S^3(\beta)\nabla^2 p + g^3(t)r_B^3(\beta)\nabla^2 p \\ + 3g(t)r_S(\beta)\nabla\left(h^2\nabla p\right) + 3g(t)r_B(\beta)\nabla\left(h^2\nabla p\right) \\ + 3g^2(t)r_S^2(\beta)\nabla(h\nabla p) + 3g^2(t)r_B^2(\beta)\nabla(h\nabla p) \\ + 3g^3(t)r_B^2(\beta)r_S(\beta)\nabla^2 p + 3g^3(t)r_S^2(\beta)r_B(\beta)\nabla^2 p \\ + 6g^2(t)r_S(\beta)r_B(\beta)\nabla(h\nabla p) \end{pmatrix} = 12\eta\frac{\partial h}{\partial t} + 6U\eta\frac{\partial h}{\partial x} \tag{2.24}$$

Solving equation (2.24) requires the exact topography of the two roughness $r_S(\beta)$ and $r_B(\beta)$. In order to avoid this, we will use the statistical representation of those variables. Applying the average operator in equation (2.24), remembering that since h is a deterministic function thus $\forall k \in \mathbb{R}$ $\mathbb{E}^{\beta}\left[h^k\right] = h^k$, yields equation (2.25).

$$\begin{pmatrix} \nabla\left(h^3\nabla\mathbb{E}^{\beta}[p]\right)+g^3(t)\nabla^2\mathbb{E}^{\beta}\left[r_S^3(\beta)p\right]+g^3(t)\nabla^2\mathbb{E}^{\beta}\left[r_B^3(\beta)p\right] \\ +3g(t)\nabla\left(h^2\nabla\mathbb{E}^{\beta}\left[r_S(\beta)p\right]\right)+3g(t)\nabla\left(h^2\nabla\mathbb{E}^{\beta}\left[r_B(\beta)p\right]\right) \\ +3g^2(t)\nabla\left(h\nabla\mathbb{E}^{\beta}\left[r_S^2(\beta)p\right]\right)+3g^2(t)\nabla\left(h\nabla\mathbb{E}^{\beta}\left[r_B^2(\beta)p\right]\right) \\ +3g^3(t)\nabla^2\mathbb{E}^{\beta}\left[r_B^2(\beta)r_S(\beta)p\right]+3g^3(t)\nabla^2\mathbb{E}^{\beta}\left[r_B(\beta)r_S^2(\beta)p\right] \\ +6g^2(t)\nabla\left(h\nabla\mathbb{E}^{\beta}\left[r_S(\beta)r_B(\beta)p\right]\right) \end{pmatrix} = 12\eta\frac{\partial h}{\partial t}+6U\eta\frac{\partial h}{\partial x} \quad \textbf{(2.25)}$$

The next step is to formally calculate the averages of the equation (2.25). Those averages represent various moments of the roughness and the pressure. The terms that are to be calculated are listed below, in ascending order in respect to h for simplicity.

$$T_1 = \nabla\left(h^3\,\mathbb{E}^{\beta}[\nabla p]\right)$$

$$T_2 = 3g(t)\nabla\left(h^2\,\mathbb{E}^{\beta}\left[r_B(\beta)\nabla p\right]\right)$$

$$T_3 = 3g(t)\nabla\left(h^2\,\mathbb{E}^{\beta}\left[r_S(\beta)\nabla p\right]\right)$$

$$T_4 = 3g^2(t)\nabla\left(h\,\mathbb{E}^{\beta}\left[r_B^2(\beta)\nabla p\right]\right)$$

$$T_5 = 6g^2(t)\nabla\left(h\,\mathbb{E}^{\beta}\left[r_B(\beta)r_S(\beta)\nabla p\right]\right)$$

$$T_6 = 3g^2(t)\nabla\left(h\,\mathbb{E}^{\beta}\left[r_S^2(\beta)\nabla p\right]\right)$$

$$T_7 = g^3(t)\mathbb{E}^{\beta}\left[r_B^3(\beta)\nabla^2 p\right]$$

$$T_8 = 3g^3(t)\mathbb{E}^{\beta}\left[r_B^2(\beta)r_S(\beta)\nabla^2 p\right]$$

$$T_9 = 3g^3(t)\mathbb{E}^{\beta}\left[r_B(\beta)r_S^2(\beta)\nabla^2 p\right]$$

$$T_{10} = g^3(t)\mathbb{E}^{\beta}\left[r_S^3(\beta)\nabla^2 p\right]$$

Applying Stein's Lemma in each one of the above terms yields the following form for the terms.

$$T_1 = \nabla\left(h^3\nabla\mathrm{m}_p\right)$$

$$T_2 = 3\sigma_B^2 g(t)\nabla\left(h^2\,\mathbb{E}^{\beta}\left[\frac{\partial\,\nabla p}{\partial r_B(\beta)}\right]\right)$$

$$T_3 = 3\sigma_S^2 g(t)\nabla\left(h^2\ \mathbb{E}^{\beta}\left[\frac{\partial\,\nabla p}{\partial r_S(\beta)}\right]\right)$$

$$T_4 = 3\sigma_B^2 g^2(t)\nabla\left(h\nabla \mathrm{m}_p\right) + 3\sigma_B^4 g^2(t)\nabla\left(h\ \mathbb{E}^{\beta}\left[\frac{\partial^2\nabla p}{\partial r_B^2(\beta)}\right]\right)$$

$$T_5 = 6\sigma_S^2\sigma_B^2 g^2(t)\nabla\left(h\ \mathbb{E}^{\beta}\left[\frac{\partial^2\nabla p}{\partial r_S(\beta)\partial r_B(\beta)}\right]\right)$$

$$T_6 = 3\sigma_S^2 g^2(t)\nabla\left(h\nabla \mathrm{m}_p\right) + 3\sigma_S^4 g^2(t)\nabla\left(h\ \mathbb{E}^{\beta}\left[\frac{\partial^2\nabla p}{\partial r_S^2(\beta)}\right]\right)$$

$$T_7 = 3\sigma_B^4 g^3(t)\mathbb{E}^{\beta}\left[\frac{\partial\,\nabla^2 p}{\partial r_B(\beta)}\right] + \sigma_B^6 g^3(t)\mathbb{E}^{\beta}\left[\frac{\partial^3\nabla^2 p}{\partial r_B^3(\beta)}\right]$$

$$T_8 = 3\sigma_B^2\sigma_S^2 g^3(t)\mathbb{E}^{\beta}\left[\frac{\partial\nabla^2 p}{\partial r_S(\beta)}\right] + 3\sigma_B^4\sigma_S^2 g^3(t)\mathbb{E}^{\beta}\left[\frac{\partial^3\nabla^2 p}{\partial r_B^2(\beta)\partial r_S(\beta)}\right]$$

$$T_9 = 3\sigma_S^2\sigma_B^2 g^3(t)\mathbb{E}^{\beta}\left[\frac{\partial\nabla^2 p}{\partial r_B(\beta)}\right] + 3\sigma_S^4\sigma_B^2 g^3(t)\mathbb{E}^{\beta}\left[\frac{\partial^3\nabla^2 p}{\partial r_S^2(\beta)\partial r_B(\beta)}\right]$$

$$T_{10} = 3\sigma_S^4 g^3(t)\mathbb{E}^{\beta}\left[\frac{\partial\,\nabla^2 p}{\partial r_S(\beta)}\right] + \sigma_S^6 g^3(t)\mathbb{E}^{\beta}\left[\frac{\partial^3\nabla^2 p}{\partial r_S^3(\beta)}\right]$$

Categorizing the previous terms into groups in respect to the order of the variational derivative of the pressure in respect to the roughness, using that $\sigma_B = \alpha_1\cdot\sigma$ and $\sigma_S = \alpha_2\cdot\sigma$, yields the following terms

$$\tilde{T}_1 = \nabla\left(\left(h^3 + 3\sigma^2 g^2(t)h\right)\nabla \mathrm{m}_p\right)$$

$$\tilde{T}_2 = 3\alpha_2^2\sigma^2 g\ (t)\nabla\left(\left(h^2 + \sigma^2 g^2(t)\right)\nabla\mathbb{E}^{\beta}\left[\frac{\partial\ p}{\partial r_S(\beta)}\right]\right)$$

$$\tilde{T}_3 = 3\alpha_1^2\sigma^2 g\ (t)\nabla\left(\left(h^2 + \sigma^2 g^2(t)\right)\nabla\mathbb{E}^{\beta}\left[\frac{\partial\ p}{\partial r_B(\beta)}\right]\right)$$

$$\tilde{T}_4 = 3\alpha_2^4\sigma^4 g^2(t)\nabla\left(h\nabla\mathbb{E}^{\beta}\left[\frac{\partial^2 p}{\partial r_S^2(\beta)}\right]\right)$$

$$\tilde{T}_5 = 3\alpha_1^4\sigma^4 g^2(t)\nabla\left(h\nabla\mathbb{E}^{\beta}\left[\frac{\partial^2 p}{\partial r_B^2(\beta)}\right]\right)$$

$$\tilde{T}_6 = 6\alpha_1^2\alpha_2^2\sigma^4 g^2(t)\nabla\left(h\nabla\mathbb{E}^{\beta}\left[\frac{\partial^2 p}{\partial r_S(\beta)\partial r_B(\beta)}\right]\right)$$

$$\tilde{T}_7 = 3\alpha_1^4\alpha_2^2\sigma^4 g^3(t)\nabla^2\mathbb{E}^{\beta}\left[\frac{\partial^3 p}{\partial r_B^2(\beta)\partial r_S(\beta)}\right]$$

$$\tilde{T}_8 = 3\alpha_1^2\alpha_2^4\sigma^6 g^3(t)\nabla^2\mathbb{E}^{\beta}\left[\frac{\partial^3 p}{\partial r_S^2(\beta)\partial r_B(\beta)}\right]$$

$$\tilde{T}_9 = g^3(t)\alpha_2^6\sigma^6\nabla^2\mathbb{E}^{\beta}\left[\frac{\partial^3 p}{\partial r_S^3(\beta)}\right]$$

$$\tilde{T}_{10} = g^3(t)\alpha_1^6\sigma^6\nabla^2\mathbb{E}^{\beta}\left[\frac{\partial^3 p}{\partial r_B^3(\beta)}\right]$$

Remark 2.1: ***The term $\tilde{T}_1$ is the exact and only term that appears in previous literature findings for isotropic roughness. All the other terms are zero, meaning that the mean values of the variational derivatives of the pressure in respect to the roughness are equal to zero.***

2.5.2. Variational Derivatives of Pressure

If we differentiate Equation (2.23) in respect to the roughness of the shaft $r_S(\beta)$ we get that

$$\nabla\left(h_T^3 \nabla \frac{\partial p}{\partial r_S(\beta)} + 3g(t) h_T^2 \nabla p \right) = 0$$

The previous equation after manipulations results in:

$$h_T^3 \frac{\partial \nabla p}{\partial r_S(\beta)} + 3g(t) h_T^2 \nabla p = C_1$$

Since p is a continuous function and since $p(0, y, t; \beta) = 0$ and $p(\pi D, y, t; \beta) = 0$, we know that p has a maxima or minima (from previous works we know that it's a maxima). Then there exists a $x_* \in [0 \quad \pi D]$ such as $\nabla p(x_*, y, t; \beta) = 0$ and $\frac{\partial \nabla(p)}{\partial r(\beta)}(x_*, y, t; \beta) = 0$. So we get that $C_1 = 0$ and the previous equation turns into

$$\nabla\left(\frac{\partial p}{\partial r_S(\beta)} \right) = -\frac{3g(t)}{h_T} \nabla(p) \qquad \textbf{(2.26)}$$

If we repeat the same for the roughness of the bearing we get that

$$\nabla\left(\frac{\partial p}{\partial r_B(\beta)} \right) = -\frac{3g(t)}{h_T} \nabla(p) \qquad \textbf{(2.27)}$$

2.5.3. Final Form of the Stochastic Reynolds Equation

Using Equations (2.26) and (2.27) and Stein's Lemma for negative powers, and categorizing the terms in respect to the averages that appear, yields the following terms

$$T_1 = \nabla\left(\left(h^3 + 3\sigma^2 g^2(t)h\right)\nabla \mathrm{m}_p\right)$$

$$T_2 = -9\sigma^2 g^2(t)\nabla\left(\left(h^2 + \sigma^2 g^2(t)\right)\mathbb{E}^{\beta}\left[\frac{\nabla p}{h_T}\right]\right)$$

$$T_3 = 9\sigma^2 g^2(t)\nabla\left(h^2\mathbb{E}^{\beta}\left[\frac{\nabla p}{h_T}\right] - h\nabla \mathrm{m}_p\right)$$

$$T_4 = -3\sigma^2 g^2(t)\nabla\left(h^2\mathbb{E}^{\beta}\left[\frac{\nabla p}{h_T}\right] - 4\sigma^2 g^2(t)\mathbb{E}^{\beta}\left[\frac{\nabla p}{h_T}\right] - h\nabla \mathrm{m}_p\right)$$

Combining the previous terms and inserting them into Equation (2.23) yields Equation (2.28).

$$\left(\nabla\left(\left(h^3 - 3\sigma^2 g^2(t)h\right)\nabla \mathrm{m}_p\right) + 3\sigma^2 g^2(t)\nabla\left(\left(\sigma^2 g^2(t) - h^2\right)\mathbb{E}^{\beta}\left[\frac{\nabla p}{h_T}\right]\right)\right) = 12\eta\frac{\partial h}{\partial t} + 6U\eta\frac{\partial h}{\partial x} \quad \textbf{(2.28)}$$

Equation (2.28) is exact, but yet not closed. In order to get the final form of the Stochastic Reynolds Equation we make the assumption that $\mathbb{E}^{\beta}\left[\frac{\nabla p}{h_T}\right] = \mathbb{F}_0(h,\sigma)\cdot\mathbb{E}^{\beta}[\nabla p]$, which yields equation (2.29).

$$\left(\nabla\left(\left(h^3 - 3\sigma^2 g^2(t)h^2\mathbb{F}_0 - 3\sigma^2 g^2(t)h + 3\sigma^4 g^4(t)\mathbb{F}_0\right)\nabla \mathrm{m}_p\right)\right) = 12\eta\frac{\partial h}{\partial t} + 6U\eta\frac{\partial h}{\partial x} \quad \textbf{(2.29)}$$

The coefficient $\mathbb{F}_0(h,\sigma)$, as well as the coefficients $\mathbb{F}_1(h,\sigma)$ and $\mathbb{F}_2(h,\sigma)$, are calculated numerically in Appendix B and C respectively. From this point on we will denote $\mathbb{F}_n(h,\sigma) \equiv \mathbb{F}_n$ for simplicity in equations.

Remark 2.2: ***Equation (2.29) is the Stochastic Reynolds Equation that we propose. We can see that by eliminating the terms including the standard deviation of the roughness, taking*** $\sigma = 0$***, yields the Deterministic Reynolds Equation*** $\nabla\left(h^3\nabla \mathrm{m}_p\right) = 12\eta\frac{\partial h}{\partial t} + 6U\eta\frac{\partial h}{\partial x}$***, where*** $\nabla \mathrm{m}_p = \nabla p$**.**

2.5.4. Boundary Conditions

Based on [9]

In order to solve the proposed Reynolds Equation, appropriate boundary conditions for the pressure distribution must be set. The most notable of them are

- The Full Sommerfeld Boundary Condition: This condition assumes that the pressure is equal to zero at the edges of the unwrapped journal bearing geometry, meaning that $p(0,y,t;\beta) = 0$ and $p(\pi D,y,t;\beta) = 0$.

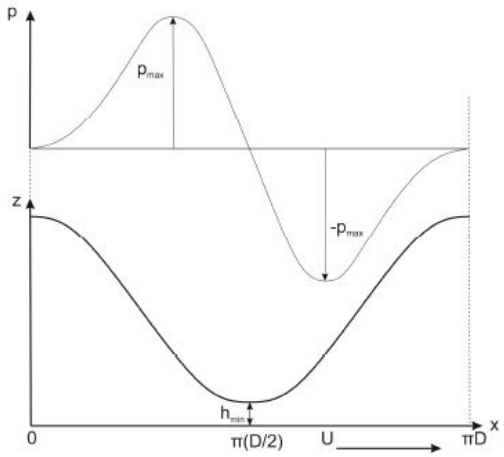

Figure 2.8: Solution of the Reynolds Equation with the Full Sommerfeld Boundary Condition

- The Half Sommerfeld Boundary Condition: This condition neglects negative pressures in the divergent region of the bearing, by setting them equal to zero, meaning that $p(0,y,t;\beta) = 0$, $p(\pi D,y,t;\beta) = 0$ and $p(x,y,t;\beta) = 0 \qquad x \in \left(\frac{\pi D}{2}, \pi D\right)$.

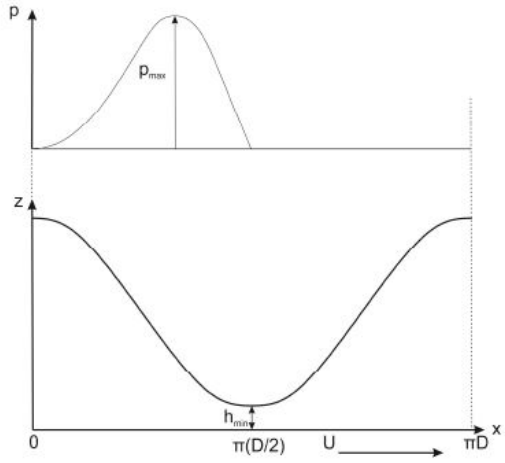

Figure 2.9: Solution of the Reynolds Equation with the Half Sommerfeld Boundary Condition

- Reynolds Boundary Condition: Reynolds suggested that no negative pressures can be sustained by the lubricant film in the diverging region, and that at the boundary between zero and non-zero pressure the following condition should apply $p = \frac{\partial p}{\partial x} = 0$. The Reynolds boundary condition gives more accurate results in comparison to the Full and Half Sommerfeld conditions, and it is used for the pressure calculations of the present work.

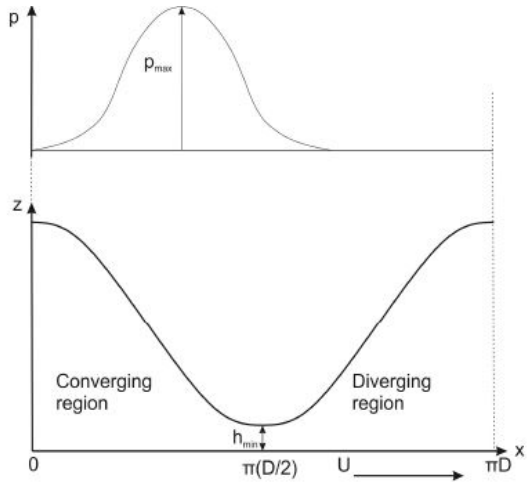

Figure 2.10: Solution of the Reynolds Equation with the Reynolds Boundary Condition

2.6. Design and Performance Parameters

2.6.1. Load Carrying Capacity

The total hydrodynamic load supporting the rotating shaft can be found by integrating the pressure exerted on the shaft surface. This load can be resolved into two mutually perpendicular components, one acting on the $z'z$ axis and one on the $x'x$ axis. The total force component projected along the line of centers is expressed by equations (2.30) and (2.31).

$$W_z = \iint_{\tilde{S}_S} p \cdot d\tilde{S}_S = \int_0^{2\pi}\int_0^L p \cdot \sin\left(\varphi + \omega - \frac{\pi}{2}\right)\left(R_S + g(t) r_S(\beta)\right) dy d\omega \quad \textbf{(2.30)}$$

$$W_x = \iint_{\tilde{S}_S} p \cdot d\tilde{S}_S = \int_0^{2\pi}\int_0^L p \cdot \cos\left(\varphi + \omega - \frac{\pi}{2}\right)\left(R_S + g(t) r_S(\beta)\right) dy d\omega \quad \textbf{(2.31)}$$

Averaging the previous equations yields equations (2.32) and (2.33).

$$\mathrm{m}_{W_z(\beta)} = \mathbb{E}^{\beta}\left[W_z(\beta)\right] = \int_0^{2\pi}\int_0^L \left(\mathrm{m}_p R_S + \alpha_2^2 \sigma^2 g(t) \mathbb{E}^{\beta}\left[\frac{\partial p}{\partial r_S(\beta)}\right]\right) \cdot \sin\left(\varphi + \omega - \frac{\pi}{2}\right) dy d\omega \quad \textbf{(2.32)}$$

$$\mathrm{m}_{W_x(\beta)} = \mathbb{E}^{\beta}\left[W_x(\beta)\right] = \int_0^{2\pi}\int_0^L \left(\mathrm{m}_p R_S + \alpha_2^2 \sigma^2 g(t) \mathbb{E}^{\beta}\left[\frac{\partial p}{\partial r_S(\beta)}\right]\right) \cdot \cos\left(\varphi + \omega - \frac{\pi}{2}\right) dy d\omega \quad \textbf{(2.33)}$$

The total load capacity W is given by equation (2.34)

$$\mathrm{m}_{W(\beta)} = \sqrt{\mathrm{m}_{W_z(\beta)}^2 + \mathrm{m}_{W_x(\beta)}^2} \quad \textbf{(2.34)}$$

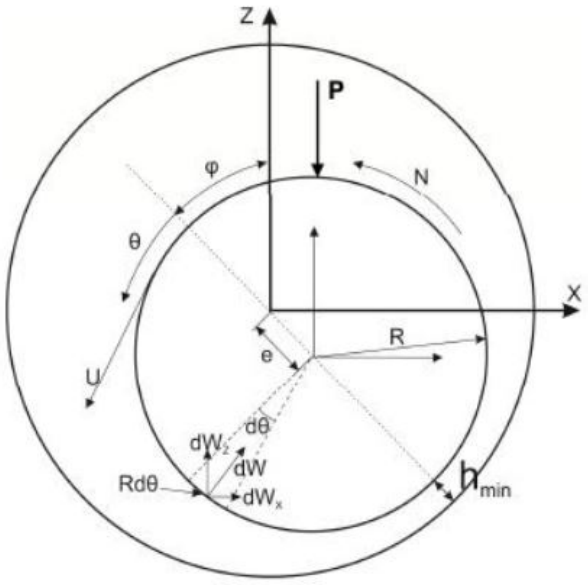

Figure 2.11: Hydrodynamic Load Components in a Journal Bearing

2.6.2. Friction Force

The friction force can be obtained by integrating the x component of the shear stress over the bearing area

$$F = \iint_{\tilde{S}_B} \tau_x \cdot d\tilde{S}_B = \iint_{\tilde{S}_B} \eta \frac{du}{dz} \cdot d\tilde{S}_B$$

If we expand the previous equation we get that

$$F = \int_0^{2\pi} \int_0^L \left(\frac{2z - h_T}{2\left(R_B + g(t) r_B(\theta)\right)} \frac{\partial p}{\partial \omega} + \frac{\eta U}{h_T} \right) \left(R_B + g(t) r_B(\theta)\right) dy d\omega$$

or else

$$F = \int_0^{2\pi} \int_0^L \frac{2z - h_T}{2} \frac{\partial p}{\partial \omega} dy d\omega + \int_0^{2\pi} \int_0^L \frac{\eta U}{h_T} \left(R_B + g(t) r_B(\theta)\right) dy d\omega \qquad \textbf{(2.35)}$$

Averaging equation (2.35) and applying Stein's Lemma, yields equation (2.36)

$$\mathrm{m}_F = \int_0^{2\pi} \int_0^L \left(\left(\frac{2z - h + 3\sigma^2 g^2(t) \mathbb{F}_0}{2} \right) \frac{\partial \mathrm{m}_P}{\partial x} + \eta U \mathbb{F}_1 - \frac{\eta U \sigma_B^2 g^2(t)}{R_B} \mathbb{F}_2 \right) dy dx \qquad \textbf{(2.36)}$$

2.6.3. Friction Coefficient

The friction coefficients μ can be calculated from equation (2.37), where m_F is the mean friction force and m_W the mean total load of the bearing.

$$\mu = \frac{\mathrm{m}_F}{\mathrm{m}_W} \qquad \textbf{(2.37)}$$

Since $\mathrm{m}_F \equiv \mathrm{m}_F(\alpha_1)$ and $\mathrm{m}_W \equiv \mathrm{m}_W(\alpha_2)$, then we know that the friction coefficient is a function of the roughness coefficients, thus $\mu \equiv \mu(a_1, \alpha_2)$. Assigning different values to the coefficients, under the restriction that $\alpha_1^2 + \alpha_2^2 = 1$, gives us different values of the friction coefficient. The optimum operating point is the point where we have $\max\{\mathrm{m}_W\}$ and $\min\{\mathrm{m}_F\}$. That point is equal to the optimization process of minimizing the friction coefficient $\min\{\mu\}$.

2.6.4. Inlet and Outlet Flow Rates

For normal bearing operation, the lubricant must be supplied to the bearing at the same rate as that of the lubricant leakage. Otherwise lubricant starvation will occur, which will generally lead to smaller values of minimum film thickness and higher values of oil temperature. The inlet and outlet rate per unit length can be calculated by

$$q_{in} = \int_0^{h_T} u dz$$

$$q_{out} = \int_0^{h_T} v dz$$

By using equations (2.8) and (2.19) for the components u and v of the velocity and the initial conditions we get that

$$q_{in} = -\frac{h_T^3}{12\eta}\frac{\partial p}{\partial x} + U\frac{h_T}{2} \quad \textbf{(2.38)}$$

$$q_{out} = -\frac{h_T^3}{12\eta}\frac{\partial p}{\partial y} \quad \textbf{(2.39)}$$

The lubricant inflow and lubricant side leakage can be calculated by the integrations given by equations (2.40) and (2.41) respectively

$$Q_{in} = \int_0^L q_{in}\Big|_{x=0} dy \quad \textbf{(2.40)}$$

$$Q_{out} = \int_0^{2\pi} q_{out}\Big|_{y=0}\left(R_B + g(t)r_B(\beta)\right)dx + \int_0^{2\pi} q_{out}\Big|_{y=L}\left(R_B + g(t)r_B(\beta)\right)dx \quad \textbf{(2.41)}$$

By averaging equations (2.40) and (2.41), and following the same methodology, we get equations (2.42) and (2.43):

$$\mathsf{m}_{in} = -\frac{1}{12\eta}\int_0^L \left(h^3 - 3\sigma^2 g^2(t)h^2\mathbb{F}_0 - 3\sigma^2 g^2(t)h + 3\sigma^4 g^4(t)\mathbb{F}_0\right)\frac{\partial \mathsf{m}_p}{\partial x}\Big|_{x=0} dy$$

$$\mathsf{m}_{out} = -\frac{1}{12\eta}\int_0^{2\pi}\left(\begin{array}{l}\left(R_B - 6\sigma_B^2 g^2(t)\mathbb{F}_1\right)h^3 - 3R_B\sigma^2 g^2(t)h^2\mathbb{F}_1 \\ -3\sigma^2 g^2(t)\left(R_B - 6\sigma_B^2 g^2(t)\mathbb{F}_1\right)h + 3R_B\sigma^4 g^4(t)\mathbb{F}_1\end{array}\right)\frac{\partial \mathsf{m}_p}{\partial y}\Big|_{y=0}^{y=L} d\theta$$

For normal bearing operation, lubricant must be supplied to the bearing at the same rate as that of the lubricant leakage; otherwise lubricant starvation will occur, leading to smaller values of minimum film thickness and higher values of oil temperature

2.6.5. Sommerfeld Number

Sommerfeld number is a non - dimensional parameter that comprises both design and operation elements. It characterizes the performance of the bearing and is used to compare similar bearings in different operational conditions or different bearing designs for a precise operation. Sommerfeld number can be calculated according to the following equation

$$S = \frac{\eta NDL}{W}\left(\frac{R}{c}\right)^2 \qquad \textbf{(2.42)}$$

where c: Bearing clearance

D: Bearing diameter

L: Bearing length

N: Shaft rotational speed

R: Bearing radius

W: Total hydrodynamic force

η: Fluid dynamic viscosity

Sommerfeld number is an important quantity in hydrodynamic lubrication analysis; proper values of Sommerfeld number assure that the shaft is rotating on a sufficient fluid film, thus avoiding direct contact with the bearing.

2.6.6. Advanced Film Thickness Geometry

Based on [25]

The area between the rotating shaft and the bearing housing, filled with lubricant oil. will be geometrically modeled based on several parameters. Those parameters can either be the constant parameters of the system $(L\,,\,R\,,\,c)$ or their represented variables of the system $(\theta\,,\,e\,,\,\varphi)$. It is evident that the film thickness h is variable and has to be calculated at every time step of the solution, before solving the Reynolds Equation. Assuming that inertia effects in the film area are neglected, the flow is laminar, the fluid is Newtonian and incompressible and that the density, the heat and thermal conductivity are constants, the film thickness geometry for a journal bearing is given by equation (2.43).

$$h = h_N + h_E + h_T + h_M \tag{2.43}$$

where h_N: the nominal part of the film thickness, given by (2.4)

h_E: the elastic deformation of the bearing housing due to hydrodynamic pressure

h_{TH}: the thermal deformation due to thermal expansion of the shaft and the bearing housing

h_M: the misalignment of the shaft and bearing housing

The elastic deformation part of the film thickness occurs due to the hydrodynamic pressures applied on the housing of the bearing, assuming that the shaft is rigid. Since marine bearings are stiff structures, elastic deformations will generally be small. So, in the present thesis, we can ignore the elastic deformation by taking $h_E = 0$.

The modification of the thermal deformation part of the film thickness has two origins; the thermal expansion of the shaft, which leads to increased diameter, thus affecting clearance, and the corresponding deformation of the bearing housing, due to uneven temperature distribution in the bearing solid domain. In general, thermal deformations become critical in applications characterized by high values of rotational speed and/or high loads. Marine shaft bearings are generally operated at very low speeds (below 120 RPM), and eccentricity values are rarely above 0.6-0.7. Therefore, the part of thermal deformation in the formula for film thickness can be ignored, thus $h_{TH} = 0$.

Under ideal shaft alignment conditions, the bearing and the shaft centerlines are parallel. In this case, bearing misalignment is defined by the angle between the centerlines of the two components. Usually though misalignment values are not zero due to improper shaft alignment, excessive loading or other operational purposes. Misalignment angles can be resolved into two perpendicular angles, one for each one of the axes of the coordinate system. Lateral misalignment angles describe shaft rotations about the vertical axis and vertical misalignment angles describe rotations of the shaft about the horizontal axis. Taking the previous into consideration, and inserting them into equation (2.43), yield the final equation (2.44) for the film thickness

$$h(\theta\,,\,z) = c\cdot\left(1 + e\cdot\cos(\theta)\right) + z\cdot\left(\psi_y\cdot\cos(\varphi+\theta) + \psi_x\cdot\sin(\varphi+\theta)\right) \tag{2.44}$$

3. Numerical Solution

3.1. Solution Algorithm

The goal of the current study is to implement an algorithm capable of solving the problem of hydrodynamic lubrication for the main bearings of internal combustion engines in ships, which have roughness. Several algorithms have been developed to solve problems concerning hydrodynamic lubrication. In this current approach, we will solve the Reynolds Equation using an in-house algorithm developed in the section of Marine Engineering of NTUA, first introduced by Raptis[26]. Some modifications were made, to introduce the new terms for the Stochastic Reynolds Equation.

At the beginning of the algorithm, all the necessary geometric details for the bearing are read via a input file; the bearing length L, diameter D, clearance c, rotational speed N and viscosity η. This file includes the solver parameters - grid points, solver type, convergence criteria - as well as the applied loads in the bearing P_X and P_Z. Also, an initial assumption is made for the eccentricity e_0 and attitude angle φ_0.

After reading the initial parameters, the algorithm discretizes the bearing in its unwrapped form into small divisions. Then, the film thickness geometry is calculated using equation (2.44), the Deterministic Reynolds Equation is solved numerically according to the Gauss - Seidel iterative method, and the pressure field is calculated. The hydrodynamic force components are then calculated, by integrating the pressure field on the shaft surface. If the initial assumptions of eccentricity and attitude angle are correct, then the equilibrium is attained and the algorithm ends. If not, new eccentricity and attitude angle values are estimated, using a Newton - Raphson method for two variables. At the end of the whole process, the bearings operational parameters are calculated and printed out on an output file.

A detailed description of the algorithm is presented in Figure (3.1), the additions or modifications to the initial algorithm include:

1. The film thickness is calculated using equation (2.44)
2. The solution of the Reynolds Equation is performed using Gauss - Seidel numerical method
3. The hydrodynamic components are calculated by equations (2.33) and (2.34). The integrations were made using Simpson's rule.
4. The inlet and leakage flow rates of the lubricant are calculated by equations (2.41) and (2.42). The integrations were made using Simpson's rule.
5. The friction force is calculated by equation (2.37) and the friction coefficient by equation (2.38). The integrations were made using Simpson's rule.

1-5 are marked in the respective sequence shown in Figure (3.1).

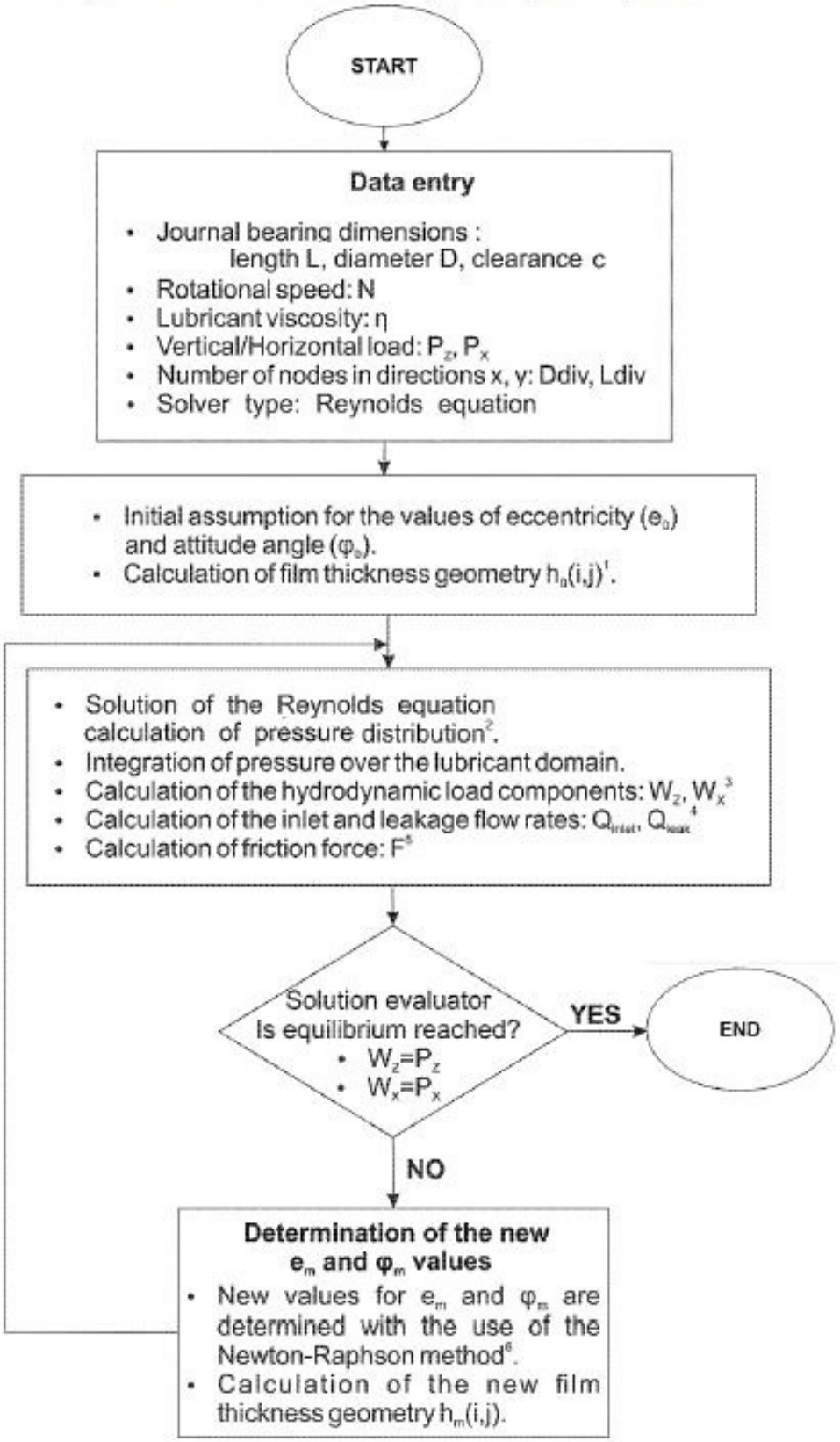

Figure3.1: Reynolds Equation - Solution Algorithm

3.2. The Finite Difference Method (FDM)

The journal bearing geometry is studied under its unwrapped domain. This unwrapped bearing is discretized by a finite element grid of L_{div} points in the $y'y$ axis and D_{div} points in the $x'x$. The L_{div} points represent the number of points alongside the length L of the bearing, while the D_{div} alongside the diameter. The unwrapped journal bearing geometry is presented in figure (3.2).

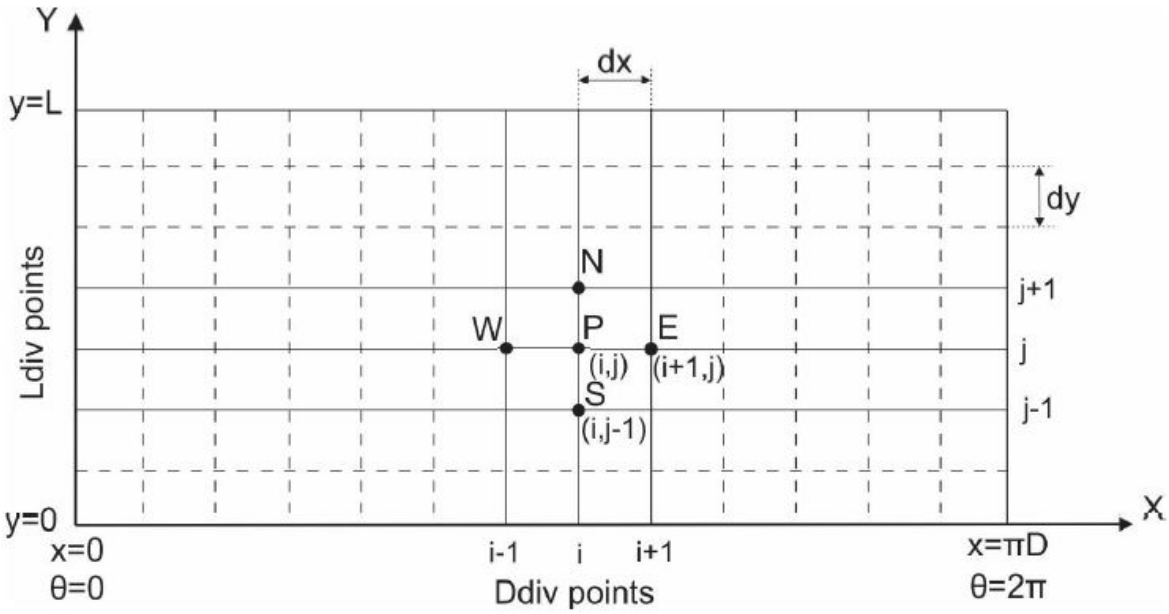

Figure 3.2: Unwrapped journal bearing geometry

In the previous figure, each point of the grid is identified by the coupled number $(i\ ,\ j)$, having four neighboring points - except for the boundary nodes. For this unwrapped journal bearing we know that

$$dx = \frac{\pi D}{D_{div}}$$

$$dy = \frac{L}{L_{div}}$$

$$x(i) = i \cdot dx$$

$$y(j) = j \cdot dy$$

$$\theta(i) = \frac{x(i)}{R} \cdot dy$$

The Reynolds Equation can be numerically solved over the lubricant domain with the use of the Finite Difference Method (FDM). The first step is to replace the derivatives of the Reynolds Equation with algebraic difference quotients which come for the Taylor series expansion

$$f(i+1,j) = f(i,j) + \left.\frac{\partial f(i,j)}{\partial x}\right|_{i,j} + \frac{\Delta x^2}{2!}\left.\frac{\partial^2 f(i,j)}{\partial x^2}\right|_{i,j} + \frac{\Delta x^3}{3!}\left.\frac{\partial^3 f(i,j)}{\partial x^3}\right|_{i,j} + \ldots$$

$$f(i-1,j) = f(i,j) - \left.\frac{\partial f(i,j)}{\partial x}\right|_{i,j} + \frac{\Delta x^2}{2!}\left.\frac{\partial^2 f(i,j)}{\partial x^2}\right|_{i,j} - \frac{\Delta x^3}{3!}\left.\frac{\partial^3 f(i,j)}{\partial x^3}\right|_{i,j} + \ldots$$

For small Δx, the terms of order $n \geq 2$ can be neglected and the finite central difference quotients for the first and second derivative can be written in the following way, achieving second order accuracy:

$$\left.\frac{\partial f(i,j)}{\partial x}\right|_{i,j} = \frac{f(i+1,j) - f(i-1,j)}{2\Delta x}$$

$$\left.\frac{\partial^2 f(i,j)}{\partial x^2}\right|_{i,j} = \frac{f(i+1,j) - 2f(i,j) + f(i-1,j)}{\Delta x^2}$$

3.2.1. Solution for the Deterministic Reynolds Equation

The Deterministic Reynolds Equation to be treated is given by equation (2.28) by setting equal to zero the terms containing the standard deviation of the roughness. This equation is listed below on equation (3.1)

$$\overbrace{\frac{\partial}{\partial x}\left(h^3\frac{\partial p}{\partial x}\right)}^{T_1}+\overbrace{h^3\frac{\partial^2 p}{\partial x^2}}^{T_2}+\underbrace{\frac{\partial}{\partial y}\left(h^3\frac{\partial p}{\partial y}\right)}_{T_3}+\underbrace{h^3\frac{\partial^2 p}{\partial y^2}}_{T_4}=\overbrace{12\eta\frac{\partial h}{\partial t}}^{T_5}+\overbrace{6U\eta\frac{\partial h}{\partial x}}^{T_6} \quad \textbf{(3.1)}$$

The terms that need to be calculated via the finite difference method are denoted on the equation. For those terms we know that

$$T_1 = \frac{h^3(i+1,j)-h^3(i-1,j)}{x(i+1)-x(i-1)}\cdot\frac{p(i+1,j)-p(i-1,j)}{x(i+1)-x(i-1)}$$

$$T_2 = h^3(i,j)\cdot\frac{p(i+1,j)-2p(i,j)+p(i-1,j)}{\left(x(i+1)-x(i)\right)\left(x(i)-x(i-1)\right)}$$

$$T_3 = \frac{h^3(i,j+1)-h^3(i,j-1)}{y(j+1)-y(j-1)}\cdot\frac{p(i,j+1)-p(i,j-1)}{y(j+1)-y(j-1)}$$

$$T_4 = h^3(i,j)\cdot\frac{p(i,j+1)-2p(i,j)+p(i,j-1)}{\left(y(j+1)-y(j)\right)\left(y(j)-y(j-1)\right)}$$

$$T_5 = 12\eta\cdot\frac{3h(i,j)\big|_m-4h(i,j)\big|_{m-1}+h(i,j)\big|_{m-2}}{2\Delta t}$$

$$T_6 = 6U\eta\frac{h(i+1,j)-h(i-1,j)}{x(i+1)-x(i-1)}$$

The pressure of the deterministic Reynolds Equation at the node $(i\,,\,j)$ comes from the solution of equation (3.2)

$$p(i,j) = \frac{G(i,j)-A(i,j)\cdot p(i+1,j)-B(i,j)\cdot p(i-1,j)-C(i,j)\cdot p(i,j+1)-D(i,j)\cdot p(i,j-1)}{E(i,j)} \quad \textbf{(3.2)}$$

where

$$A(i,j) = \frac{h^3(i+1,j)-h^3(i-1,j)}{\left(x(i+1)-x(i-1)\right)^2}+\frac{h^3(i,j)}{\left(x(i+1)-x(i)\right)\left(x(i)-x(i-1)\right)}$$

$$B(i,j) = -\frac{h^3(i+1,j) - h^3(i-1,j)}{\left(x(i+1) - x(i-1)\right)^2} + \frac{h^3(i,j)}{\left(x(i+1) - x(i)\right)\left(x(i) - x(i-1)\right)}$$

$$C(i,j) = \frac{h^3(i,j+1) - h^3(i,j-1)}{\left(y(j+1) - y(j-1)\right)^2} + \frac{h^3(i,j)}{\left(y(j+1) - y(j)\right)\left(y(j) - y(j-1)\right)}$$

$$D(i,j) = -\frac{h^3(i,j+1) - h^3(i,j-1)}{\left(y(j+1) - y(j-1)\right)^2} + \frac{h^3(i,j)}{\left(y(j+1) - y(j)\right)\left(y(j) - y(j-1)\right)}$$

$$E(i,j) = -2\frac{h^3(i,j)}{\left(x(i+1) - x(i)\right)\left(x(i) - x(i-1)\right)} - 2\frac{h^3(i,j)}{\left(y(j+1) - y(j)\right)\left(y(j) - y(j-1)\right)}$$

$$G(i,j) = 12\eta \cdot \frac{3h(i,j)\big|_m - 4h(i,j)\big|_{m-1} + h(i,j)\big|_{m-2}}{2\Delta t} + 6U\eta\frac{h(i+1,j) - h(i-1,j)}{x(i+1) - x(i-1)}$$

3.2.2. Solution for Christensen's Approach of the Reynolds Equation

Christensen's Approach of Reynolds Equation is given by equation (2.24) by setting equal to zero the terms containing any derivative of the pressure in respect to the roughness. This equation is listed below on equation (3.3)

$$\left(\begin{array}{l} \overbrace{\dfrac{\partial h^3}{\partial x}\dfrac{\partial \mathrm{m}_p}{\partial x}}^{T_1} + \overbrace{3\sigma^2 g^2(t)\dfrac{\partial h}{\partial x}\left(\dfrac{\partial \mathrm{m}_p}{\partial x}\right)}^{T_2} + \overbrace{\left(h^3 + 3\sigma^2 g^2(t)h\right)\dfrac{\partial^2 \mathrm{m}_p}{\partial x^2}}^{T_3} + \\ \underbrace{\dfrac{\partial h^3}{\partial y}\dfrac{\partial \mathrm{m}_p}{\partial y}}_{T_4} + \underbrace{3\sigma^2 g^2(t)\dfrac{\partial h}{\partial y}\left(\dfrac{\partial \mathrm{m}_p}{\partial y}\right)}_{T_5} + \underbrace{\left(h^3 + 3\sigma^2 g^2(t)h\right)\dfrac{\partial^2 \mathrm{m}_p}{\partial y^2}}_{T_6} \end{array}\right) = \overbrace{12\eta\frac{\partial h}{\partial t}}^{T_7} + \overbrace{6U\eta\frac{\partial h}{\partial x}}^{T_8} \qquad \textbf{(3.3)}$$

The terms that need to be calculated via the finite difference method are denoted on the equation. For those terms we know that

$$T_1 = \frac{h^3(i+1,j) - h^3(i-1,j)}{x(i+1) - x(i-1)} \cdot \frac{\mathrm{m}_p(i+1,j) - \mathrm{m}_p(i-1,j)}{x(i+1) - x(i-1)}$$

$$T_2 = 3\sigma^2 g^2(t)\frac{h(i+1,j) - h(i-1,j)}{x(i+1) - x(i-1)} \cdot \frac{\mathrm{m}_p(i+1,j) - \mathrm{m}_p(i-1,j)}{x(i+1) - x(i-1)}$$

$$T_3 = \left(h^3(i,j) + 3\sigma^2 g^2(t)h(i,j)\right) \cdot \frac{\mathrm{m}_p(i+1,j) - 2\mathrm{m}_p(i,j) + \mathrm{m}_p(i-1,j)}{\left(x(i+1) - x(i)\right)\left(x(i) - x(i-1)\right)}$$

$$T_4 = \frac{h^3(i,j+1) - h^3(i,j-1)}{y(j+1) - y(j-1)} \cdot \frac{\mathrm{m}_p(i,j+1) - \mathrm{m}_p(i,j-1)}{y(j+1) - y(j-1)}$$

$$T_5 = 3\sigma^2 g^2(t)\frac{h(i,j+1) - h(i,j-1)}{y(j+1) - y(j-1)} \cdot \frac{\mathrm{m}_p(i,j+1) - \mathrm{m}_p(i,j-1)}{y(j+1) - y(j-1)}$$

$$T_6 = \left(h^3(i,j) + 3\sigma^2 g^2(t)h(i,j)\right) \cdot \frac{\mathrm{m}_p(i,j+1) - 2\mathrm{m}_p(i,j) + \mathrm{m}_p(i,j-1)}{\left(y(j+1) - y(j)\right)\left(y(j) - y(j-1)\right)}$$

$$T_7 = 12\eta \cdot \frac{3h(i,j)\big|_m - 4h(i,j)\big|_{m-1} + h(i,j)\big|_{m-2}}{2\Delta t}$$

$$T_8 = 6U\eta\frac{h(i+1,j) - h(i-1,j)}{x(i+1) - x(i-1)}$$

The pressure of Christensen's approach of the Reynolds Equation at the central node comes from the solution of equation (3.4)

$$\mathrm{m}_p(i,j) = \frac{G(i,j) - A\cdot\mathrm{m}_p(i+1,j) - B\cdot\mathrm{m}_p(i-1,j) - C\cdot\mathrm{m}_p(i,j+1) - D\cdot\mathrm{m}_p(i,j-1)}{E(i,j)} \qquad \textbf{(3.4)}$$

where

$$A(i,j) = \frac{h^3(i+1,j) - h^3(i-1,j)}{\left(x(i+1) - x(i-1)\right)^2} + 3\sigma^2 g^2(t)\frac{h(i+1,j) - h(i-1,j)}{\left(x(i+1) - x(i-1)\right)^2} + \frac{\left(h^3(i,j) + 3\sigma^2 g^2(t)h(i,j)\right)}{\left(x(i+1) - x(i)\right)\left(x(i) - x(i-1)\right)}$$

$$B(i,j) = -\frac{h^3(i+1,j) - h^3(i-1,j)}{\left(x(i+1) - x(i-1)\right)^2} - 3\sigma^2 g^2(t)\frac{h(i+1,j) - h(i-1,j)}{\left(x(i+1) - x(i-1)\right)^2} + \frac{\left(h^3(i,j) + 3\sigma^2 g^2(t)h(i,j)\right)}{\left(x(i+1) - x(i)\right)\left(x(i) - x(i-1)\right)}$$

$$C(i,j) = \frac{h^3(i,j+1) - h^3(i,j-1)}{\left(y(j+1) - y(j-1)\right)^2} + 3\sigma^2 g^2(t)\frac{h(i,j+1) - h(i,j-1)}{\left(y(j+1) - y(j-1)\right)^2} + \frac{\left(h^3(i,j) + 3\sigma^2 g^2(t)h(i,j)\right)}{\left(y(j+1) - y(j)\right)\left(y(j) - y(j-1)\right)}$$

$$D(i,j) = -\frac{h^3(i,j+1) - h^3(i,j-1)}{\left(y(j+1) - y(j-1)\right)^2} - 3\sigma^2 g^2(t)\frac{h(i,j+1) - h(i,j-1)}{\left(y(j+1) - y(j-1)\right)^2} + \frac{\left(h^3(i,j) + 3\sigma^2 g^2(t)h(i,j)\right)}{\left(y(j+1) - y(j)\right)\left(y(j) - y(j-1)\right)}$$

$$E(i,j) = -2\frac{\left(h^3(i,j) + 3\sigma^2 g^2(t)h(i,j)\right)}{\left(x(i+1) - x(i)\right)\left(x(i) - x(i-1)\right)} - 2\frac{\left(h^3(i,j) + 3\sigma^2 g^2(t)h(i,j)\right)}{\left(y(j+1) - y(j)\right)\left(y(j) - y(j-1)\right)}$$

$$G(i,j) = 12\eta\cdot\frac{3h(i,j)\big|_m - 4h(i,j)\big|_{m-1} + h(i,j)\big|_{m-2}}{2\Delta t} + 6U\eta\frac{h(i+1,j) - h(i-1,j)}{x(i+1) - x(i-1)}$$

3.2.3. Solution for Proposed Approach of the Reynolds Equation

The current proposal of Reynolds Equation is given by equation (2.24). This equation is listed below on equation (3.5)

$$\left(\begin{array}{l}
\overbrace{\frac{\partial h^3}{\partial x}\frac{\partial \mathrm{m}_p}{\partial x}}^{T_1} - \overbrace{3\sigma^2 g^2(t) h^2 \frac{\partial \mathbb{F}_0}{\partial x}\frac{\partial \mathrm{m}_p}{\partial x}}^{T_2} - \overbrace{3\sigma^2 g^2(t)\mathbb{F}_0 \frac{\partial h^2}{\partial x}\frac{\partial \mathrm{m}_p}{\partial x}}^{T_3} - \overbrace{3\sigma^2 g^2(t)\frac{\partial h}{\partial x}\frac{\partial \mathrm{m}_p}{\partial x}}^{T_4} \\
+ \overbrace{3\sigma^4 g^4(t)\frac{\partial \mathbb{F}_0}{\partial x}\frac{\partial \mathrm{m}_p}{\partial x}}^{T_5} + \overbrace{\left(h^3 - 3\sigma^2 g^2(t) h^2 \mathbb{F}_0 - 3\sigma^2 g^2(t) h + 3\sigma^4 g^4(t)\mathbb{F}_0\right)\frac{\partial^2 \mathrm{m}_p}{\partial x^2}}^{T_6} \\
+ \underbrace{\frac{\partial h^3}{\partial y}\frac{\partial \mathrm{m}_p}{\partial y}}_{T_7} - \underbrace{3\sigma^2 g^2(t) h^2 \frac{\partial \mathbb{F}_0}{\partial y}\frac{\partial \mathrm{m}_p}{\partial y}}_{T_8} - \underbrace{3\sigma^2 g^2(t)\mathbb{F}_0 \frac{\partial h^2}{\partial y}\frac{\partial \mathrm{m}_p}{\partial y}}_{T_9} - \underbrace{3\sigma^2 g^2(t)\frac{\partial h}{\partial y}\frac{\partial \mathrm{m}_p}{\partial y}}_{T_{10}} \\
+ \underbrace{3\sigma^4 g^4(t)\frac{\partial \mathbb{F}_0}{\partial y}\frac{\partial \mathrm{m}_p}{\partial y}}_{T_{11}} + \underbrace{\left(h^3 - 3\sigma^2 g^2(t) h^2 \mathbb{F}_0 - 3\sigma^2 g^2(t) h + 3\sigma^4 g^4(t)\mathbb{F}_0\right)\frac{\partial^2 \mathrm{m}_p}{\partial y^2}}_{T_{12}}
\end{array}\right) = \overbrace{12\eta\frac{\partial h}{\partial t}}^{T_{13}} + \overbrace{6U\eta\frac{\partial h}{\partial x}}^{T_{14}} \quad \textbf{(3.5)}$$

The terms that need to be calculated via the finite difference method are denoted on the equation. For those terms we know that

$$T_1 = \frac{h^3(i+1,j) - h^3(i-1,j)}{x(i+1) - x(i-1)} \cdot \frac{\mathrm{m}_p(i+1,j) - \mathrm{m}_p(i-1,j)}{x(i+1) - x(i-1)}$$

$$T_2 = -3\sigma^2 g^2(t) h^2(i,j) \frac{\mathbb{F}_0(i+1,j) - \mathbb{F}_0(i-1,j)}{x(i+1) - x(i-1)} \cdot \frac{\mathrm{m}_p(i+1,j) - \mathrm{m}_p(i-1,j)}{x(i+1) - x(i-1)}$$

$$T_3 = -3\sigma^2 g^2(t) \mathbb{F}_0(i,j) \frac{h^2(i+1,j) - h^2(i-1,j)}{x(i+1) - x(i-1)} \cdot \frac{\mathrm{m}_p(i+1,j) - \mathrm{m}_p(i-1,j)}{x(i+1) - x(i-1)}$$

$$T_4 = -3\sigma^2 g^2(t) \frac{h(i+1,j) - h(i-1,j)}{x(i+1) - x(i-1)} \cdot \frac{\mathrm{m}_p(i+1,j) - \mathrm{m}_p(i-1,j)}{x(i+1) - x(i-1)}$$

$$T_5 = 3\sigma^4 g^4(t) \frac{\mathbb{F}_0(i+1,j) - \mathbb{F}_0(i-1,j)}{x(i+1) - x(i-1)} \cdot \frac{\mathrm{m}_p(i+1,j) - \mathrm{m}_p(i-1,j)}{x(i+1) - x(i-1)}$$

$$T_6 = \left(\begin{array}{l} h^3(i,j) - 3\sigma^2 g^2(t) h^2(i,j)\mathbb{F}_0(i,j) \\ -3\sigma^2 g^2(t) h(i,j) + 3\sigma^4 g^4(t)\mathbb{F}_0(i,j) \end{array}\right) \cdot \frac{\mathrm{m}_p(i+1,j) - 2\mathrm{m}_p(i,j) + \mathrm{m}_p(i-1,j)}{\left(x(i+1) - x(i)\right)\left(x(i) - x(i-1)\right)}$$

$$T_7 = \frac{h^3(i,j+1) - h^3(i,j-1)}{y(j+1) - y(j-1)} \cdot \frac{\mathrm{m}_p(i,j+1) - \mathrm{m}_p(i,j-1)}{y(j+1) - y(j-1)}$$

$$T_8 = -3\sigma^2 g^2(t) h^2(i,j) \frac{\mathbb{F}_0(i,j+1) - \mathbb{F}_0(i,j-1)}{y(j+1) - y(j-1)} \cdot \frac{\mathrm{m}_p(i,j+1) - \mathrm{m}_p(i,j-1)}{y(j+1) - y(j-1)}$$

$$T_9 = -3\sigma^2 g^2(t) \mathbb{F}_0(i,j) \frac{h^2(i,j+1) - h^2(i,j-1)}{y(j+1) - y(j-1)} \cdot \frac{\mathrm{m}_p(i,j+1) - \mathrm{m}_p(i,j-1)}{y(j+1) - y(j-1)}$$

$$T_{10} = -3\sigma^2 g^2(t) \frac{h(i+1,j) - h(i-1,j)}{y(j+1) - y(j-1)} \cdot \frac{\mathrm{m}_p(i+1,j) - \mathrm{m}_p(i-1,j)}{y(j+1) - y(j-1)}$$

$$T_{11} = 3\sigma^4 g^4(t) \cdot \frac{\mathbb{F}_0(i+1,j) - \mathbb{F}_0(i-1,j)}{y(j+1) - y(j-1)} \cdot \frac{\mathrm{m}_p(i+1,j) - \mathrm{m}_p(i-1,j)}{y(j+1) - y(j-1)}$$

$$T_{12} = \begin{pmatrix} h^3(i,j) - 3\sigma^2 g^2(t) h^2(i,j) \mathbb{F}_0(i,j) \\ -3\sigma^2 g^2(t) h(i,j) + 3\sigma^4 g^4(t) \mathbb{F}_0(i,j) \end{pmatrix} \cdot \frac{\mathrm{m}_p(i,j+1) - 2\mathrm{m}_p(i,j) + \mathrm{m}_p(i,j-1)}{\big(y(j+1) - y(j)\big)\big(y(j) - y(j-1)\big)}$$

$$T_{13} = 12\eta \cdot \frac{3h(i,j)\big|_m - 4h(i,j)\big|_{m-1} + h(i,j)\big|_{m-2}}{2\Delta t}$$

$$T_{14} = 6U\eta \frac{h(i+1,j) - h(i-1,j)}{x(i+1) - x(i-1)}$$

The pressure of the proposed approach of the Reynolds Equation at the central node comes from the solution of equation (3.6)

$$\mathrm{m}_p(i,j) = \frac{G(i,j) - A \cdot \mathrm{m}_p(i+1,j) - B \cdot \mathrm{m}_p(i-1,j) - C \cdot \mathrm{m}_p(i,j+1) - D \cdot \mathrm{m}_p(i,j-1)}{E(i,j)} \quad \textbf{(3.6)}$$

where

$$\begin{aligned} A(i,j) = {} & \frac{h^3(i+1,j) - h^3(i-1,j)}{\big(x(i+1) - x(i-1)\big)^2} - 3\sigma^2 g^2(t) h^2(i,j) \frac{\mathbb{F}_0(i+1,j) - \mathbb{F}_0(i-1,j)}{\big(x(i+1) - x(i-1)\big)^2} \\ & - 3\sigma^2 g^2(t) \mathbb{F}_0(i,j) \frac{h^2(i+1,j) - h^2(i-1,j)}{\big(x(i+1) - x(i-1)\big)^2} - 3\sigma^2 g^2(t) \frac{h(i+1,j) - h(i-1,j)}{\big(x(i+1) - x(i-1)\big)^2} \\ & + 3\sigma^4 g^4(t) \cdot \frac{\mathbb{F}_0(i+1,j) - \mathbb{F}_0(i-1,j)}{\big(x(i+1) - x(i-1)\big)^2} \\ & + \frac{h^3(i,j) - 3\sigma^2 g^2(t) h^2(i,j) \mathbb{F}_0(i,j) - 3\sigma^2 g^2(t) h(i,j) + 3\sigma^4 g^4(t) \mathbb{F}_0(i,j)}{\big(x(i+1) - x(i)\big)\big(x(i) - x(i-1)\big)} \end{aligned}$$

$$B(i,j) = -\frac{h^3(i+1,j)-h^3(i-1,j)}{\left(x(i+1)-x(i-1)\right)^2} + 3\sigma^2 g^2(t)h^2(i,j)\frac{\mathbb{F}_0(i+1,j)-\mathbb{F}_0(i-1,j)}{\left(x(i+1)-x(i-1)\right)^2}$$
$$+ 3\sigma^2 g^2(t)\mathbb{F}_0(i,j)\frac{h^2(i+1,j)-h^2(i-1,j)}{\left(x(i+1)-x(i-1)\right)^2} + 3\sigma^2 g^2(t)\frac{h(i+1,j)-h(i-1,j)}{\left(x(i+1)-x(i-1)\right)^2}$$
$$- 3\sigma^4 g^4(t)\cdot\frac{\mathbb{F}_0(i+1,j)-\mathbb{F}_0(i-1,j)}{\left(x(i+1)-x(i-1)\right)^2}$$
$$+ \frac{h^3(i,j) - 3\sigma^2 g^2(t)h^2(i,j)\mathbb{F}_0(i,j) - 3\sigma^2 g^2(t)h(i,j) + 3\sigma^4 g^4(t)\mathbb{F}_0(i,j)}{\left(x(i+1)-x(i)\right)\left(x(i)-x(i-1)\right)}$$

$$C(i,j) = \frac{h^3(i,j+1)-h^3(i,j-1)}{\left(y(j+1)-y(j-1)\right)^2} - 3\sigma^2 g^2(t)h^2(i,j)\frac{\mathbb{F}_0(i,j+1)-\mathbb{F}_0(i,j-1)}{\left(y(j+1)-y(j-1)\right)^2}$$
$$- 3\sigma^2 g^2(t)\mathbb{F}_0(i,j)\frac{h^2(i,j+1)-h^2(i,j-1)}{\left(y(j+1)-y(j-1)\right)^2} - 3\sigma^2 g^2(t)\frac{h(i,j+1)-h(i,j-1)}{\left(y(j+1)-y(j-1)\right)^2}$$
$$+ 3\sigma^4 g^4(t)\cdot\frac{\mathbb{F}_0(i,j+1)-\mathbb{F}_0(i,j-1)}{\left(y(j+1)-y(j-1)\right)^2}$$
$$+ \frac{h^3(i,j) - 3\sigma^2 g^2(t)h^2(i,j)\mathbb{F}_0(i,j) - 3\sigma^2 g^2(t)h(i,j) + 3\sigma^4 g^4(t)\mathbb{F}_0(i,j)}{\left(y(j+1)-y(j)\right)\left(y(j)-y(j-1)\right)}$$

$$D(i,j) = -\frac{h^3(i,j+1)-h^3(i,j-1)}{\left(y(j+1)-y(j-1)\right)^2} + 3\sigma^2 g^2(t)h^2(i,j)\frac{\mathbb{F}_0(i,j+1)-\mathbb{F}_0(i,j-1)}{\left(y(j+1)-y(j-1)\right)^2}$$
$$+ 3\sigma^2 g^2(t)\mathbb{F}_0(i,j)\frac{h^2(i,j+1)-h^2(i,j-1)}{\left(y(j+1)-y(j-1)\right)^2} + 3\sigma^2 g^2(t)\frac{h(i,j+1)-h(i,j-1)}{\left(y(j+1)-y(j-1)\right)^2}$$
$$- 3\sigma^4 g^4(t)\cdot\frac{\mathbb{F}_0(i,j+1)-\mathbb{F}_0(i,j-1)}{\left(y(j+1)-y(j-1)\right)^2}$$
$$+ \frac{h^3(i,j) - 3\sigma^2 g^2(t)h^2(i,j)\mathbb{F}_0(i,j) - 3\sigma^2 g^2(t)h(i,j) + 3\sigma^4 g^4(t)\mathbb{F}_0(i,j)}{\left(y(j+1)-y(j)\right)\left(y(j)-y(j-1)\right)}$$

$$E(i,j) = -2\frac{h^3(i,j) - 3\sigma^2 g^2(t)h^2(i,j)\mathbb{F}_0(i,j) - 3\sigma^2 g^2(t)h(i,j) + 3\sigma^4 g^4(t)\mathbb{F}_0(i,j)}{\left(x(i+1)-x(i)\right)\left(x(i)-x(i-1)\right)}$$
$$- 2\frac{h^3(i,j) - 3\sigma^2 g^2(t)h^2(i,j)\mathbb{F}_0(i,j) - 3\sigma^2 g^2(t)h(i,j) + 3\sigma^4 g^4(t)\mathbb{F}_0(i,j)}{\left(y(j+1)-y(j)\right)\left(y(j)-y(j-1)\right)}$$

$$G(i,j) = 12\eta\cdot\frac{3h(i,j)\big|_m - 4h(i,j)\big|_{m-1} + h(i,j)\big|_{m-2}}{2\Delta t} + 6U\eta\frac{h(i+1,j)-h(i-1,j)}{x(i+1)-x(i-1)}$$

4. Validation of Modeling

The proposed approach solution for the Reynolds Equation will be validated against the results published in literature findings, [4], [12], [27] and [28]. This validation will be carried out for both a slider and a journal bearing. For each bearing, a comparison between the results of the proposed approach for a rough bearing and the results of a rough bearing under Christensen's approach will be held. The validation of the proposed approach will be performed, for both cases, in two separate steps.

Firstly, we will run the case of a slider bearing. The validation will be held for a constant geometric profile and roughness profile, and then the results will be generalized for different slider bearings geometry and surface roughness. Main findings and comparison between the rough and the smooth bearings will be summarized according to the operational parameter.

The second step is performing the previous validation for the case of a journal bearing. The results are compared with literature findings for each one of the operational parameters. Also, an approach to see the extension of the results from the slider bearing to a journal bearing is performed.

For each case, the basic geometric and operational parameters of the bearing are presented, alongside with the main equations for the calculation of the bearing parameters, the derivation of which is performed in Chapter 2. The Reynolds Equation is solved using the Finite Difference method, via the algorithm mentioned in Chapter 3.

In the figures presented in the current chapter, Christensen’s results are marked with a dashed line, while the proposed approach’s results are marked with solid lines. The results for a smooth bearing are denoted with a blue straight line.

4.1. Slider Bearing

Validation based on[4], [9] and[12]

The present solution algorithm was validated by comparing the calculated operational characteristics of the bearing with the expected results of literature. A comparison with Christensen's approach of the Reynolds Equation is also presented. In the case of the slider bearing, we will use two dimensionless ratios; one for the standard deviation and one for the film geometry, denoted as r and k respectively. The ratios are given by equations (4.1) and (4.2).

$$r = \frac{\sigma}{h_{\min}} \tag{4.1}$$

$$k = \frac{h_{\max} - h_{\min}}{h_{\min}} \tag{4.2}$$

The slider bearing used in the calculations for the validation has the following geometric and operating parameters:

- Slider Length $L = 0.05 \ \ m$
- Film thickness $h_{\min} = 50 \ \ \mu m$
- Dynamic viscosity $\eta = 0.037 \ \ Pa \cdot sec$
- Sliding speed $U = 12 \ \ m/sec$

In general, literature findings suggest that an increase of the pressure profile, the load carrying capacity and the friction force is anticipated, while the friction coefficient is expected to decrease. Each one of the design and performance parameters of the slider bearing is calculated for the case of smooth bearing, meaning no roughness, and for a rough bearing. The rough bearing consists of two parameters; the roughness profile of the upper part and the roughness profile of the lower part, which is the moving part of the bearing. In the case of rough bearing, the parameters are calculated for both Christensen's approach and proposed approach of the Reynolds Equation, and a comparison between the approaches is held. Since each one of the approaches is based on different assumptions, we expect the equations used for calculating the operational characteristics to differ. Thus the equations used for the calculations are listed below for each one of the approaches.

For a Smooth Slider Bearing

$$W = \int_0^B p dx$$

$$F = \int_0^B \left(\frac{h}{2} \frac{\partial p}{\partial x} + \frac{\eta U}{h} \right) dx$$

$$\mu = \frac{F}{W}$$

For a Rough Slider Bearing (Christensen's Approach)

$$\mathsf{m}_W = \mathbb{E}^{\beta}\left[W(\beta)\right] = \int_0^B \mathsf{m}_p dx$$

$$\mathsf{m}_F = \mathbb{E}^{\beta}\left[F(\beta)\right] = \int_0^B \left(\frac{h}{2}\frac{\partial \mathsf{m}_P}{\partial x} + \eta U R_B \mathbb{F}_1\right) dx$$

$$\mu = \frac{\mathsf{m}_F}{\mathsf{m}_W}$$

For a Rough Slider Bearing (Proposed Approach)

$$\mathsf{m}_W = \mathbb{E}^{\beta}\left[W(\beta)\right] = \int_0^B \mathsf{m}_p dx$$

$$\mathsf{m}_F = \mathbb{E}^{\beta}\left[F(\beta)\right] = \int_0^B \left(\frac{h - 3\sigma^2 g^2(t)\mathbb{F}_0}{2}\frac{\partial \mathsf{m}_P}{\partial x} + \eta U \mathbb{F}_1\right) dx$$

$$\mu = \frac{\mathsf{m}_F}{\mathsf{m}_W}$$

where

σ_{up}: The standard deviation of the upper part of the slider bearing

σ_{low}: The standard deviation of the lower, moving, part of the slider bearing

$\mathbb{F}_0$: The correlation coefficient between the mean pressure and mean film thickness

$\mathbb{F}_1$: The first negative moment of the stochastic film thickness

We observe that the equations based on Christensen's approach differ from the equations proposed in the current approach. Those differences are based on Christensen's assumption that the unit flow rates in both directions are of zero (or negligible) variance ([13]). The previous assumption, as was shown in Remark (2.1), is equal to assuming $\mathbb{E}^{\beta}\left[\frac{\partial^n p}{\partial^n r_S(\beta)}\right] = 0$ for $n \in \mathbb{N}^*$, which results in $\mathbb{F}_0 = 0$.

Remark 4.1: ***We notice that both Christensen's equations and the proposed equations for a rough bearing yield the equations of a smooth bearing, by setting the deviations of each part equal to 0, as proposed in Remark (2.2).***

4.1.1. Initial Validation of the Proposed Solution

First we will compare the results acquired for a slider bearing with convergence ratio $k = 1$ for a smooth bearing and for a rough bearing with deviation ratios $\sigma_{low} = 0$ and $\sigma_{up} = 0.2 \cdot h_0$. For the rough bearing, we utilized both the proposed approach and Christensen's approach to compare the results. The simulation results for the pressure profile are given in Figure (4.1), while the rest operational parameters are summarized in Table (4.1).

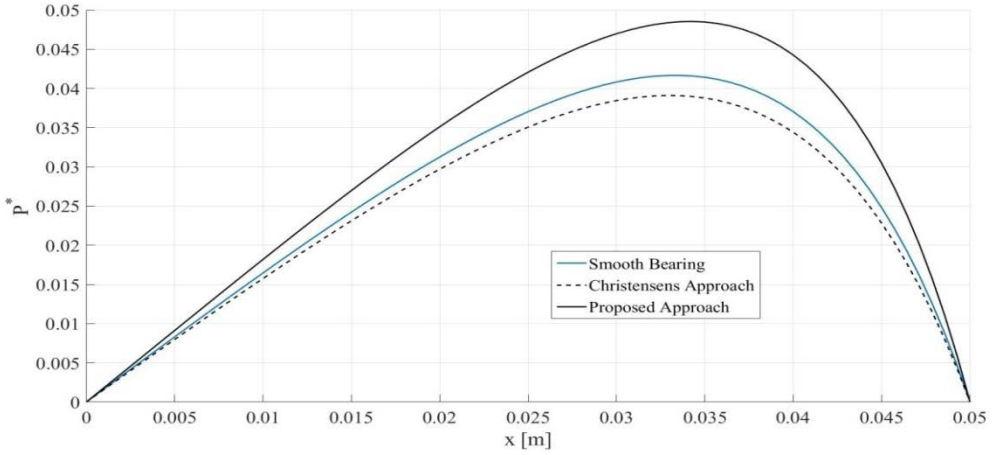

Figure 4.1: Pressure Profile for $\sigma_{low} = 0$, $\sigma_{up} = 0.2 \cdot h_0$ and $k = 1$

	Units	Smooth Bearing	Christensen's Approach	Proposed Approach
Maximum Pressure	MPa	2.219	2.083	2.586
Non Dimensional Maximum Pressure	(-)	0.0417	0.0391	0.0485
Load Carrying	kN	70.54	66.39	81.49
Non Dimensionless Load Carrying	(-)	0.0265	0.0249	0.0306
Friction Force	N	342.92	347.52	351.58
Non Dimensionless Friction Force	(-)	0.772	0.783	0.792
Friction Coefficient	(-)	0.0049	0.0054	0.0044
Non Dimensionless Friction Coefficient	(-)	4.9820	5.3848	4.3970

Table 4.1: Operational parameters of a slider bearing for $\sigma_{low} = 0$, $\sigma_{up} = 0.2 \cdot h_0$ and $k = 1$

We notice that the proposed solution of the Reynolds Equation for rough bearings complies with the findings in literature, while Christensen's approach is unsuited for calculating the increase in the pressure and load carrying capacity, which results in a higher friction coefficient. To further quantify the results for each approach, we have calculated and summarized the differences of the rough bearing operational parameters, for both approaches, from those of a smooth bearing in Table (4.2).

Ratios	Units	Christensen's Approach	Proposed Approach
Maximum Pressure	%	-6.13	16.54
Load Carrying	%	-5.88	15.52
Friction Force	%	1.34	2.52
Friction Coefficient	%	8.09	11.74

Table 4.2: Difference in [%] of operational parameters of a slider bearing for $\sigma_{low} = 0$, $\sigma_{up} = 0.2 \cdot h_0$ and $k = 1$

4.1.2. Maximum Pressure

Figures (4.2) ~ (4.3) show the maximum value of non-dimensional pressure for a smooth bearing and a rough bearing. Figure (4.2) was plotted for the case of convergence ratio $k = [0\,,\,5]$, and for deviation ratios $r_{low} = 0$ and $r_{up} = 0.2$. In Figure (4.3) different deviation ratios are plotted in the same plot, both for the proposed approach and for Christensen's approach.

We observe that the results of the previous validation can be extended for different values of convergence ratio and deviation ratios. As expected from the previous validation, we notice that the calculated maximum pressure of the proposed approach is of higher values than that of a smooth bearing, while Christensen's approach is lower.

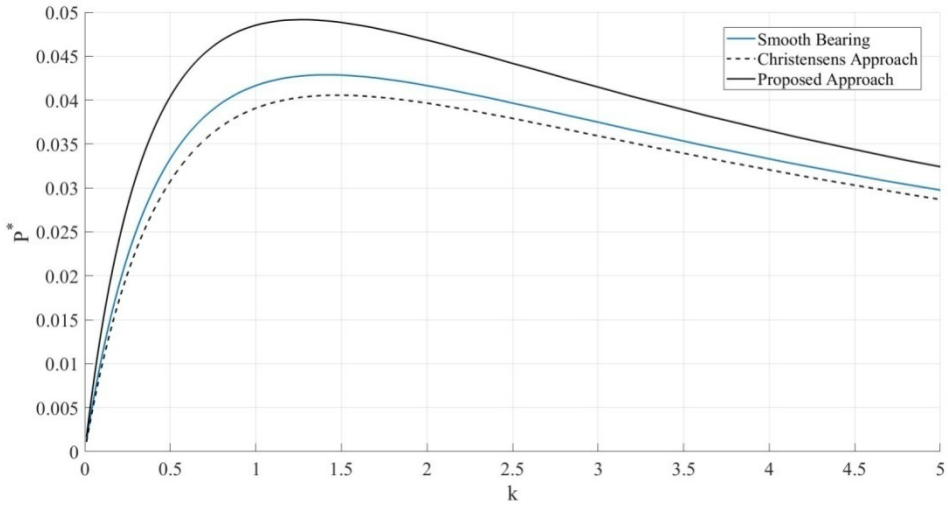

Figure 4.2: Non Dimensional Maximum Pressure for $\sigma_{low} = 0$ and $\sigma_{up} = 0.2 \cdot h_0$

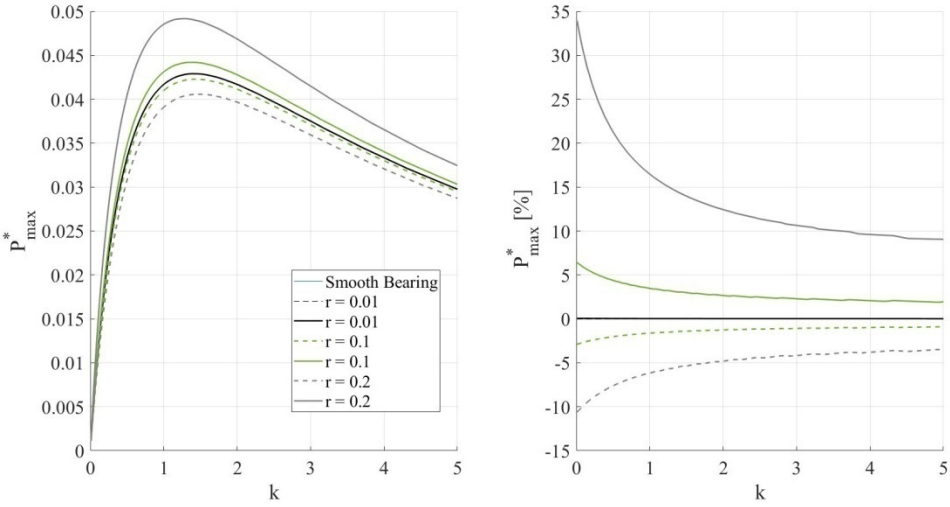

Figure 4.3: Non Dimensional Maximum Pressure for $r_{up} = \{0.01\,,\,0.1\,,\,0.2\}$

We also observe that while $r \to 0$, i.e. the deviation is getting smaller, the differences for both approaches are nearing the values of a smooth bearing. This can be seen in Figure (4.4), in which we have plotted the difference of the maximum pressure in a rough bearing and a smooth bearing, for different values of deviation ratios and for convergence ration $k = 2$. Figure (4.4) was plotted only for the proposed approach.

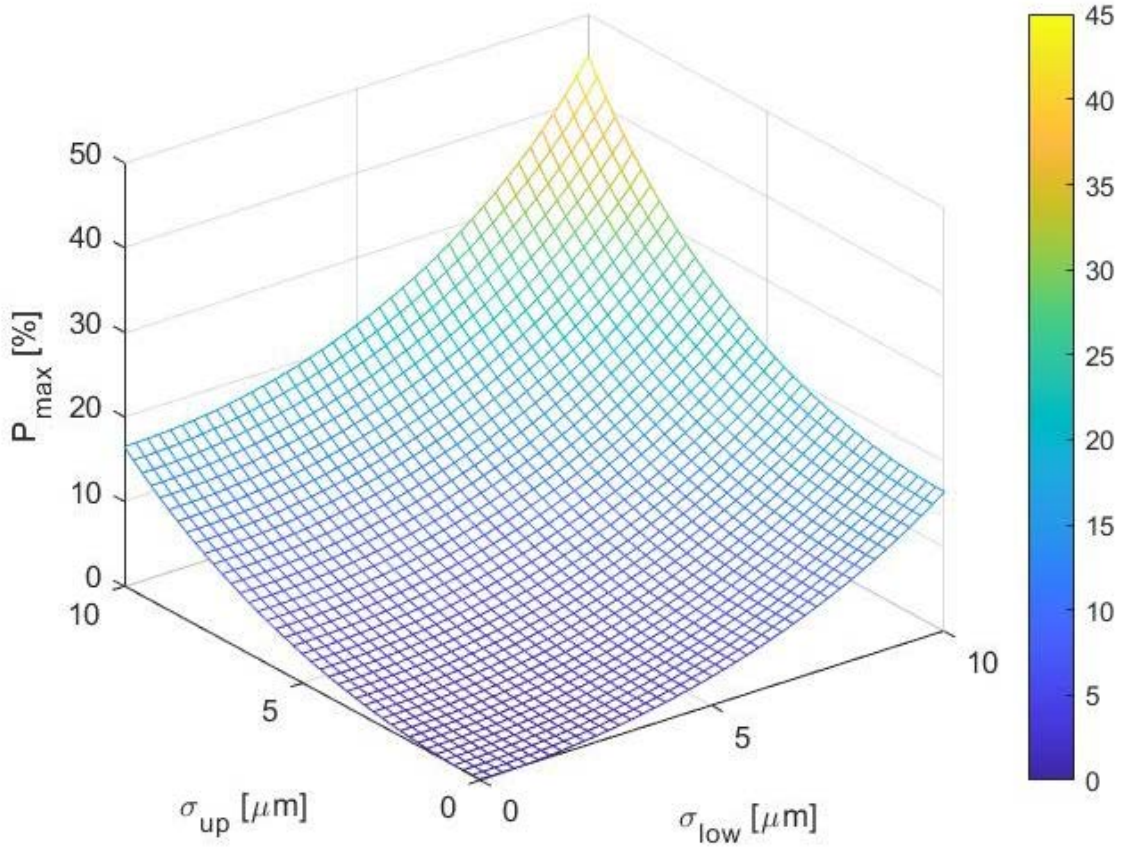

Figure 4.4: Non Dimensional Maximum Pressure for $k = 2$

We observe that while $r_{up} \to 0$ and $r_{low} \to 0$ then the difference of the maximum pressure reaches zero, meaning that the maximum pressure is equal to the maximum pressure of a smooth bearing.

4.1.3. Load Carrying Capacity

Figures (4.5) ~ (4.6) show the normalized load carrying capacity for a smooth bearing and a rough bearing. Figure (4.5) was plotted for the case of convergence ratio $k = [0\,,\,5]$, and for deviation ratios $r_{low} = 0$ and $r_{up} = 0.2$. In Figure (4.6) different deviation ratios are plotted in the same plot, both for the proposed approach and for Christensen's approach.

Similar to the maximum pressure case, the results of the initial validation can be extended for different values of convergence ratio and deviation ratios. As expected, we notice that the calculated load carrying capacity of the proposed approach is higher than that of a smooth bearing, while Christensen's approach is lower.

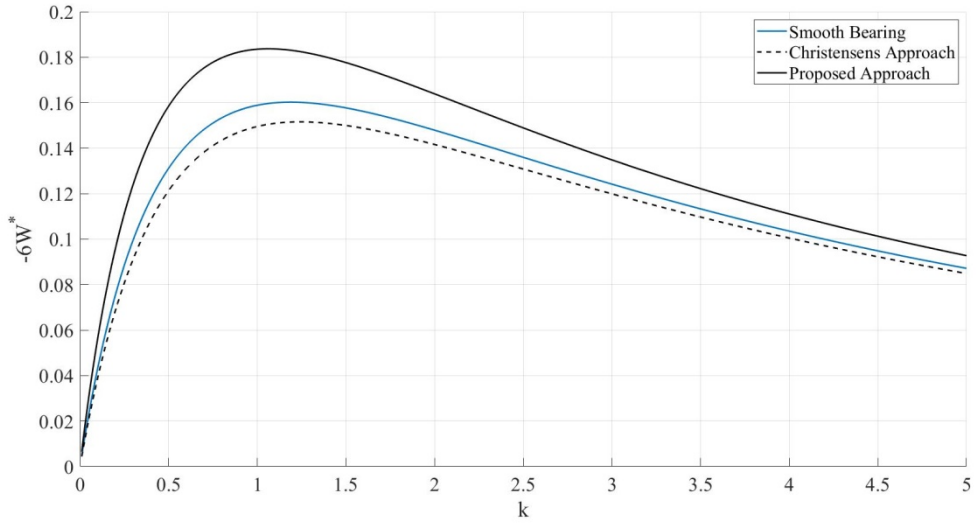

Figure 4.5: Non Dimensional Load Carrying Capacity for $\sigma_{low} = 0$ and $\sigma_{up} = 0.2 \cdot h_0$

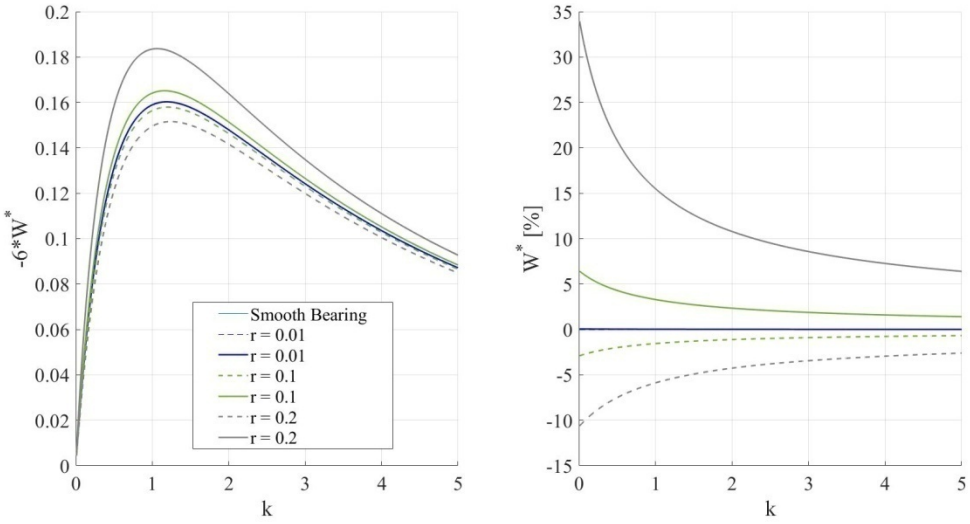

Figure 4.6: Non Dimensional Load Carrying Capacity for $r_{low} = \{0.01\,,\,0.1\,,\,0.2\}$

We observe that while $r \to 0$, i.e. the deviation is getting smaller, the differences for both approaches are nearing the values of a smooth bearing, similar to the maximum pressure results. This can be seen in Figure (4.7), in which we have plotted the difference of the load carrying capacity in a rough bearing and a smooth bearing, for different values of deviation ratios and for convergence ration $k = 2$. Figure (4.7) was plotted only for the proposed approach.

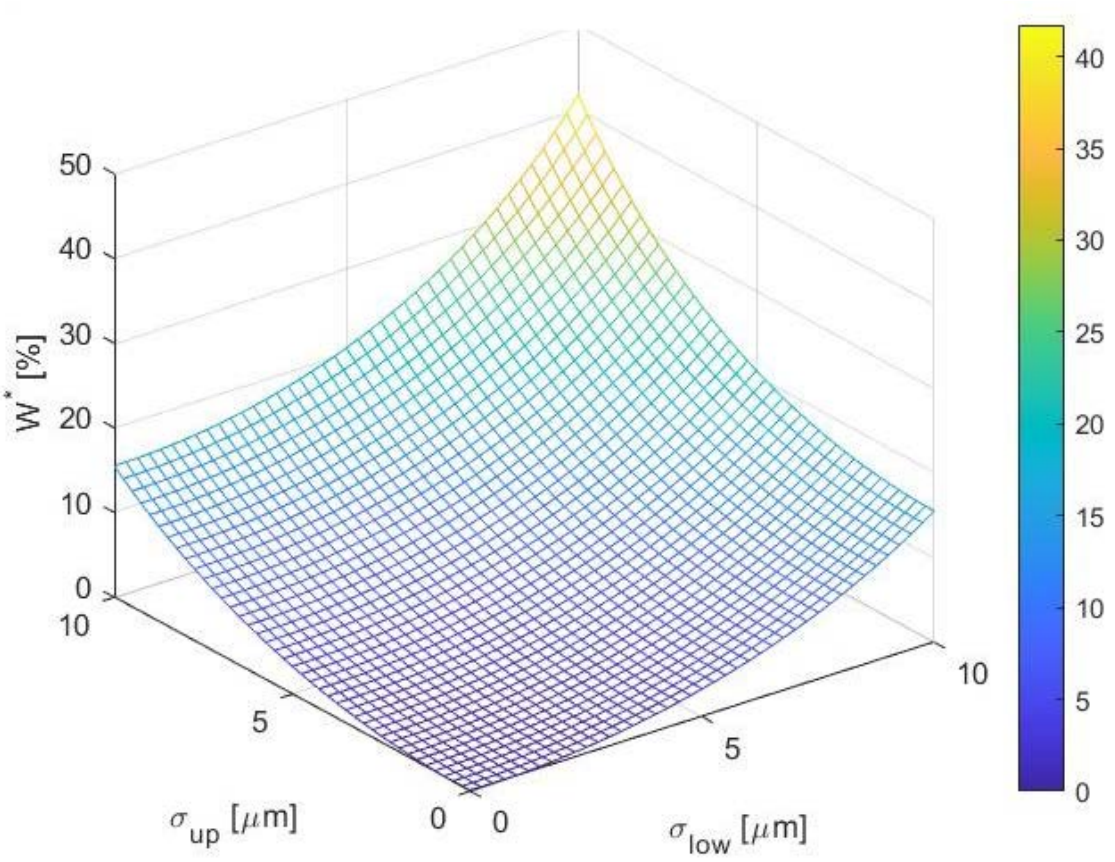

Figure 4.7: Non Dimensional Load Carrying Capacity for $k = 2$

We observe that while $r_{up} \to 0$ and $r_{low} \to 0$ then the difference of the maximum pressure reaches zero, meaning that the maximum pressure is equal to the maximum pressure of a smooth bearing.

Remark 4.2: ***Although literature findings predict a pressure build up in the parallel slider bearing ($k = 0$), both the previous approaches fail to predict this, as it can be seen in figure (4.6). This is due to the assumption that the stochastic roughness is a stochastic variable and not a stochastic function of space.***

4.1.4. Friction Force

Figures (4.8) ~ (4.9) show the normalized friction force for a smooth bearing and a rough bearing. Figure (4.8) was plotted for the case of convergence ratio $k = [0\,,\,5]$, and for deviation ratios $r_{low} = 0$ and $r_{up} = 0.2$. In Figure (4.9) different deviation ratios are plotted in the same plot, both for the proposed approach and for Christensen's approach.

Similar to the other operational parameters, the results of the initial validation for the friction force can be extended for different values of convergence ratio and deviation ratios. As expected, we notice that the calculated friction force of the proposed approach is higher than that of a smooth bearing. When it comes to Christensen's approach, we observe that the friction force starts from higher values up to some convergence ratio k^*, after which lower values than that of a smooth bearing are calculated.

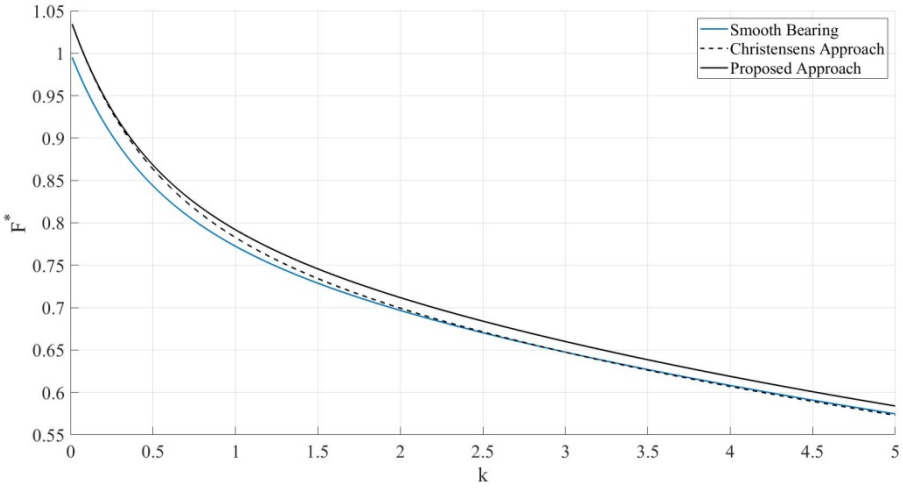

Figure 4.8: Non Dimensional Friction Force for $\sigma_{low} = 0$ and $\sigma_{up} = 0.2 \cdot h_0$

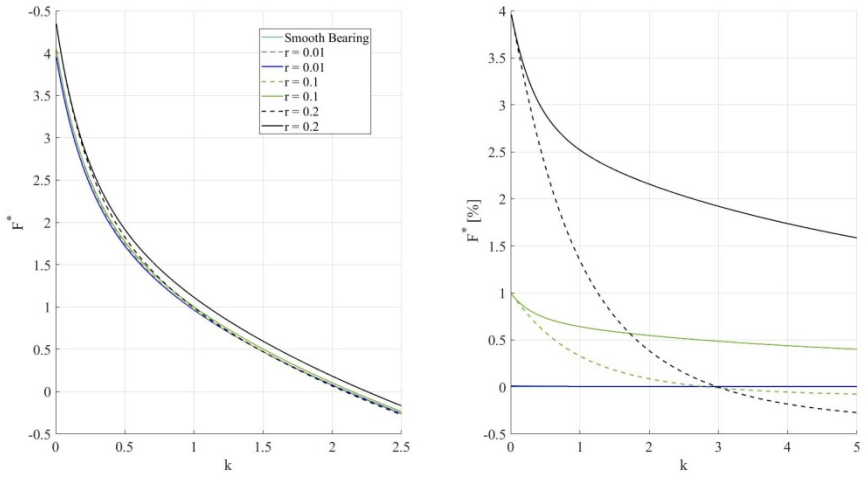

Figure 4.9: Non Dimensional Friction Force for $r_{low} = \{0.01\,,\,0.1\,,\,0.2\}$

We observe that while $r \to 0$, i.e. the deviation is getting smaller, the differences for both approaches are nearing the values of a smooth bearing, similar to the results of the other operational parameters. This can be seen in Figure (4.10), in which we have plotted the difference of the friction force in a rough bearing and a smooth bearing, for different values of deviation ratios and for convergence ration $k = 2$. Figure (4.10) was plotted only for the proposed approach.

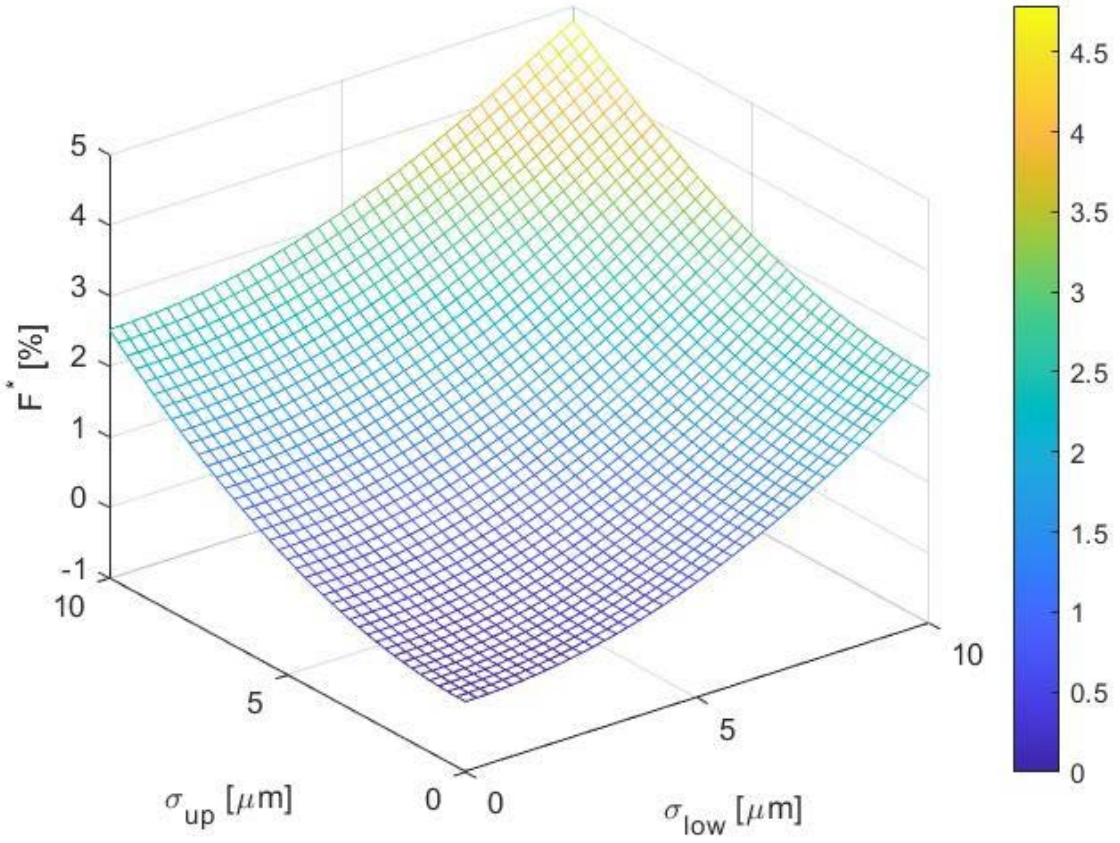

Figure 4.10: Non Dimensional Friction Force for $k = 2$

We observe that while $r_{up} \to 0$ and $r_{low} \to 0$ then the difference of the maximum pressure reaches zero, meaning that the maximum pressure is equal to the maximum pressure of a smooth bearing.

4.1.5. Coefficient of Friction

Figures (4.11) ~ (4.12) show the value of non-dimensional coefficient of friction for a smooth bearing and a rough bearing. Figure (4.11) was plotted for the case of convergence ratio $k = [0\,,\,5]$, and for deviation ratios $r_{low} = 0$ and $r_{up} = 0.2$. In Figure (4.12) different deviation ratios are plotted in the same plot, both for the proposed approach and for Christensen's approach.

We observe that the results of the initial validation of the friction coefficient can also be extended for different values of convergence ratio and deviation ratios. As expected from the previous validation, we notice that the coefficient of friction calculated from the proposed approach has lower values than that of a smooth bearing, while Christensen's approach is giving higher values. This is due to the fact that Christensen's approach calculates smaller values for the load carrying capacity, which in addition to the higher values of friction force result in a total higher coefficient of friction.

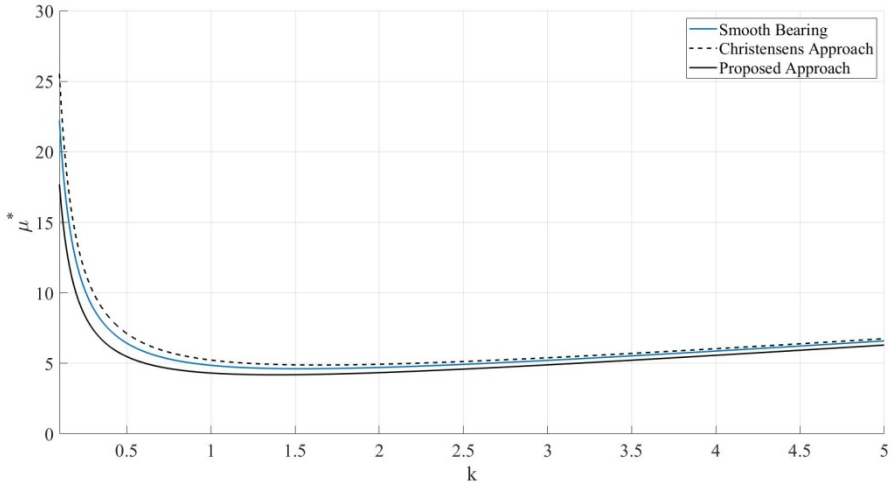

Figure 4.11: Non Dimensional Coefficient of Friction for $\sigma_{low} = 0$ and $\sigma_{up} = 0.2 \cdot h_0$

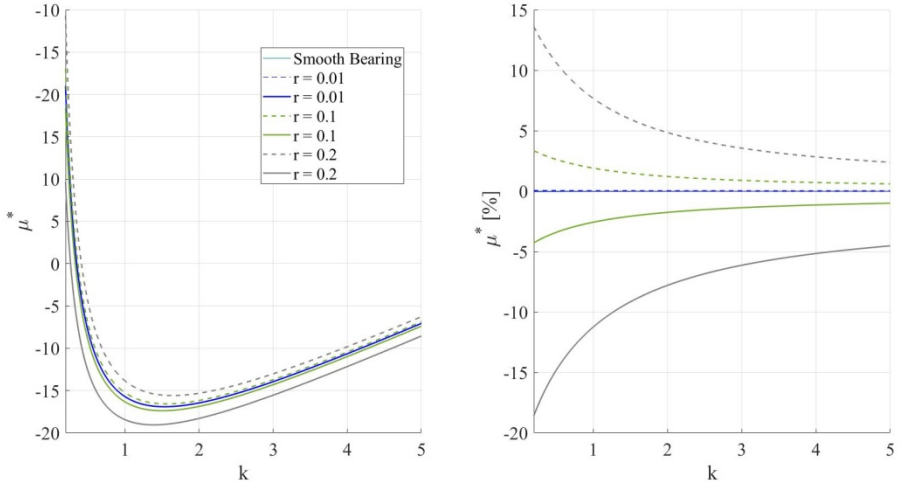

Figure 4.12: Non Dimensional Coefficient of Friction for $r_{low} = \{0.01\,,\,0.1\,,\,0.2\}$

We also observe that while $r \to 0$, i.e. the deviation is getting smaller, the differences for both approaches, similar to the other operational parameters, are nearing the values of a smooth bearing. This can be seen in Figure (4.13), in which we have plotted the difference of the friction coefficient in a rough bearing and a smooth bearing, for different values of deviation ratios and for convergence ratio $k = 2$. Figure (4.13) was plotted only for the proposed approach.

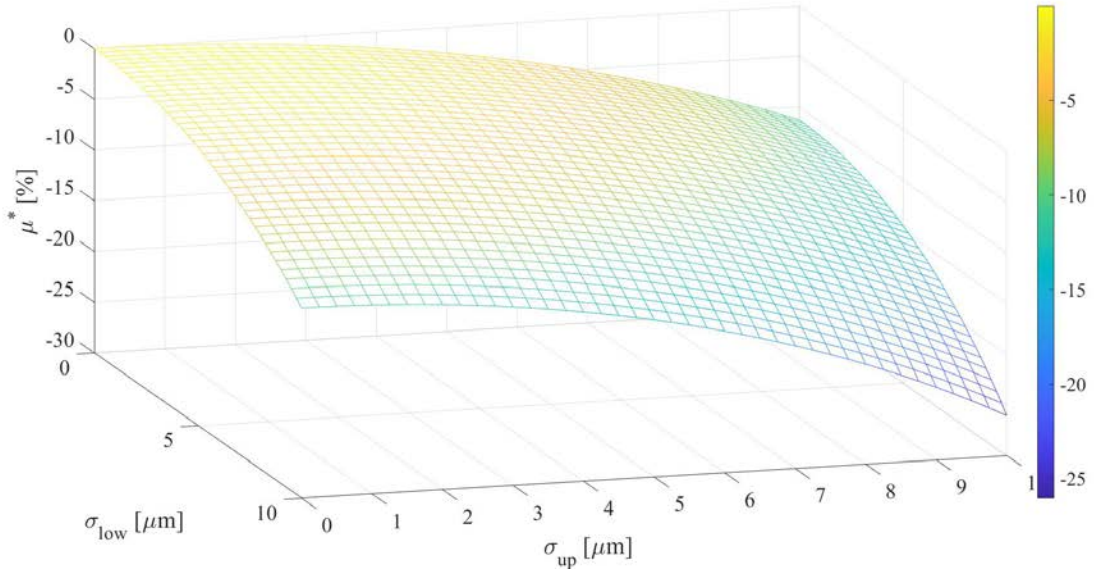

Figure 4.13: Non Dimensional Coefficient of Friction for $k = 2$

We observe that while $r_{up} \to 0$ and $r_{low} \to 0$ then the difference of the maximum pressure reaches zero, meaning that the maximum pressure is equal to the maximum pressure of a smooth bearing.

4.2. Journal Bearing

Validation based on [6], [27], [28] and [29]

Following the validation of the proposed solution of the Reynolds Equation in a wide slider bearing, we now progress in the validation of the solution for a journal bearing. The present solution algorithm was validated by comparing the calculated operational characteristics of the rough journal bearing with the respective parameters of a smooth journal bearing for the same geometry, meaning the same eccentricity ratio and attitude angle. The external load for the smooth bearing varied from 30 kN to 120 kN so as to cover different values of Sommerfeld number S and eccentricity ratios e.

The journal bearing we test for this validation has the following geometric and operating parameters:

- Bearing Diameter $D = 1.0 \ m$
- Bearing Length $L = 2.1 \ m$
- Radial Clearance $C = 0.0005 \ m$
- Rotational Speed $N = 90 \ RPM$
- Lubricant Viscosity $\eta = 0.001 \ Pa \cdot sec$

In general, literature findings suggest that an increase of the pressure profile, the load carrying capacity and the friction force is anticipated, while the friction coefficient is expected to decrease. Each one of the design and performance parameters is calculated for the case of smooth bearing, meaning no roughness, and for a rough bearing. The rough bearing consists of two parameters; the roughness profile of the bearing and the roughness profile of shaft, which is the moving part of the bearing. In the case of rough bearing, the parameters are calculated for both Christensen's approach and proposed approach of the Reynolds Equation, and a comparison between the two approaches is held. Since each one of the approaches is based on different assumptions, we expect the equations for calculating the operational characteristics to differ. Thus the equations used for the calculations are listed below for each one of the approaches.

For a Smooth Journal Bearing

$$W_z = \int_0^{2\pi}\int_0^L p \cdot R \cdot \sin\left(\varphi + \omega - \frac{\pi}{2}\right) dy d\omega$$

$$W_x = \int_0^{2\pi}\int_0^L p \cdot R \cdot \cos\left(\varphi + \omega - \frac{\pi}{2}\right) dy d\omega$$

$$F = \int_0^{\pi D}\int_0^L \left(\frac{h}{2}\frac{\partial \mathrm{m}_P}{\partial x} + \frac{\eta U}{h}\right) dy dx$$

$$\mu = \frac{F}{W}$$

For a Rough Slider Bearing (Christensen's Approach)

$$\mathrm{m}_{W_z(\beta)} = \int_0^{2\pi}\int_0^{L} \mathrm{m}_p R_S \cdot \sin\left(\varphi + \omega - \frac{\pi}{2}\right) dy d\omega$$

$$\mathrm{m}_{W_x(\beta)} = \int_0^{2\pi}\int_0^{L} \mathrm{m}_p R_S \cdot \cos\left(\varphi + \omega - \frac{\pi}{2}\right) dy d\omega$$

$$\mathrm{m}_F = \mathbb{E}^{\beta}\left[F(\beta)\right] = \int_0^{\pi D}\int_0^{L}\left(\frac{h}{2}\frac{\partial \mathrm{m}_P}{\partial \omega} + \eta U \mathbb{F}_1\right) dx dy$$

$$\mu = \frac{\mathrm{m}_F}{\mathrm{m}_W}$$

For a Rough Slider Bearing (Proposed Approach)

$$\mathrm{m}_{W_z(\beta)} = \int_0^{2\pi}\int_0^{L}\left(\mathrm{m}_p R_S + \sigma_S^2 g(t)\mathbb{E}^{\beta}\left[\frac{\partial\, p}{\partial r_S(\beta)}\right]\right)\cdot \sin\left(\varphi + \omega - \frac{\pi}{2}\right) dy d\omega$$

$$\mathrm{m}_{W_x(\beta)} = \int_0^{2\pi}\int_0^{L}\left(\mathrm{m}_p R_S + \sigma_S^2 g(t)\mathbb{E}^{\beta}\left[\frac{\partial\, p}{\partial r_S(\beta)}\right]\right)\cdot \cos\left(\varphi + \omega - \frac{\pi}{2}\right) dy d\omega$$

$$\mathrm{m}_F = \mathbb{E}^{\beta}\left[F(\beta)\right] = \int_0^{\pi D}\int_0^{L}\left(\frac{h - 3\sigma^2 g^2(t)\mathbb{F}_0}{2}\frac{\partial \mathrm{m}_P}{\partial \omega} + \eta U \mathbb{F}_1 - \frac{\eta U \sigma_B^2}{R_B}\mathbb{F}_2\right) dx dy$$

$$\mu = \frac{\mathrm{m}_F}{\mathrm{m}_W}$$

where σ_B: The standard deviation of the bearing

σ_S: The standard deviation of the shaft

$\mathbb{F}_0$: The correlation coefficient between the mean pressure and mean film thickness

$\mathbb{F}_1$: The first negative moment of the stochastic film thickness

$\mathbb{F}_2$: The second negative moment of the stochastic film thickness

Remark 4.3: ***We notice that both Christensen's equations and the proposed equations for a rough bearing yield the equations of a smooth bearing, by setting the deviations of each part equal to 0, as proposed in Remark (2.2).***

4.2.1. Maximum Pressure

Figures (4.14) ~ (4.16) show the maximum value of non-dimensional pressure for a smooth bearing and a rough bearing. Figure (4.14) was plotted for the case of external load $W = [30, 120]\ kN$, and for shaft and bearing standard deviation $\sigma_S = 0$ and $\sigma_B = 10\ \mu m$ respectively. In Figure (4.15) the maximum pressure value is plotted for different bearing standard deviations and for external loads $W = [30, 120]\ kN$.

We notice that the proposed solution of the Reynolds Equation for rough journal bearings calculates the expected pressure build up mentioned in literature findings, in contrast to Christensen's approach which does not.

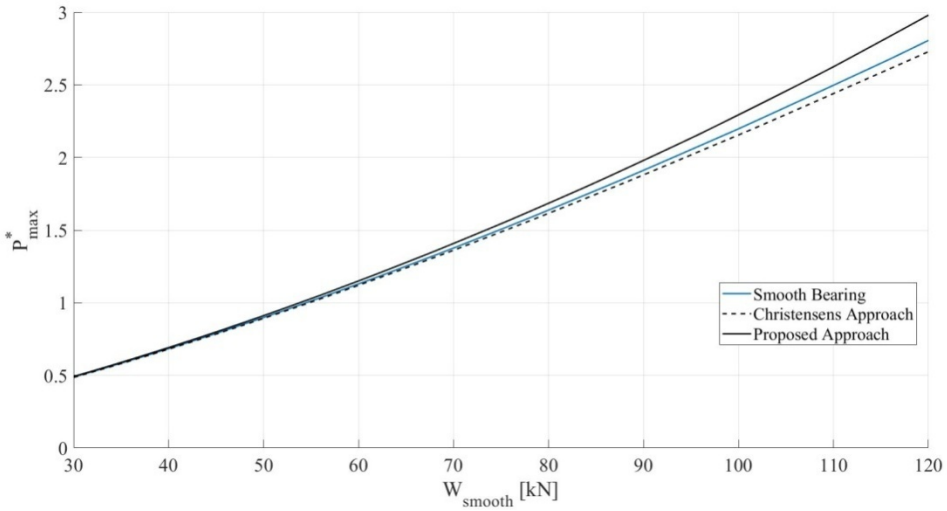

Figure 4.14: Non Dimensional Maximum Pressure for $\sigma_S = 0$ and $\sigma_B = 10\ \mu m$

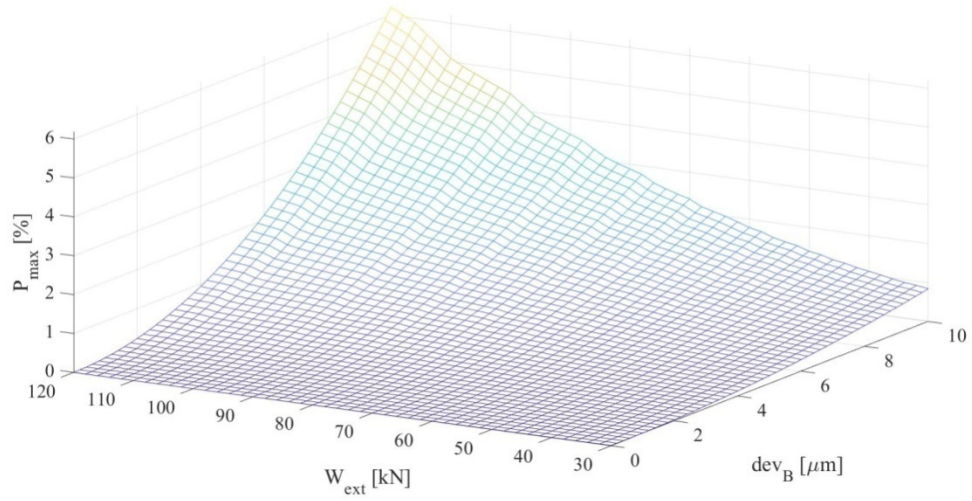

Figure 4.15: Non Dimensional Maximum Pressure for $\sigma_B = [0, 10]\ \mu m$

We also observe that while $\sigma \rightarrow 0$, i.e. the deviation is getting smaller, the differences for both approaches are nearing the values of a smooth bearing. This can be also seen in Figure (4.16), in which we have plotted the difference of the maximum pressure in a rough bearing and a smooth bearing, for different values of deviation and for external load $W = 120\ kN$. Figure (4.16) was plotted only for the proposed approach.

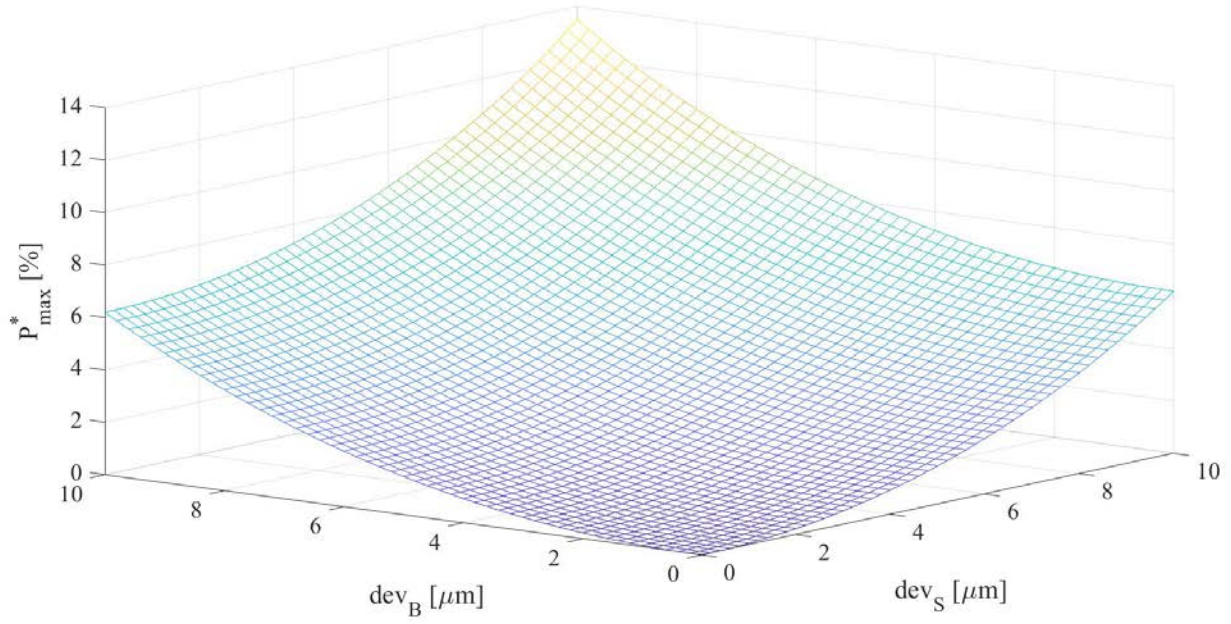

Figure 4.16: Non Dimensional Maximum Pressure for $W = 120\ kN$

We observe that while $\sigma_S \rightarrow 0$ and $\sigma_B \rightarrow 0$ then the difference of the maximum pressure reaches zero, meaning that the maximum pressure is equal to the maximum pressure of a smooth bearing.

4.2.2. Load Carrying Capacity

Figures (4.17) ~ (4.19) show the normalized load carrying capacity for a smooth and a rough journal bearing. Figure (4.17) was plotted for the case of external load $W = [30, 120]\ kN$, and for standard deviations in the shaft and bearing $\sigma_S = 0$ and $\sigma_B = 10\ \mu m$ respectively. In Figure (4.18) the value of the calculated load is plotted for different bearing standard deviations and for external loads $W = [30, 120]\ kN$.

Similar to the maximum pressure case, the results for the load carrying capacity of the proposed approach of the Reynolds Equation are in harmony with literature findings. As expected, we notice that the calculated load carrying capacity of the proposed approach is higher than that of a smooth bearing, while Christensen's approach is lower.

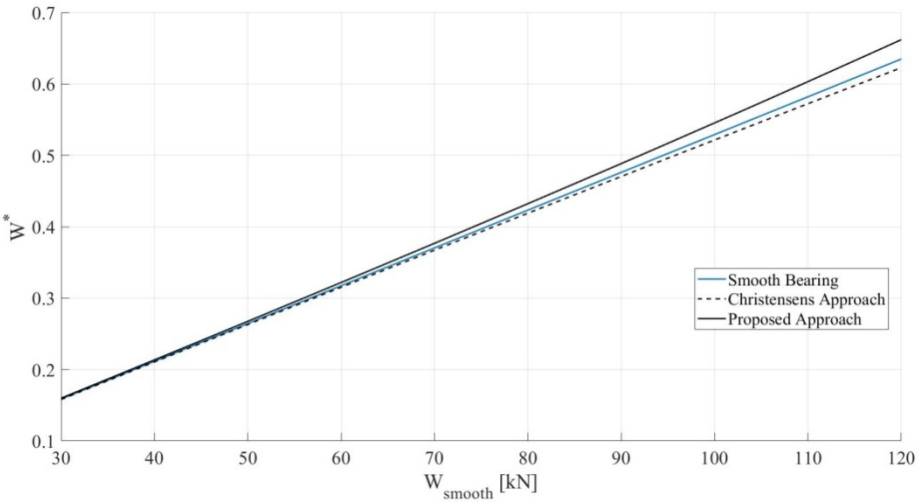

Figure 4.17: Non Dimensional Load Carrying Capacity for $\sigma_S = 0$ and $\sigma_B = 10\ \mu m$

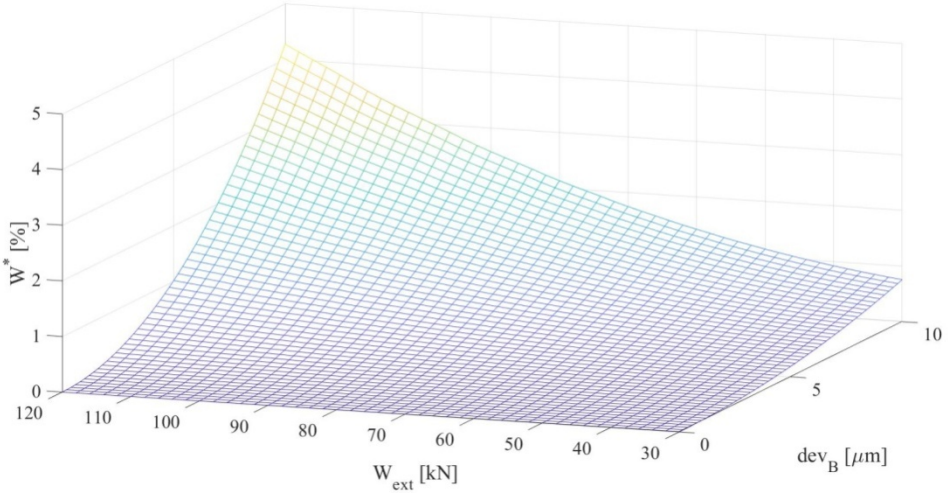

Figure 4.18: Non Dimensional Load Carrying Capacity for $\sigma_B = [0, 10]\ \mu m$

We observe that while $\sigma \to 0$, i.e. the deviation is getting smaller, the differences for both approaches are getting closer to the values of a smooth bearing, similar to the maximum pressure results. This can be seen in Figure (4.19), in which we have plotted the difference of the load carrying capacity of a rough bearing from the one of a smooth bearing, for different values of deviation and for external load $W = 120 \ kN$. Figure (4.19) was plotted only for the proposed approach.

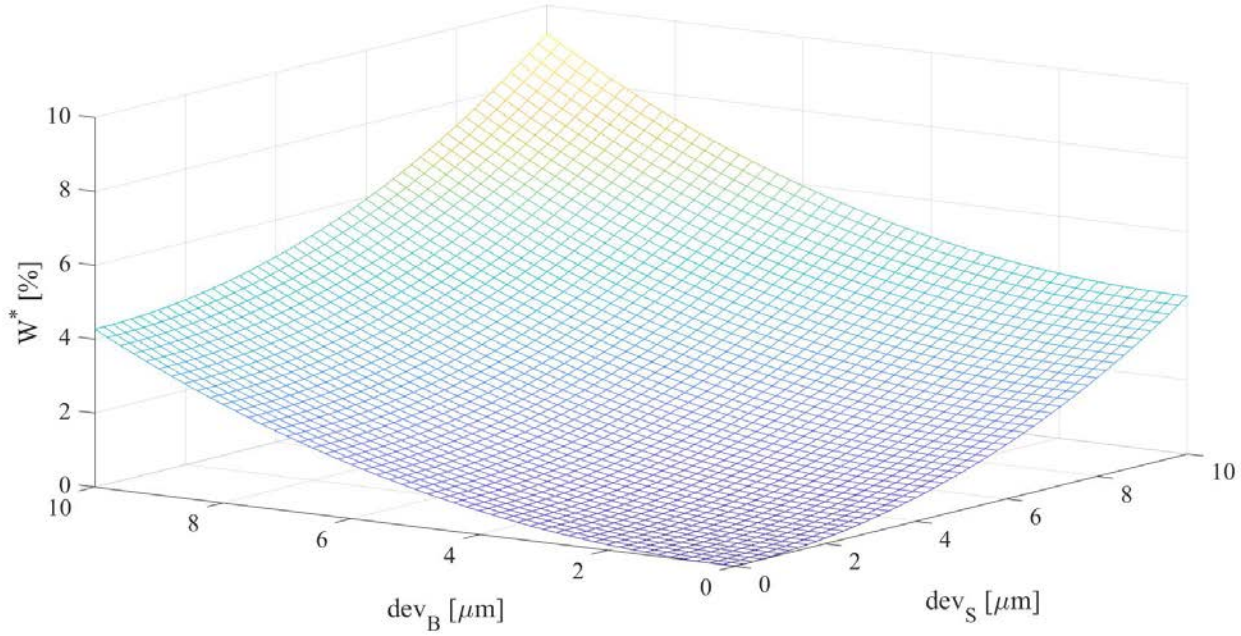

Figure 4.19: Non Dimensional Load Carrying Capacity for $W = 120 \ kN$

We observe that while $\sigma_S \to 0$ and $\sigma_B \to 0$ the difference of the bearings load carrying capacity reaches zero, meaning it is equal to the load carrying capacity of a smooth bearing.

4.2.3. Friction Force

Figures (4.20) ~ (4.22) show the normalized friction force for a smooth bearing and a rough bearing. Figure (4.20) was plotted for the case of external load $W = [30, 120]\ kN$, and for deviation in the shaft $\sigma_S = 0$ and in the bearing $\sigma_B = 10\ \mu m$. In Figure (4.21) the friction force is plotted for different bearing standard deviations and for external loads $W = [30, 120]\ kN$.

We observe that the results calculated for the friction force by the proposed approach of the Reynolds Equation are validated against literature findings. We also observe that the friction force calculated by Christensen's approach has increased values in relation to the friction force calculated for the smooth bearing.

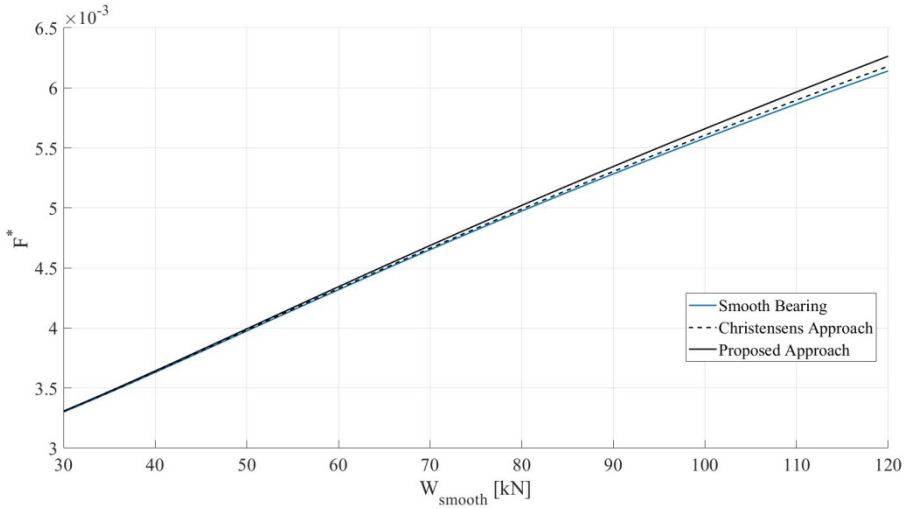

Figure 4.20: Non Dimensional Friction Force for $\sigma_S = 0$ and $\sigma_B = 10\ \mu m$

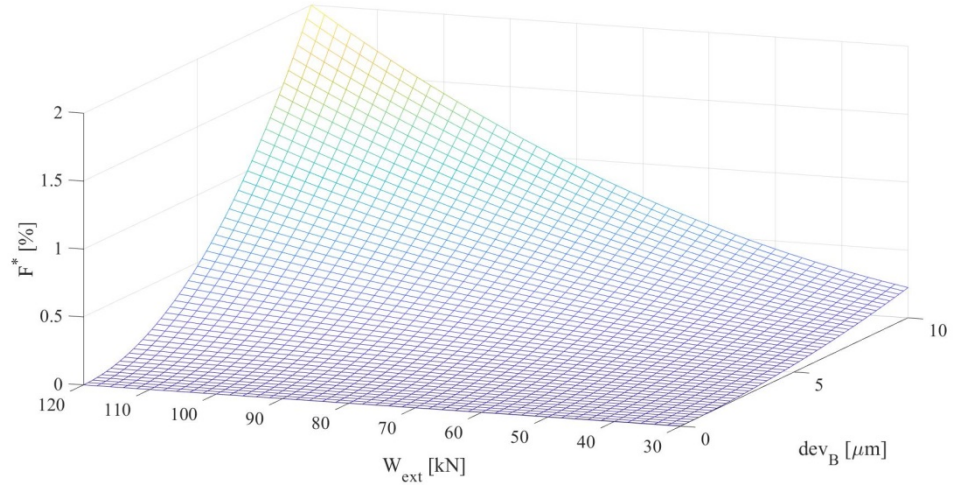

Figure 4.21: Non Dimensional Friction Force for $\sigma_B = [0, 10]\ \mu m$

We observe that while $\sigma \to 0$, i.e. the deviation is getting smaller, the differences for both approaches are nearing the values of a smooth bearing, similar to the results of the other operational parameters. This can be seen in Figure (4.22), in which we have plotted the difference of the friction force in a rough bearing and a smooth bearing, for different values of standard deviation and for external load $W = 120 \ kN$. Figure (4.22) was plotted only for the proposed approach.

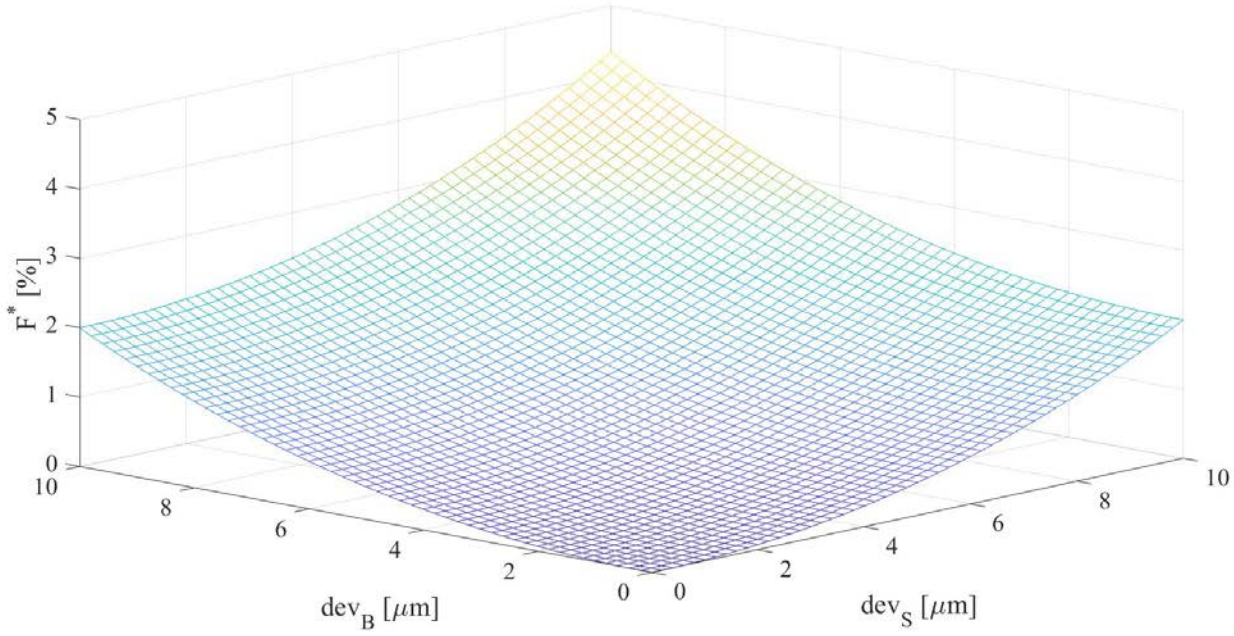

Figure 4.22: Non Dimensional Friction Force for $W = 120 \ kN$

4.2.4. Coefficient of Friction

Figures (4.23) ~ (4.24) show the value of non-dimensional coefficient of friction for a smooth bearing and a rough bearing. Figure (4.23) was plotted for the case of external load $W = [30, 120]\ kN$, and for standard deviation $\sigma_S = 0$ and $\sigma_B = 10\ \mu m$. In Figure (4.24) the calculated value of the coefficient of friction is plotted for different bearing standard deviations and for external loads $W = [30, 120]\ kN$.

We observe that, similar to the other operational parameters, the calculations are according to the ones found in literature. As expected, we notice that the coefficient of friction calculated from the proposed approach has lower values than that of a smooth bearing, while Christensen's approach is giving higher values. This is due to the fact that Christensen's approach calculates smaller values for the load carrying capacity, which in addition to the higher values of friction force result in a total higher coefficient of friction.

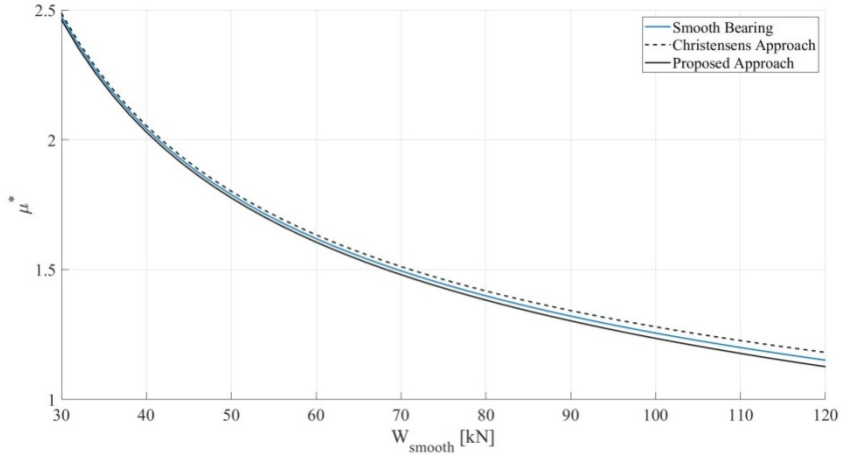

Figure 4.23: Non Dimensional Coefficient of Friction for $\sigma_S = 0$ and $\sigma_B = 10\ \mu m$

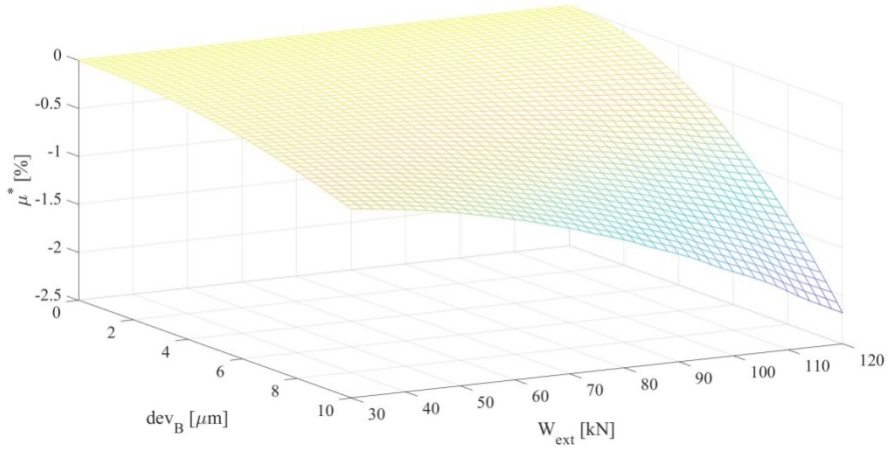

Figure 4.24: Non Dimensional Coefficient of Friction for $\sigma_B = [0, 10]\ \mu m$

We also observe that while $\sigma \rightarrow 0$, i.e. the deviation is getting smaller, the differences for both approaches, similar to the other operational parameters, are nearing the values of a smooth bearing. This can be seen in Figure (4.25), in which we have plotted the difference of the friction coefficient in a rough bearing and a smooth bearing, for different values of deviation and for external load $W = 120\ kN$. Figure (4.25) was plotted only for the proposed approach.

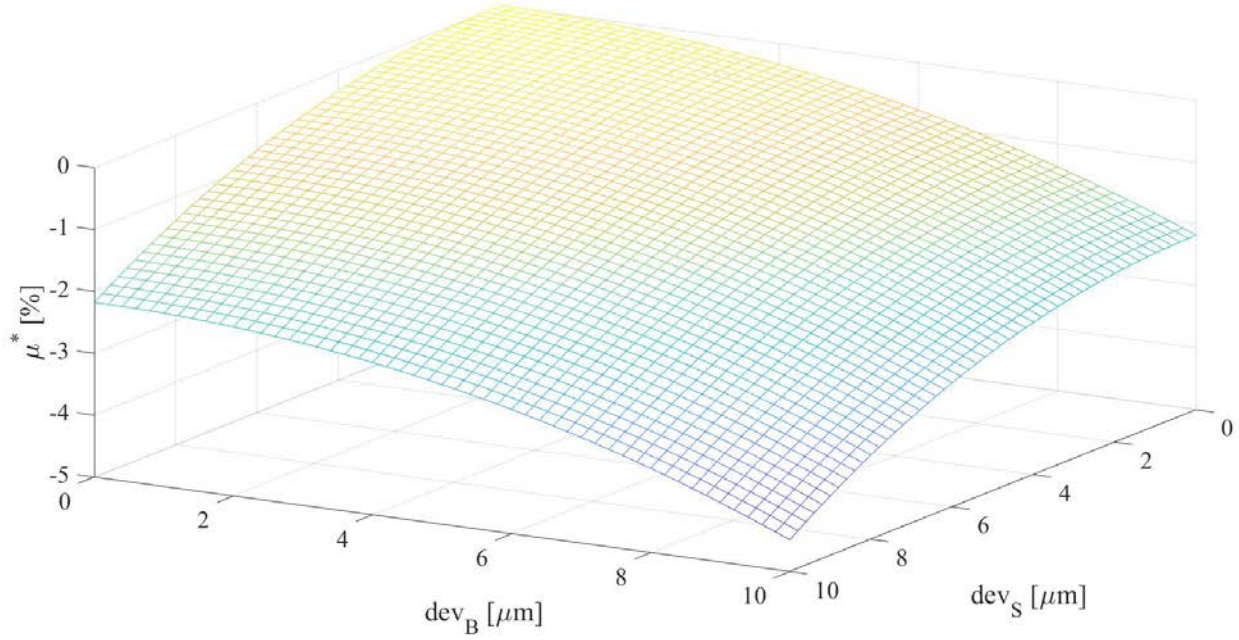

Figure 4.25: Non Dimensional Coefficient of Friction for $W = 120\ kN$

5. Numerical Simulations

Following the validation of the proposed solution of the Reynolds Equation in both a slider and a journal bearing, we now progress in numerical simulations of the solution for a journal bearing in real operational conditions; meaning we kept the load constant while the geometric parameters could vary to reach the hydrodynamic equilibrium. This was done in order to see how a rough journal bearing operates in a specific external load in contrast to a smooth bearing, and how the operational parameters of the bearing alter due to the constant external load. The external load varied from 30 kN to 110 kN so as to cover different values of Sommerfeld number S and eccentricity ratios e, keeping in mind that the bearing operates in the hydrodynamic regime.

The journal bearing we use in the below numerical simulation, is the same as the one used in Chapter 4, and its geometric and operating parameters are listed below

- Bearing Diameter $D = 1.0 \ \ m$
- Bearing Length $L = 2.1 \ \ m$
- Radial Clearance $C = 0.0005 \ \ m$
- Rotational Speed $N = 90 \ \ RPM$
- Lubricant Viscosity $\eta = 0.001 \ \ Pa \cdot sec$

Each one of the design and performance parameters for the slider bearing is calculated for a smooth bearing and for a rough bearing. The equations used for the calculations of both bearings are the following.

For a Smooth Journal Bearing

$$W_z = \int_0^{2\pi}\int_0^L p \cdot R \cdot \sin\left(\varphi + \omega - \frac{\pi}{2}\right) dy d\omega$$

$$W_x = \int_0^{2\pi}\int_0^L p \cdot R \cdot \cos\left(\varphi + \omega - \frac{\pi}{2}\right) dy d\omega$$

$$F = \int_0^{\pi D}\int_0^L \left(\frac{h}{2}\frac{\partial \mathrm{m}_P}{\partial x} + \frac{\eta U}{h}\right) dy dx$$

$$\mu = \frac{F}{W}$$

For a Rough Slider Bearing (Proposed Approach)

$$\mathrm{m}_{W_z(\beta)} = \int_0^{2\pi}\int_0^L \left(\mathrm{m}_p R_S + \sigma_S^2 g(t) \mathbb{E}^{\beta}\left[\frac{\partial\, p}{\partial r_S(\beta)}\right]\right) \cdot \sin\left(\varphi + \omega - \frac{\pi}{2}\right) dy d\omega$$

$$\mathrm{m}_{W_x(\beta)} = \int_0^{2\pi}\int_0^{L}\left(\mathrm{m}_p R_S + \sigma_S^2 g(t)\mathbb{E}^{\beta}\left[\frac{\partial\, p}{\partial r_S(\beta)}\right]\right)\cdot\cos\left(\varphi+\omega-\frac{\pi}{2}\right)dyd\omega$$

$$\mathrm{m}_F = \mathbb{E}^{\beta}\left[F(\beta)\right] = \int_0^{\pi D}\int_0^{L}\left(\frac{h-3\sigma^2 g^2(t)\mathbb{F}_0}{2}\frac{\partial \mathrm{m}_P}{\partial\omega}+\eta U\mathbb{F}_1-\frac{\eta U\sigma_B^2}{R_B}\mathbb{F}_2\right)dxdy$$

$$\mu = \frac{\mathrm{m}_F}{\mathrm{m}_W}$$

where

σ_B: The standard deviation of the bearing

σ_S: The standard deviation of the shaft

$\mathbb{F}_0$: The correlation coefficient between the mean pressure and mean film thickness

$\mathbb{F}_1$: The first negative moment of the stochastic film thickness

$\mathbb{F}_2$: The second negative moment of the stochastic film thickness

5.1.1. Attitude Angle

The first parameter that we will check is the one of the attitude angle. Figure (5.1) shows the maximum pressure for $W_{ext} = [30 , 120]\ kN$ and some selective standard deviations, while Figures (5.2) and (5.3) depict the effect of the stochastic roughness for different external loads and standard deviations.

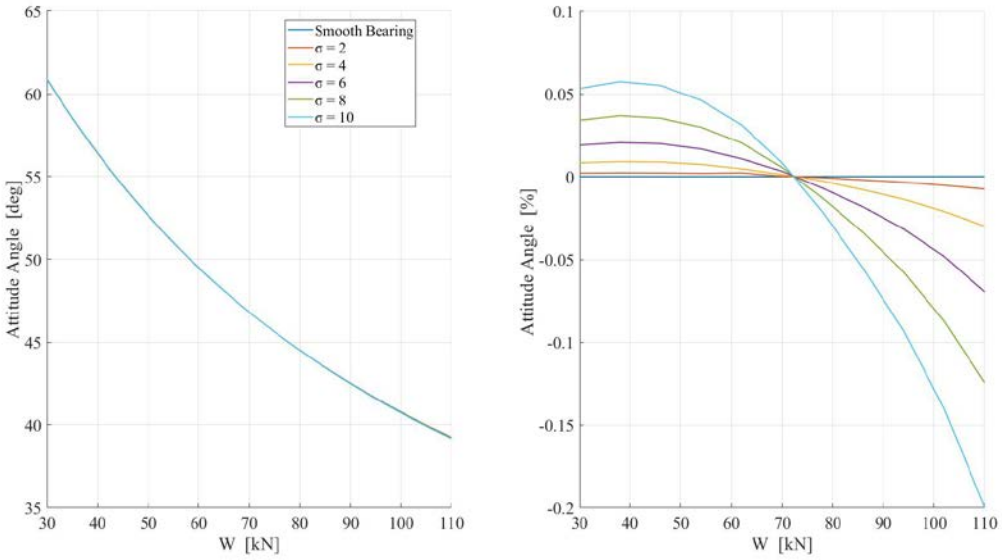

Figure 5.1: Attitude Angle for $\sigma_B = \{0 , 2 , 4 , 6 , 8 , 10\}\ \mu m$

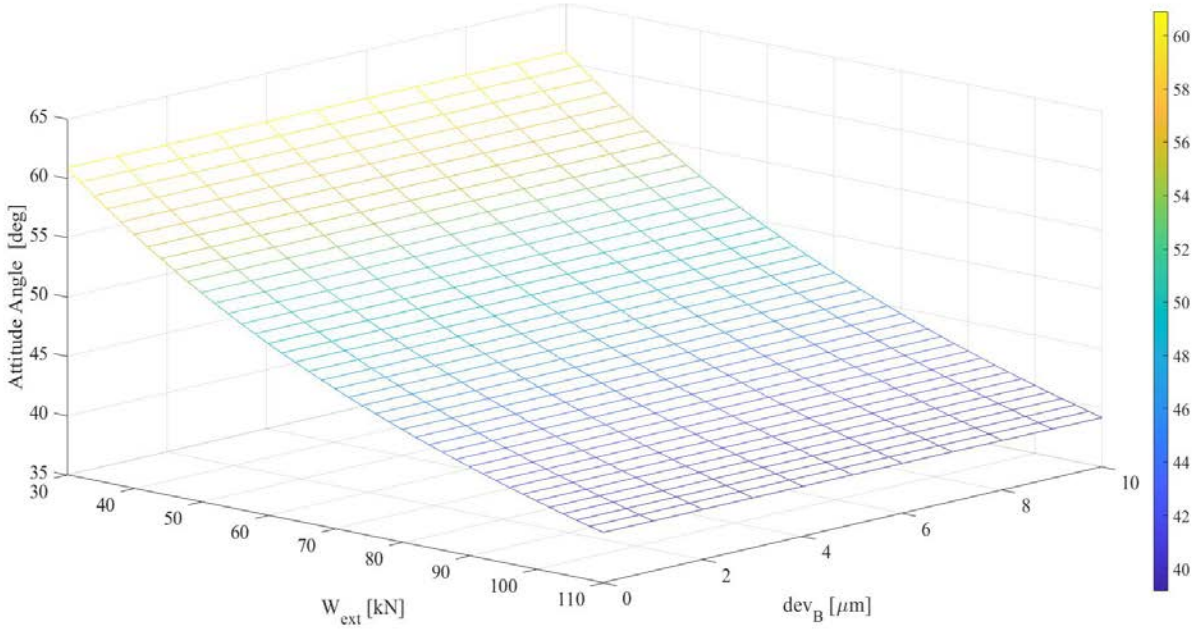

Figure 5.2: Attitude Angle for $\sigma_B = [0 , 10]\ \mu m$

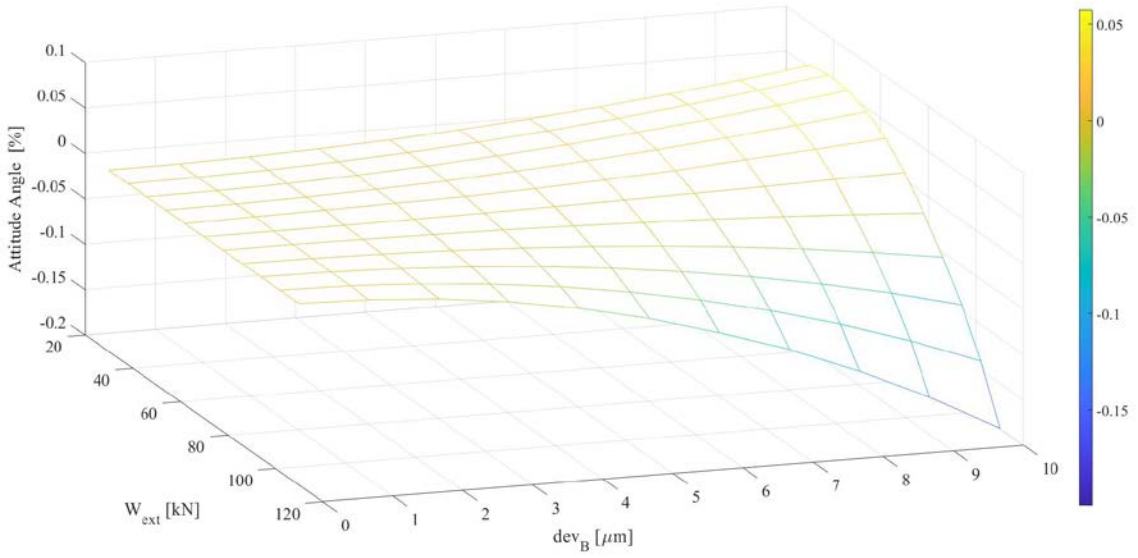

Figure 5.3: Difference of Attitude Angle in [%] for $\sigma_B = [0\ ,10]\ \ \mu m$

Generally, we see that the attitude angle tends to not alter significantly in respect to the attitude angle a smooth bearing has. For external loads $W_{ext} \leq 72\ \ kN$ we see that the attitude angle tends to get higher values, while for external loads $W_{ext} \geq 72\ \ kN$ higher values. For $W_{ext} = 40\ \ kN$ we observe that the attitude angle, for all the standard deviations, has a maximum value. Since attitude angle is highly correlated with the hydrodynamic load and is a component strongly dependent from the numerical execution of the solution algorithm, it cannot be further evaluated.

5.1.2. Geometry Results

We know that the film thickness is a function of the eccentricity ratio e and the bearing clearance c. The analytical expression of the film thickness is given by equation (2.4), which is also given below.

$$h = c \cdot \left(1 + \varepsilon \cdot \cos\left(\theta\right)\right)$$

Regarding the eccentricity ratio e figures (5.4) ~ (5.6) were plotted. Figure (5.4) displays the values of eccentricity ratio, as well as their difference from their respective values of a smooth bearing, for a selective set of standard deviations and for $W_{ext} = \left[30 , 120\right]$ kN. In figure (5.5) we plotted the values of eccentricity ratio for a rough journal bearing under different external load and for different standard deviations, while in figure (5.6) we plotted the difference of the eccentricity ratio from the smooth bearing.

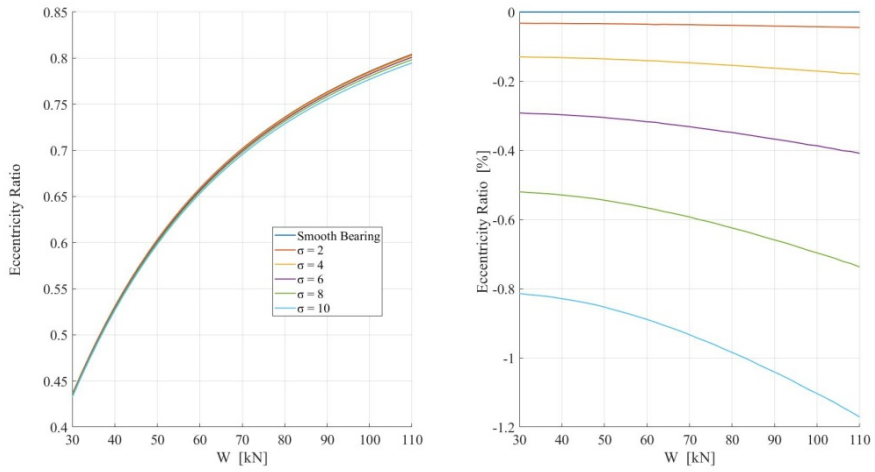

Figure5.4: Eccentricity Ratio for $\sigma_B = \left\{0 , 2 , 4 , 6 , 8 , 10\right\}$ μm

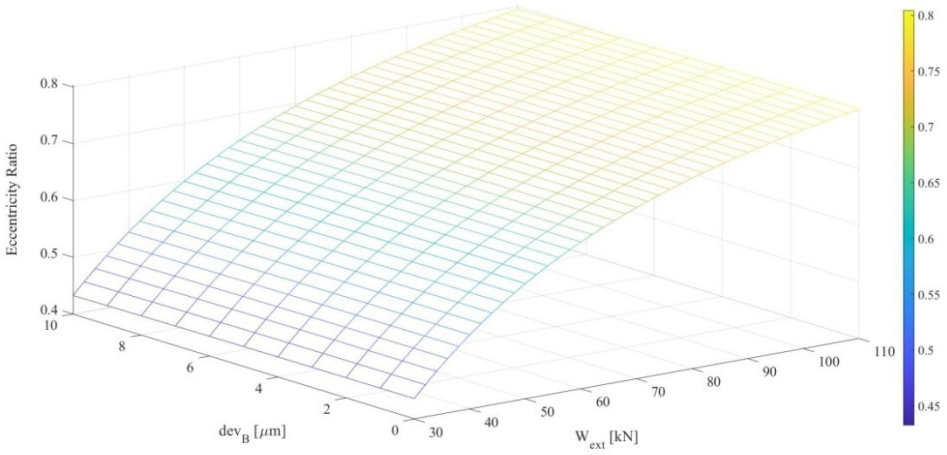

Figure5.5: Eccentricity Ratio for $\sigma_B = \left[0 , 10\right]$ μm

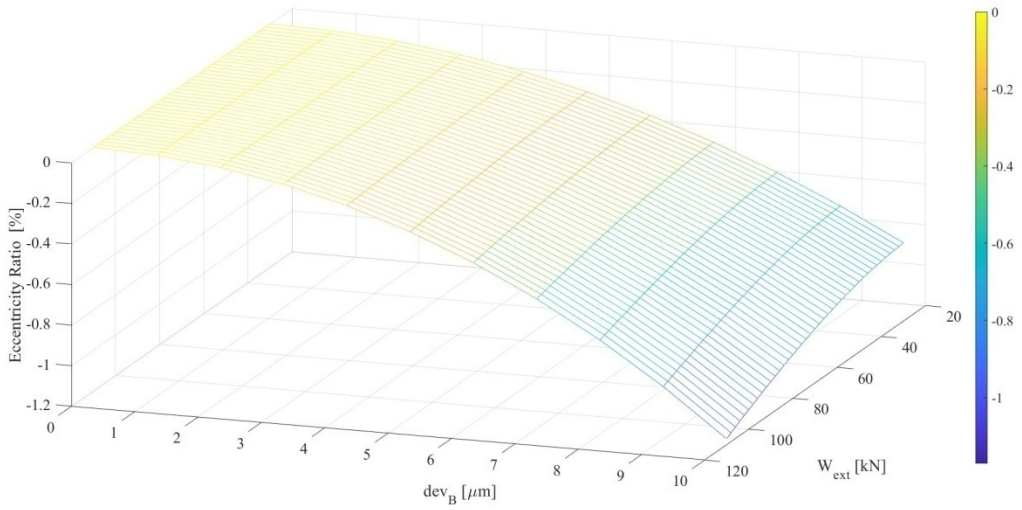

Figure5.6: Difference Eccentricity Ratio in [%] for $\sigma_B = [0, 10]\ \mu m$

As far as the geometry profile of the film thickness is concerned, it is easy to observe that it depends on the value of the eccentricity ratio. Thus, alongside with the results acquired for the eccentricity ratio, we also plotted the results for the film thickness. In Figure (5.7) the minimum values of the deterministic film thickness are displayed for a selective set of standard deviations, in respect to the external load. In Figures (5.8) and (5.9) we plotted the dimensional values of minimum film thickness for a rough journal bearing under different external load and for different standard deviations as well as their difference from those of a smooth bearing. The values of the film thickness presented in the figures are the values of the deterministic part, thus are the mean values of the film thickness.

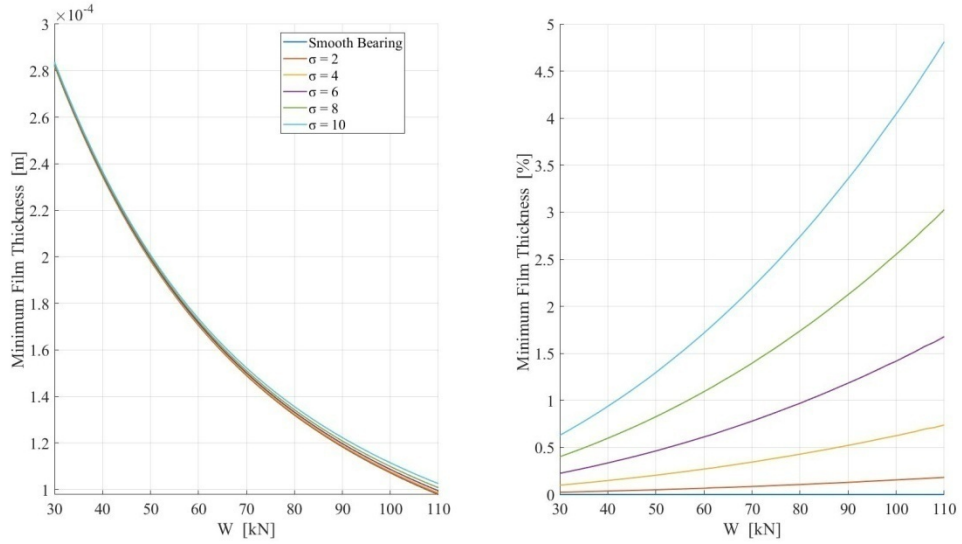

Figure5.7: Minimum Film Thickness for $\sigma_B = \{0, 2, 4, 6, 8, 10\}\ \mu m$

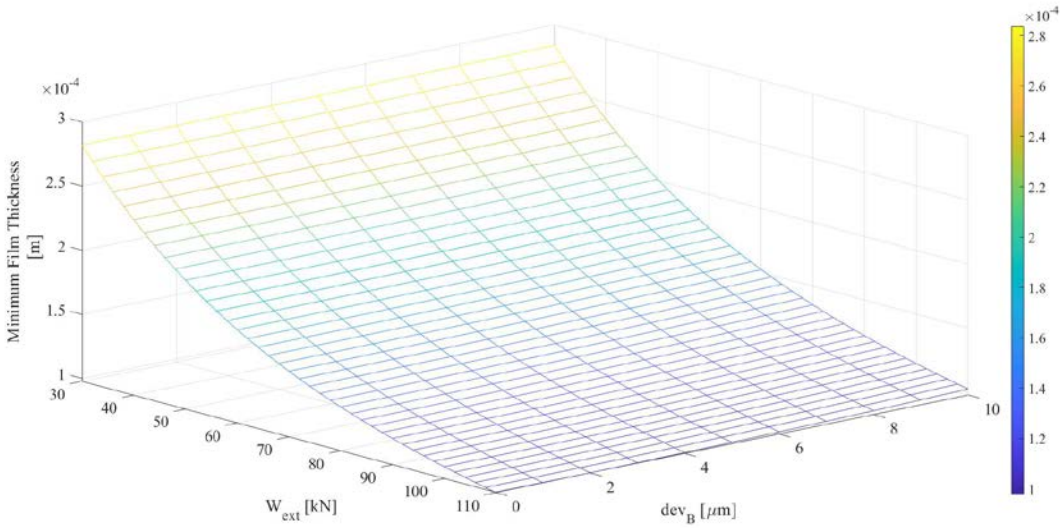

Figure5.8: Minimum Film Thickness for $\sigma_B = [0\,,10]\ \mu m$

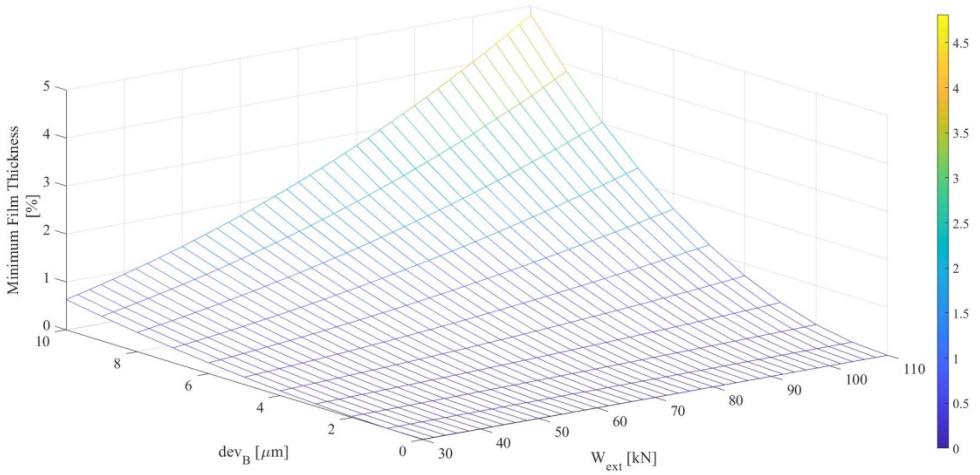

Figure5.9: Difference of Minimum Film Thickness in [%] for $\sigma_B = [0\,,10]\ \mu m$

Firstly we observe that as the standard deviation approaches zero, thus as the rough bearing is getting smoother, the effect of the roughness tends to zero for both the eccentricity ratio and the film thickness. This was expected from remark (2.2) as well as from the validation based on a rough slider bearing; as deviation reaches zero the results acquired tend to reach those of a smooth bearing. We also observe that as the standard deviation is going to higher values, the eccentricity ratio of the journal bearing is decreasing and the minimum value of the film thickness is increasing. The effect of this decrease and increase respectively is rising as we approach higher external loads. This means, that the rough bearing tends to operate under more steady conditions, e.g. avoiding the possibility of metal to metal contact between the shaft and the bearing.

5.1.3. Maximum Pressure

In this sub section, the effects of stochastic roughness on the maximum pressure are plotted. Figure (5.10) shows the maximum pressure for $W_{ext} = [30 , 120]\ kN$ and some selective standard deviations, while Figures (5.11) and (5.12) depict the effect of the stochastic roughness for different external loads and standard deviations.

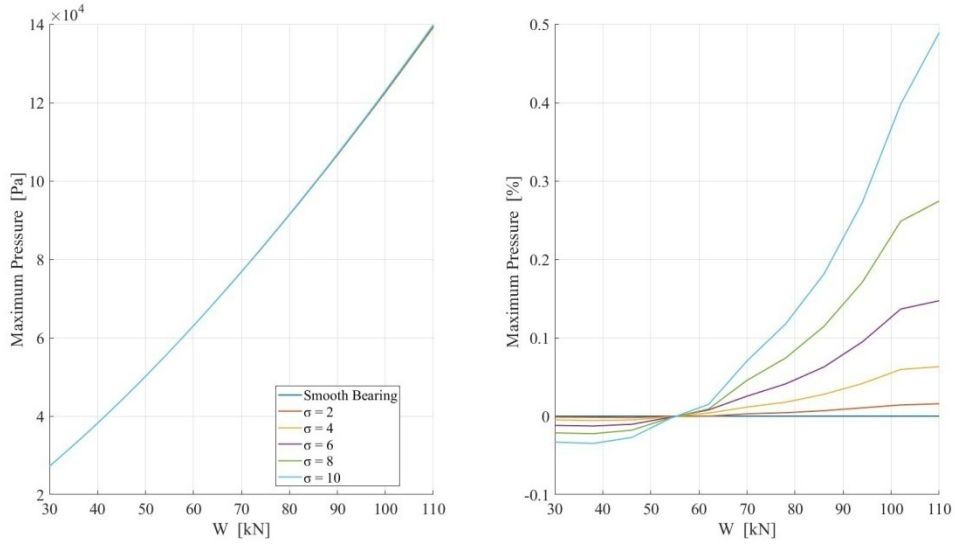

Figure5.10: Maximum Pressure for $\sigma_B = \{0 , 2 , 4 , 6 , 8 , 10\}\ \mu m$

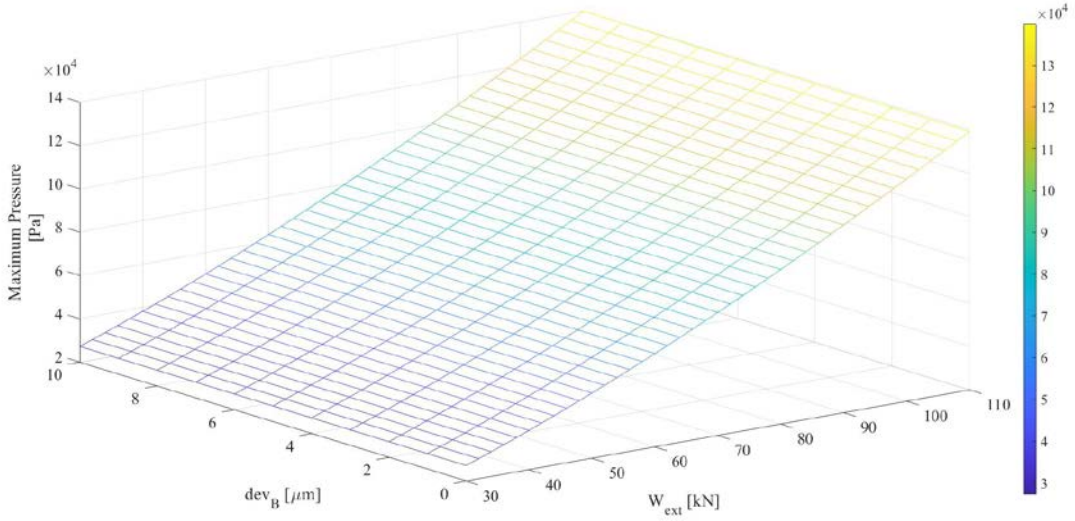

Figure5.11: Maximum Pressure for $\sigma_B = [0 , 10]\ \mu m$

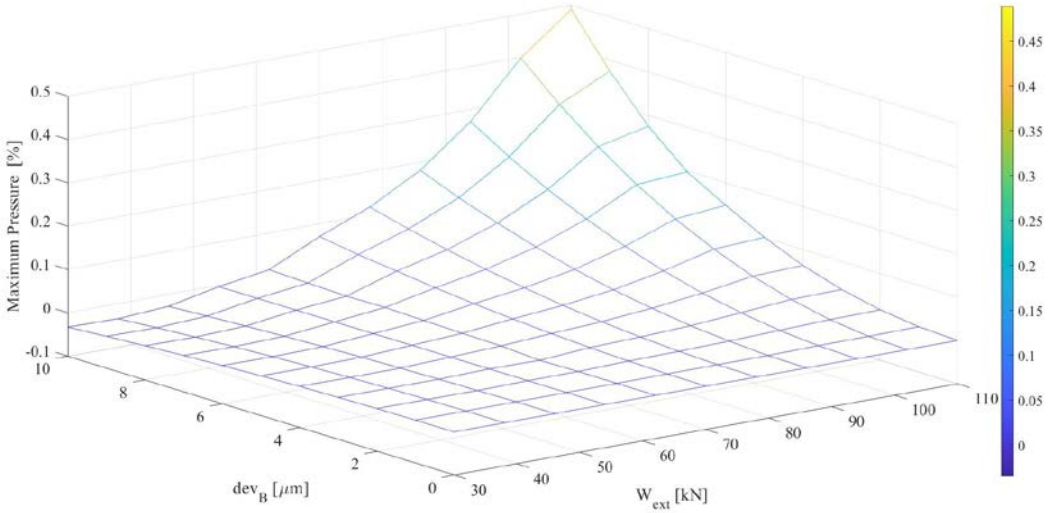

Figure5.12: Difference of Maximum Pressure in [%] for $\sigma_B = [0\ ,10]\ \mu m$

From the previous figures we observe that for small external loads $W_{ext} \leq 50\ \ kN$ the maximum pressure generated is slightly smaller ($\leq 0.03\ \%$) than that of a smooth bearing, while for $W_{ext} \geq 50\ \ kN$ the maximum pressure gradually increases.

The above observation can be explained by looking over the operational conditions of the bearing. In external loads $W_{ext} \leq 50\ \ kN$, the pressure build up in the journal bearing with constant geometry was of small values. Thus keeping the external load constant, a decreased pressure generation occurred in the bearing. For the journal bearing to withstand this lower load, a different pressure profile is generated that is characterized by smaller values of pressure.

5.1.4. Power Loss& Friction Torque

The extend of the effect of the surface roughness to the friction force, can be studied by analyzing the results for the Power Loss and Friction Torque, given by equations (5.1) and (5.2) respectively.

$$\mathrm{m}_{PL} = \mathrm{m}_F \cdot U \tag{5.1}$$

$$\mathrm{m}_{T_F} = \mathrm{m}_F \cdot \frac{D}{2} \tag{5.2}$$

In respect to the previous equations, Figures (5.13) ~ (5.15) for the power loss and Figure (5.16) ~ (5.18) for the friction torque were plotted. Figures (5.13) and (5.16) display the values of power loss and friction torque, as well as their difference from their respective values of a smooth bearing, for a selective set of standard deviations and for $W_{ext} = [30\,,120]\ kN$. In figures (5.14) and (5.17) we plotted the mentioned values for a rough journal bearing under different external load and for different standard deviations, while in Figures (5.15) and (5.18) we plotted the difference of the values from the respective values of a smooth bearing.

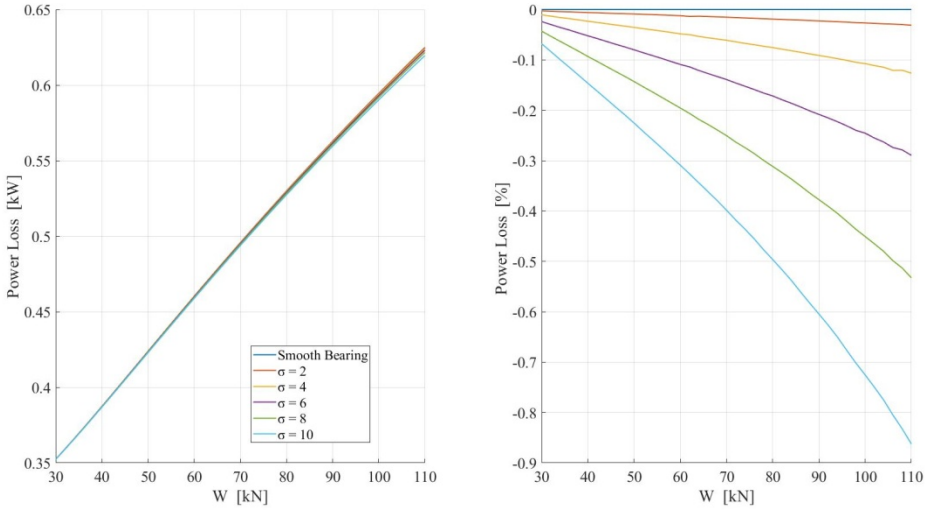

Figure 5.13: Power Loss for $\sigma_B = \{0\,,2\,,4\,,6\,,8\,,10\}\ \mu m$

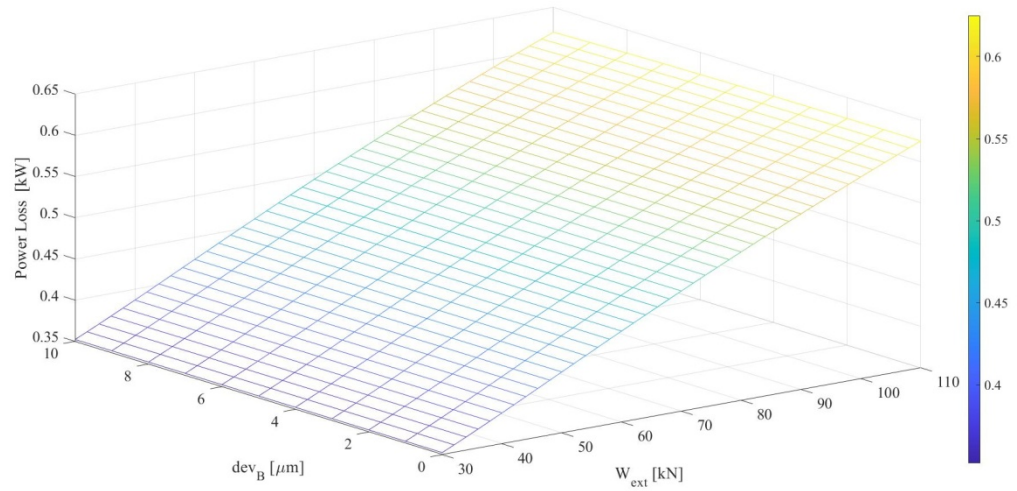

Figure 5.14: Power Loss for $\sigma_B = [0, 10]\ \mu m$

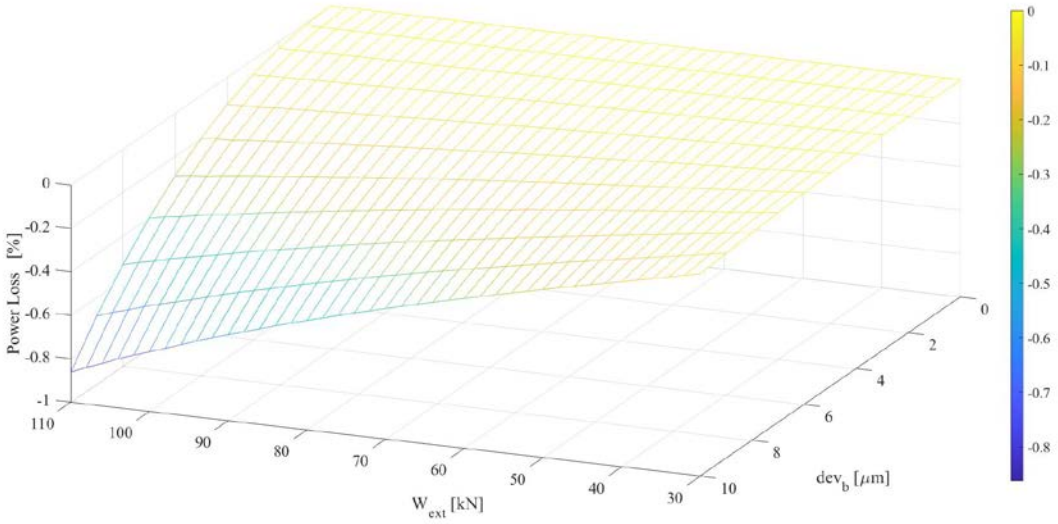

Figure 5.15: Difference of Power Loss in [%] for $\sigma_B = [0, 10]\ \mu m$

We observe that the power loss is decreasing with increasing values of standard deviation, which is due to a decreasing friction force. The same results can be also seen in Figures (5.16) ~ (5.18) regarding the friction torque.

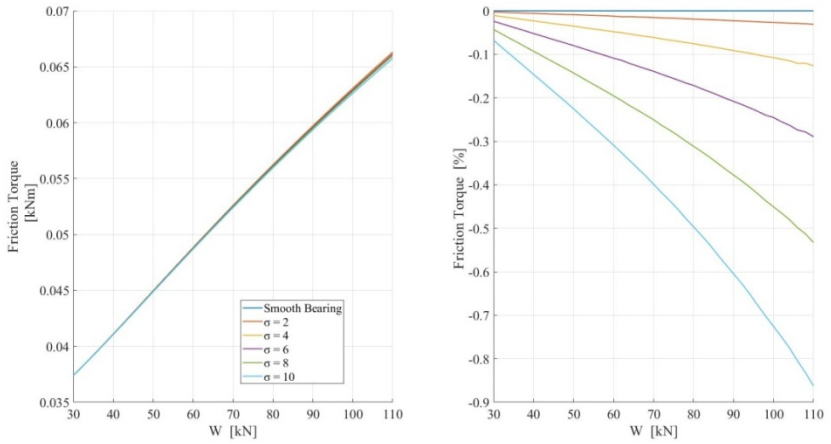

Figure 5.16: Friction Torque for $\sigma_B = \{0\ ,\ 2\ ,\ 4\ ,\ 6\ ,\ 8\ ,\ 10\}\ \ \mu m$

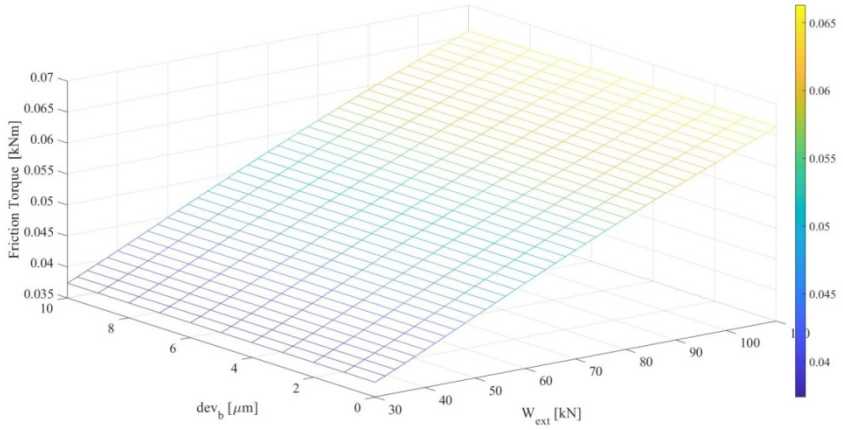

Figure 5.17: Friction Torque for $\sigma_B = [0\ ,\ 10]\ \ \mu m$

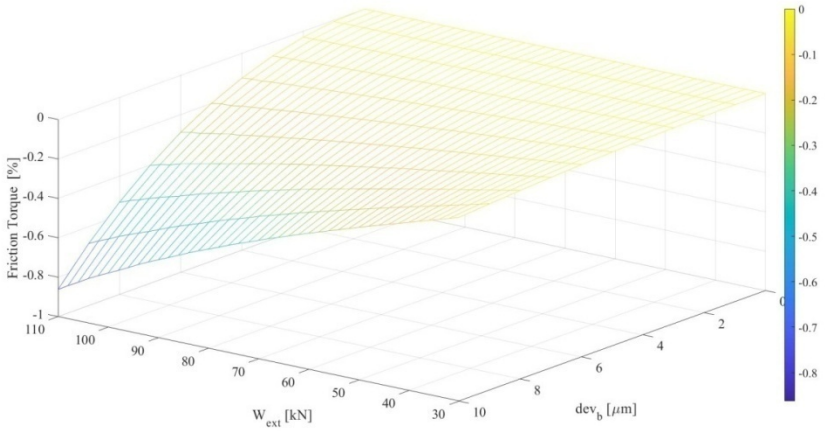

Figure 5.18: Difference of Friction Torque in [%] for $\sigma_B = [0\ ,\ 10]\ \ \mu m$

5.1.5. Friction Coefficient

Lastly we have quantified the effect that surface roughness has on the coefficient of friction. Since we have kept the external load, thus the load carrying capacity of the bearing, constant and the friction force is decreasing, we except that the friction coefficient will also decrease. In order to evaluate this, we have produced Figures (5.19) ~ (5.21). Figure (5.19) displays the values of the coefficient of friction, as well as their difference from their respective values of a smooth bearing, for a selective set of standard deviations and for $W_{ext} = [30 , 120]\ kN$. In figure (5.20) we plotted the values of friction coefficient for a rough journal bearing under different external load and for different standard deviations, while in figure (5.21) we plotted its difference of the from the smooth bearing.

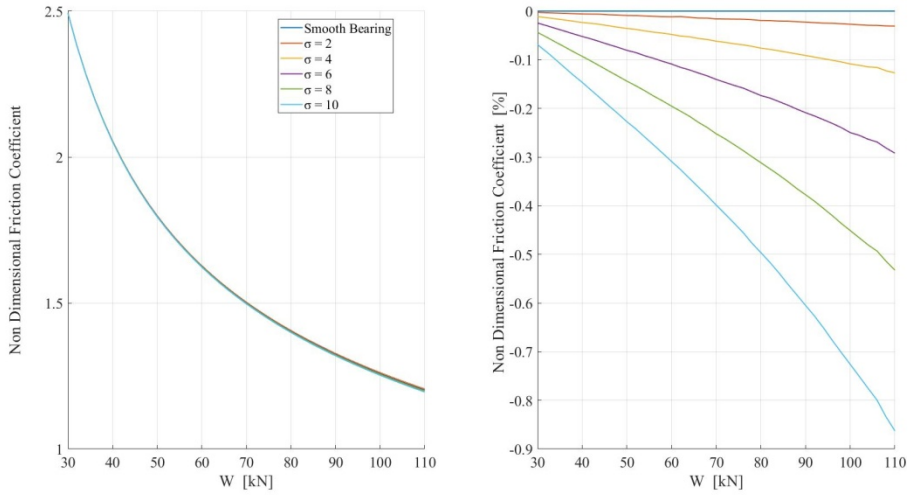

Figure 5.19: Normalized Friction Coefficient for $\sigma_B = \{0 , 2 , 4 , 6 , 8 , 10\}\ \mu m$

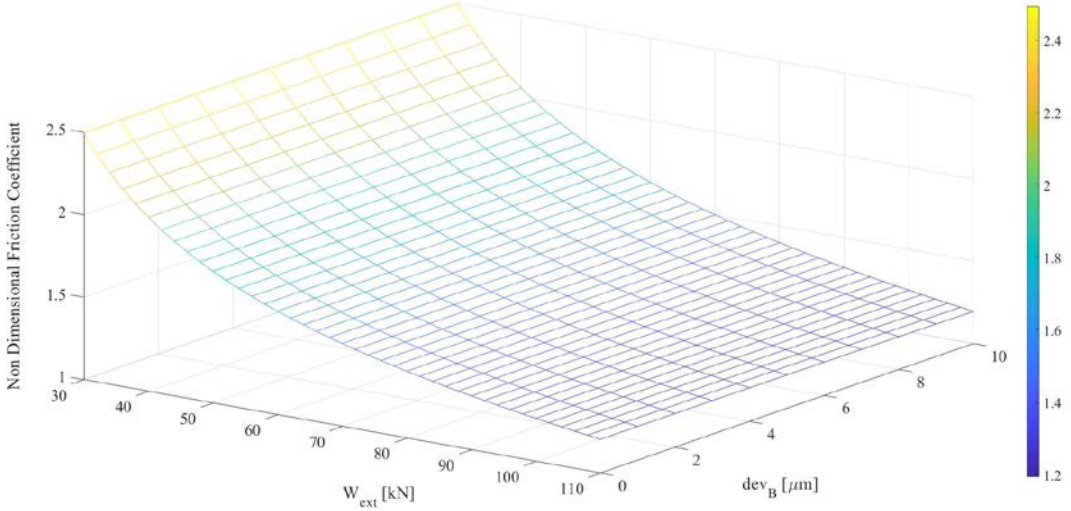

Figure 5.20: Normalized Friction Coefficient for $\sigma_B = [0 , 10]\ \mu m$

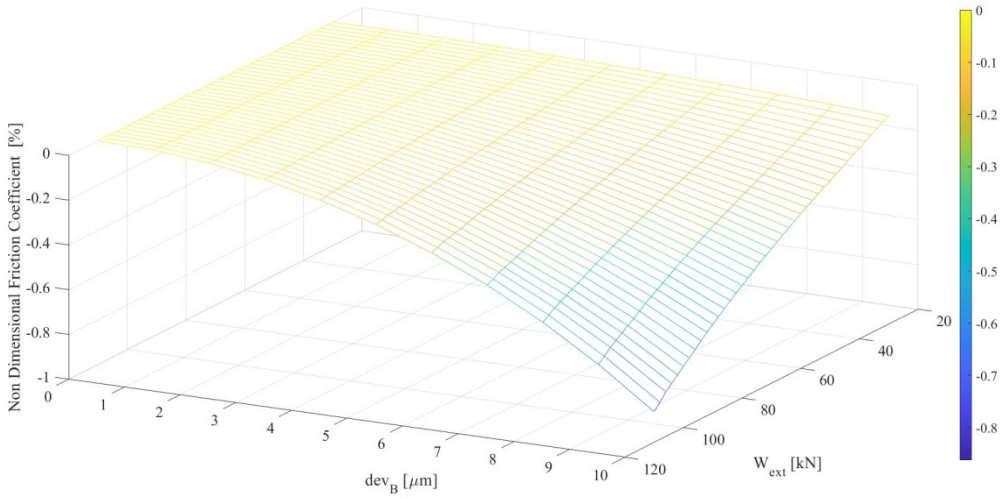

Figure 5.21: Difference of Friction Coefficient in [%] for $\sigma_B = [0\,,10]\ \mu m$

We observe that the friction coefficient is decreasing with increasing values of standard deviation, but in smaller rates compared to the results acquired in Chapter (4.2). This is because, by keeping the external load constant, a decreased pressure generation occurred in the bearing. This "reduced" profile pressure, results in smaller values of friction and load carrying capacity, which result in higher normalized friction coefficients.

We have to point out, that the friction coefficient in the case of rough bearing is still of smaller values than that of a smooth bearing. The previous comparison was held between the friction coefficient of the rough bearing in the case of constant geometry, i.e. e and φ constant, and in the case of constant operational condition, i.e. W_{ext} constant.

6. Results & Discussion

In the present thesis a novel stochastic solution of the Reynolds Equation for rough slider and journal bearings is derived and solved. Different geometric and roughness profiles, as well as operational conditions are tested, and the effect of stochastic roughness in hydrodynamic lubrication problems of journal bearings is quantified accordingly. The differential equations presented in the current analysis were solved using the Finite Difference method.

In the case of slider bearings, the introduction of surface roughness leads to an increase in the pressure and the load carrying capacity of the bearing. As the sliders convergence ratio tends to 0, thus the bearing tends to be parallel, we notice a significant increase in both those parameters, up to 35 %, which is in accordance with calculations for rough parallel bearings. The friction force calculated is also higher in comparison to that of a smooth bearing, exhibiting an increase of up to 4%. However, the friction coefficient of a rough bearing, being the ratio of friction force over load capacity, is smaller than that of a smooth bearing, exhibiting decrease which reaches 20%. We notice that the values of all the calculated operational parameters asymptotically tend to a constant value as the convergence ratio increase; physically this mean that as the bearing gets steeper the effect of the roughness tends to be constant.

As far as the journal bearing is taken into consideration, we observe that the mean pressure generated exhibits slightly higher values, in comparison to those of a smooth bearing, of the order of 1%. The minimum film thickness of a rough journal bearing tends to take higher values in comparison to that of smooth bearings, with difference reaching 6%. This means that the rough bearings tend to operate on higher minimum film thicknesses, aiding in avoiding the metal to metal contact. As a consequence, the rougher the bearing the more it operates on smaller eccentricity values. Furthermore, the friction force, and thus consequently the friction torque and power losses, takes lower values than the ones of a smooth bearing, with differences up to 1%. Lastly, the friction coefficient tends to decrease in value as the deviation is getting higher or the Sommerfeld number is decreasing.

At this point, we have to comment that, on first sight, the maximum differences calculated in the journal bearing were notably lower than those of a slider bearing. This can be explained by calculating the respective “convergence ratio” and “deviation ratio” of the journal bearing. Since the eccentricity varied from 0.4 to 0.8, the minimum film thickness took values in $[100\,,\,300]\ \mu m$, and thus the maximum deviation ratio calculated was $r_{\max} \simeq 0.1$, while the maximum convergence ration is $k_{\max} = 8$. So if we compare the results acquired for the same deviation ratio, we see that they are of the same level.

7. Future Work

Future work, in continuation of the present analysis, can include the following topics

- Calculations for the variance of the stochastic quantities mentioned in the previous analysis, such as the pressure, the load capacity and the friction force.
- Modification of the proposed solution by assuming the stochastic roughness as a stochastic function of space and time, rather than a stochastic variable
- Extension of the present model to account for inertia effects, hydrophobic surfaces, thermal effects in the lubricant domain and elastic deformations of the bearing structure
- Extension of the current approach to account for wear in the surfaces, via altering the statistical quantities of surface roughness; for example, the average of the surface roughness would be a time dependent function
- Extension of the suggested Reynolds Equation to account for more complex, and realistic, operational conditions

8. Literature

[1] T. A. Stolarski, *Tribology in Machine Design*, 1st Edition. Oxford: Butterworth-Heinemann, 2000.

[2] Kenneth J. Stout and L. Blunt, *Three - Dimensional Surface Topography*, 2nd Edition. London: Penton Press, 2000.

[3] A. G. M. Michell, *Lubrication; Its Principles & Practice*. London: Blackie, 1950.

[4] M. E. Salama, "The Effect of Macro-Roughness on the Performance of Parallel Thrust Bearings," *Proceedings of the Institution of Mechanical Engineers*, vol. 163, no. 1, pp. 149–161, 1950, doi: 10.1243/PIME_PROC_1950_163_019_02.

[5] R. A. Burton, "Effects of Two-Dimensional, Sinusoidal Roughness on the Load Support Characteristics of a Lubricant Film," *Journal of Basic Engineering*, vol. 85, no. 2, pp. 258–262, 1963, doi: 10.1115/1.3656572.

[6] D. Dowson and T.L. Whomes, "The effect of surface roughness upon the lubrication of rigid cylindrical rollers I. Theoretical," *Wear*, vol. 18, no. 2, pp. 129–140, Aug. 1971, doi: 10.1016/0043-1648(71)90161-X.

[7] J. A. Greenwood and J. B. P. Williamson, "Contact of Nominally Flat Surfaces," *Proc. R. Soc. Lond. A*, vol. 295, no. 1442, pp. 300–319, 1966, doi: 10.1098/rspa.1966.0242.

[8] Donald H. Buckley, *Surface Effects in Adhesion, Friction, Wear and Lubrication.* Amsterdam ; New York : New York: Elsevier Scientific Pub. Co. ; Distributors for the U.S. and Canada, Elsevier North-Holland, 1981.

[9] G. W. Stachowiak and A. W. Batchelor, *Engineering tribology*, 4th Edition. Oxford: Elsevier/Butterworth-Heinemann, 2014.

[10] Oscar Pinkus, "The Reynolds Centennial: A Brief History of the Theory of Hydrodynamic Lubrication," *Journal of Tribology*, vol. 109, no. 1, pp. 2–15, 1987, doi: 10.1115/1.3261322.

[11] G. Bayada and M. Chambat, "New Models in the Theory of the Hydrodynamic Lubrication of Rough Surfaces," *Journal of Tribology*, vol. 110, no. 3, pp. 402–407, 1988, doi: 10.1115/1.3261642.

[12] S. T. Tzeng and E. Saibel, "Surface Roughness Effect on Slider Bearing Lubrication," *A S L E Transactions*, vol. 10, no. 3, pp. 334–348, 1967, doi: 10.1080/05698196708972191.

[13] H. Christensen, "Stochastic Models for Hydrodynamic Lubrication of Rough Surfaces," *Proceedings of the Institution of Mechanical Engineers*, vol. 184, no. 1, pp. 1013–1026, 1969, doi: 10.1243/PIME_PROC_1969_184_074_02.

[14] H. Christensen and K. Tonder, "The Hydrodynamic Lubrication of Rough Journal Bearings," *Journal of Lubrication Technology*, vol. 95, no. 2, pp. 166–172, 1973, doi: 10.1115/1.3451759.

[15] Nadir Patir and H. S. Cheng, "An Average Flow Model for Determining Effects of Three-Dimensional Roughness on Partial Hydrodynamic Lubrication," *Journal of Lubrication Technology*, vol. 100, no. 1, pp. 12–17, 1978, doi: 10.1115/1.3453103.

[16] Nadir Patir and H. S. Cheng, "Application of Average Flow Model to Lubrication Between Rough Sliding Surfaces," *Journal of Lubrication Technology*, vol. 101, no. 2, pp. 220–229, 1979, doi: 10.1115/1.3453329.

[17] Kristian Tønder, "The Lubrication of Unidirectional Striated Roughness: Consequences for Some General Roughness Theories," *Journal of Tribology*, vol. 108, no. 2, pp. 167–170, 1986, doi: 10.1115/1.3261155.

[18] Kristian Tønder, "Surface Roughness Induced Effects in Hydrodynamic Lubrication," in *Tribology Issues and Opportunities in MEMS*, Dordrecht: Springer Netherlands, 1998, pp. 185–206.

[19] M B Dobrica and M Fillon, "About the Validity of Reynolds Equation and Inertia Effects in Textured Sliders of Infinite Width," *Proceedings of the Institution of Mechanical Engineers, Part J: Journal of Engineering Tribology*, vol. 223, no. 1, pp. 69–78, 2009, doi: 10.1243/13506501JET433.

[20] M. M. Khonsari and E. Richard Booser, *Applied Tribology: Bearing Design and Lubrication: Bearing Design and Lubrication*. Chichester, UK: John Wiley & Sons, Ltd, 2017.

[21] John Piotrowski, *Shaft Alignment Handbook*, 3rd Edition. Boca Raton: CRC Press, 2007.

[22] Bharat Bhushan, Ed., *Modern Tribology Handbook*. Boca Raton, FL: CRC Press, 2001.

[23] William A. Glaeser, *Materials for tribology*. Amsterdam ; New York: Elsevier Science, 1992.
[24] M.V.S. Babu, A. Rama Krishna, and K.N.S. Suman, "Review of Journal Bearing Materials and Current Trends," *AJMST*, 2015, doi: 10.7726/ajmst.2015.1006.
[25] Georgios Nikitas Rossopoulos, "Tribological Study of the Stern Tube Bearing of Marine Vessels," National Technical University of Athens, Athens, 2018.
[26] Leonidas Raptis, "Software Development for the Solution of Hydrodynamic Lubrication Problems in main Bearings of marine Diesel Engines," National Technical University of Athens, Athens, 2014.
[27] S.T. Tzeng and E. Saibel, "On the effects of surface roughness in the hydrodynamic lubrication theory of a short journal bearing," *Wear*, vol. 10, no. 3, pp. 179–184, May 1967, doi: 10.1016/0043-1648(67)90002-6.
[28] D. Dowson and T.L. Whomes, "The effect of surface roughness upon the lubrication of rigid cylindrical rollers. II. Experimental," *Wear*, vol. 18, no. 2, pp. 141–151, Aug. 1971, doi: 10.1016/0043-1648(71)90162-1.
[29] Prerit Vyas, "Effects of Stochastic (Random) Surface Roughness on Hydrodynamic Lubrication of Deterministic Asperity," University of Kentucky, Kentucky, 2005.
[30] Charles M. Stein, "Estimation of the Mean of a Multivariate Normal Distribution," *Ann. Statist.*, vol. 9, no. 6, pp. 1135–1151, 1981, doi: 10.1214/aos/1176345632.
[31] H. Christensen and K. Tønder, "The Hydrodynamic Lubrication of Rough Bearing Surfaces of Finite Width," *Transactions of the ASME*, pp. 324–329, 1971.
[32] Haym Benaroya and Seon Mi Han, *Probability Models in Engineering and Science*. Boca Raton: Taylor & Francis, 2005.

Appendix A: The Stein's Lemma

Let $X(\beta)$ be a stochastic variable, following the natural distribution with zero mean value and deviation σ^2, and $g(X(\beta))$ a function of that stochastic variable. It was proposed and proved by Charles M. Stein in [30], that the following equation is valid.

$$\mathbb{E}^{\beta}\left[X(\beta)g(X(\beta))\right] = \sigma^2\,\mathbb{E}^{\beta}\left[\frac{\partial g(X(\beta))}{\partial X(\beta)}\right]$$

If we suppose that $X(\beta)$ is the stochastic roughness and $g(X(\beta))$ is the stochastic pressure, then we can calculate the averages that appear in the proposed solution. Those integrals have the form of $\mathbb{E}^{\beta}\left[r^n(\beta)p\right]$, where $n = \{0,1,2,3\}$. The calculated averages are found below.

$$\mathbb{E}^{\beta}[p] = \mathrm{m}_p$$

$$\mathbb{E}^{\beta}\left[r(\beta)p\right] = \sigma^2\mathbb{E}^{\beta}\left[\frac{\partial p}{\partial r(\beta)}\right]$$

$$\mathbb{E}^{\beta}\left[r^2(\beta)p\right] = \sigma^2\left(\mathrm{m}_p + \sigma^2\mathbb{E}^{\beta}\left[\frac{\partial^2 p}{\partial r^2(\beta)}\right]\right)$$

$$\mathbb{E}^{\beta}\left[r^3(\beta)p\right] = \sigma^4\left(3\mathbb{E}^{\beta}\left[\frac{\partial p}{\partial r(\beta)}\right] + \sigma^2\mathbb{E}^{\beta}\left[\frac{\partial^3 p}{\partial r^3(\beta)}\right]\right)$$

By using Stein's lemma we can also calculate the negative averages $\mathbb{E}^{\beta}\left[\left(h + g(t)r(\beta)\right)^{-n}p\right]$, where $n = \{2,3\}$, which are calculated below.

$$\mathbb{E}^{\beta}\left[\frac{\nabla p}{h_T^2}\right] = \frac{h}{4g_S^2(t)\left(\sigma_S^2+\sigma_B^2\right)}\mathbb{E}^{\beta}\left[\frac{\nabla p}{h_T}\right] - \frac{1}{4g_S^2(t)\left(\sigma_S^2+\sigma_B^2\right)}\nabla\mathrm{m}_p$$

$$\mathbb{E}^{\beta}\left[\frac{\nabla p}{h_T^3}\right] = \frac{h^2 - 4g^2(t)\left(\sigma_S^2+\sigma_B^2\right)}{20g^4(t)\left(\sigma_S^2+\sigma_B^2\right)^2}\mathbb{E}^{\beta}\left[\frac{\nabla p}{h_T}\right] - \frac{h}{20g^4(t)\left(\sigma_S^2+\sigma_B^2\right)^2}\nabla\mathrm{m}_p$$

$$\mathbb{E}^{\beta}\left[\frac{\nabla p}{h_T^4}\right] = \frac{h\left(h^2 - 9\left(\sigma_S^2+\sigma_B^2\right)g^2(t)\right)}{120g^6(t)\left(\sigma_S^2+\sigma_B^2\right)^3}\mathbb{E}^{\beta}\left[\frac{\nabla p}{h_T}\right] - \frac{h^2 - 5\left(\sigma_S^2+\sigma_B^2\right)}{120g^6(t)\left(\sigma_S^2+\sigma_B^2\right)^3}\nabla\mathrm{m}_p$$

Appendix B: Moments Concerning The Stochastic Film Thickness

As mentioned in Chapter (2), the stochastic roughness are assumed to be random variables, each one following a different normal distribution. For those variables we know that their mean and standard deviation is given by equations (B.1) and (B.2) for $r_B(\beta)$ and (B.3) and (B.4) for $r_B(\beta)$.

$$\mathsf{m}_{r_S(\beta)} = 0 \tag{B.1}$$

$$\mathsf{C}_{r_B(\beta)r_B(\beta)} = \sigma_{\mathrm{B}}^2 \tag{B.2}$$

$$\mathsf{m}_{r_B(\beta)} = 0 \tag{B.3}$$

$$\mathsf{C}_{r_S(\beta)r_S(\beta)} = \sigma_S^2 \tag{B.4}$$

For the stochastic film thickness, we know that its two first central moments are given by equations (B.5) and (B.6)

$$\mathsf{m}_{h_T} = \mathbb{E}^{\beta}\left[h_T\right] = \mathbb{E}^{\beta}\left[h\right] + \mathbb{E}^{\beta}\left[r_B(\beta)\right] + \mathbb{E}^{\beta}\left[r_S(\beta)\right] = h \tag{B.5}$$

$$\mathsf{C}_{h_T h_T} = \mathbb{E}^{\beta}\left[h_T^2\right] - \left(\mathbb{E}^{\beta}\left[h_T\right]\right)^2 = \sigma^2 \tag{B.6}$$

In our approach, we propose to use the Taylor Expansion for calculating the factor $\mathbb{F}_0$. According to [32] the Taylor Expansion for the moments of functions of random variables reads as following

Let $f_1(X, Y) = \dfrac{X}{Y}$ be a function of the random variable X and Y. Then by using the Taylor Expansion we know that

$$\mathbb{E}^{\beta}\left[\frac{X}{Y}\right] = \frac{\mathbb{E}^{\beta}[X]}{\mathbb{E}^{\beta}[Y]} - \frac{Cov(X, Y)}{\left(\mathbb{E}^{\beta}[Y]\right)^2} + \frac{\mathbb{E}^{\beta}[X]}{\left(\mathbb{E}^{\beta}[Y]\right)^3} \cdot Var(Y)$$

Utilizing the Taylor Expansion for the correlation factor $\mathbb{F}_0$, with X being the pressure and Y the stochastic film thickness we get equations (B.7)

$$\mathbb{E}^{\beta}\left[\frac{\nabla p}{h_T}\right] = \frac{\mathbb{E}^{\beta}[\nabla p]}{\mathbb{E}^{\beta}\left[h_T\right]} - \frac{Cov\left(\nabla p, h_T\right)}{\left(\mathbb{E}^{\beta}\left[h_T\right]\right)^2} + \frac{\mathbb{E}^{\beta}[\nabla p]}{\left(\mathbb{E}^{\beta}\left[h_T\right]\right)^3} Var\left(h_T\right) \tag{B.7}$$

where $\mathbb{E}^{\beta}[\nabla p] = \nabla \mathsf{m}_p$

$\mathbb{E}^{\beta}\left[h_T\right] = h$

$Cov\left(\nabla p\,,\, h_T\right) = \mathbb{E}^{\beta}\left[h_T \cdot \nabla p\right] - \mathbb{E}^{\beta}\left[h_T\right]\mathbb{E}^{\beta}\left[\nabla p\right]$

$Var\left(h_T\right) = \mathbb{E}^{\beta}\left[h_T^2\right] - \left(\mathbb{E}^{\beta}\left[h_T\right]\right)^2$

After calculations we get that

$$\mathbb{E}^{\beta}\left[\frac{\nabla p}{h_T}\right] = \frac{h^2 + \sigma^2 g^2(t)}{h\left(h^2 - 3\sigma^2 g^2(t)\right)}\nabla \mathsf{m}_p$$

or else

$$\mathbb{F}_0 = \frac{h^2 + \sigma^2 g^2(t)}{h\left(h^2 - 3\sigma^2 g^2(t)\right)}\nabla \mathsf{m}_p \qquad \textbf{(B.8)}$$

Appendix C: Choosing the right approximation for the distribution

As mentioned in the introduction, it is known that the roughness height distribution is a Gaussian distribution, or is really close to it up to three standard deviations. Although this distribution allows us to use various mathematical tools, for instance the Stein's Lemma, in terms of calculating, the cost of the Gaussian probability density function is a rather incontinent one to use. So, we will try to approach the various moments found in the proposed analysis rather than calculating them directly.

In Christensen's papers (i.e. [13] and [31]), a polynomial form approximating the Gaussian distribution is chosen. Its mathematical expression is given by equation (C1), while an illustration of the function is given in Figure (C.1).

$$\mathsf{f}_{r(\beta)}(w) = \begin{cases} \dfrac{35}{32\tilde{C}^7}\left(\tilde{C}^2 - w^2\right)^3, & \tilde{C} \le w \le \tilde{C} \\ 0, & \text{elsewhere} \end{cases} \qquad ,\tilde{C} = 3\sigma g(t) \quad \textbf{(C.1)}$$

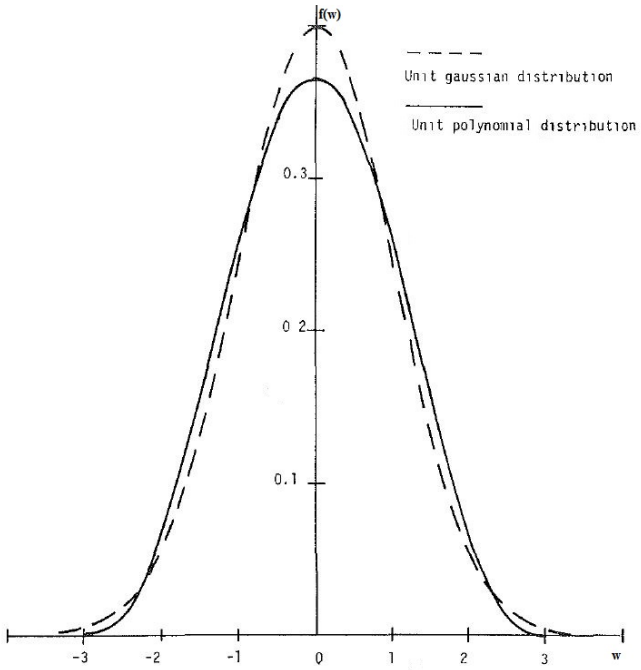

Figure C.1: Probability Density Function (PDF) of roughness heights

Using the previous approximation of the Gaussian distribution, the first two negative moments of the stochastic film thickness, denoted as $\mathbb{F}_1$ and $\mathbb{F}_2$ respectively, are given by equations (C.2) and (C.3)

$$\mathbb{F}_1^{(A)} = \frac{35}{32\tilde{C}^7}\left\{\left(\tilde{C}^2 - h^2\right)^3 \ln\left(\frac{h+\tilde{C}}{h-\tilde{C}}\right) + \frac{2}{15}\tilde{C}h\left(15h^4 - 40\tilde{C}^2h^2 + 33\tilde{C}^4\right)\right\} \qquad \textbf{(C.2)}$$

$$\mathbb{F}_2^{(A)} = \frac{35}{32C^7}\left\{6h\left(\tilde{C}^2 - h^2\right)^2 \ln\left(\frac{h+\tilde{C}}{h-\tilde{C}}\right) - \frac{4}{5}\tilde{C}\left(15h^4 - 25\tilde{C}^2h^2 + 8\tilde{C}^4\right)\right\} \qquad \textbf{(C.3)}$$

In our approach, we propose to use the Taylor Expansion for the moments of functions of random variables. According to [32] the Taylor Expansion for the moments of functions of random variables reads as following

Let $f_1(X)$ be a function of a random variable X. Then by using the Taylor Expansion we know that

$$\mathbb{E}^{\beta}\left[f(X)\right] = f\left(\mathbb{E}^{\beta}[X]\right) + \frac{1}{2} f''\left(\mathbb{E}^{\beta}[X]\right) \cdot Var\left(h_T\right)$$

Utilizing the Taylor Expansion for the first and the second negative moment of the stochastic film thickness, meaning $f_1(x) = \frac{1}{x}$ and $f_1(x) = \frac{1}{x^2}$ respectively, we get equations (C.4) and (C.5).

$$\mathbb{F}_1^{(B)} = \frac{h^2 + \sigma^2 g^2(t)}{h^3} \tag{C.4}$$

$$\mathbb{F}_2^{(B)} = \frac{h^2 + 3\sigma^2 g^2(t)}{h^4} \tag{C.5}$$

At first, we checked the coefficient of the first negative moment of the film thickness numerically in a rough slider bearing for deviation ratio $r = [0.02\ ,\ 0.2]$. Their numerical value in respect to x and r was plotted in Figure (C.2), while in Figure (C.3) their difference was plotted.

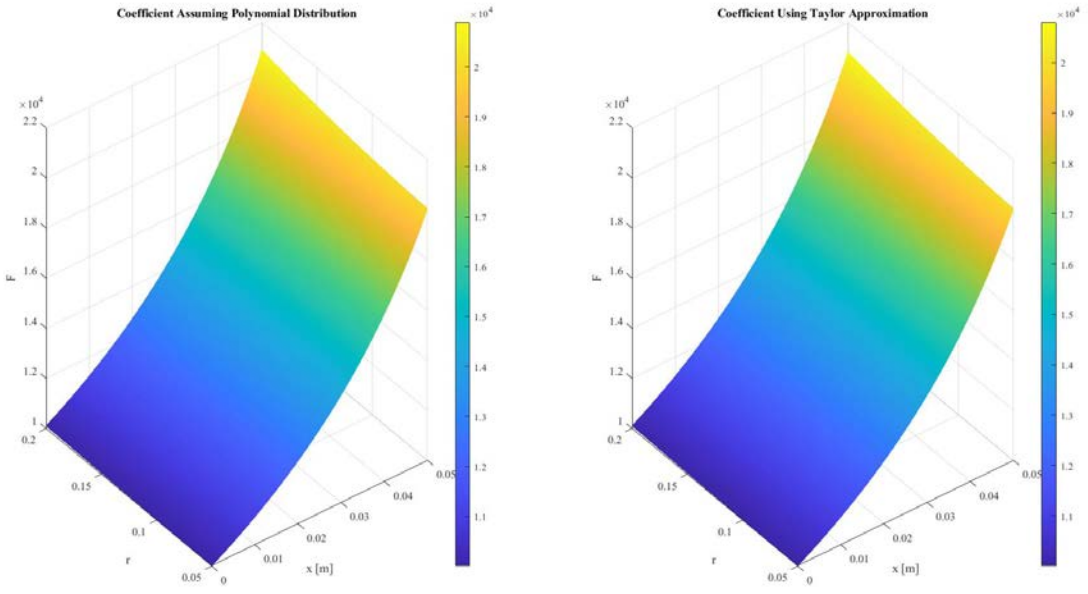

Figure C.2: Numerical Values For the First Negative Moment of The Film Thickness for $r = [0.02\ ,\ 0.2]$

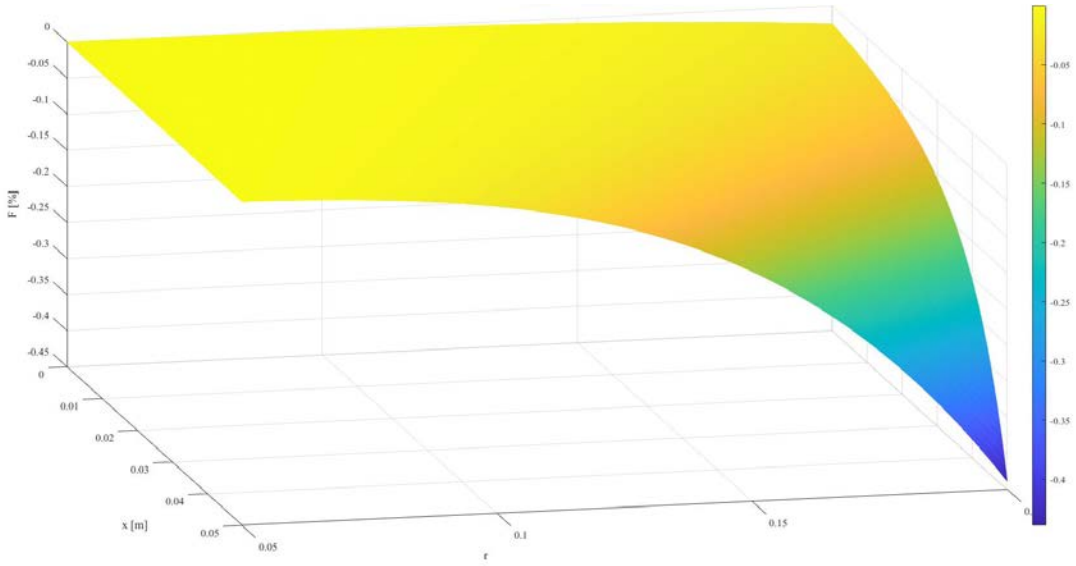

Figure C.3: Difference of the two coefficients for $r = [0.02 , 0.2]$

We observe that their difference is negligible, and that they behave smoothly throughout the bearing, meaning in respect to x, and the deviation, meaning in respect to r. But when we tested the same moment for $r = [0.001 , 0.2]$ we get Figures (C.4) and (C.5).

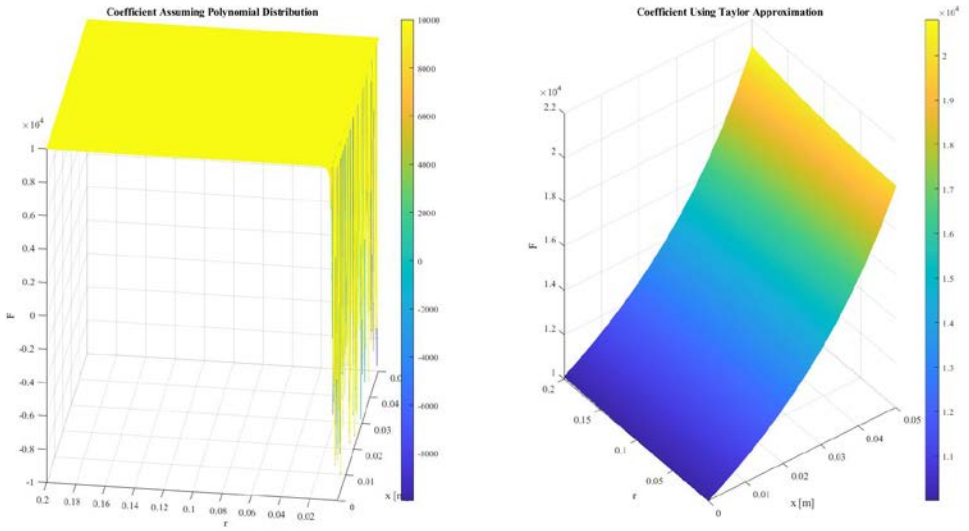

Figure C.4: Numerical Values For the First Negative Moment of The Film Thickness for $r = [0.0001 , 0.2]$

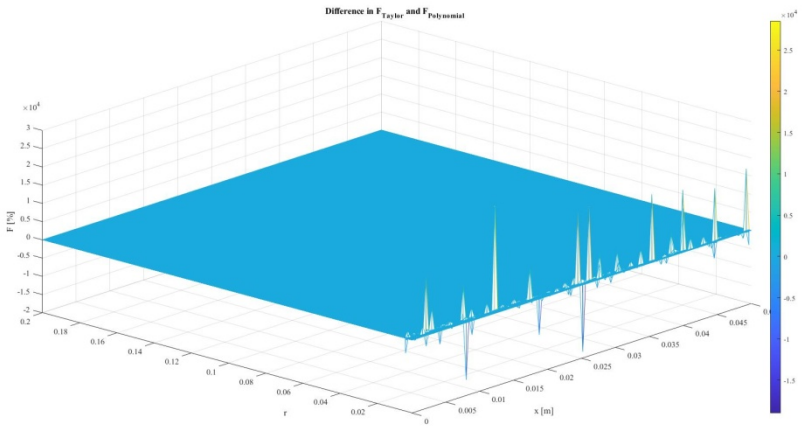

Figure C.5: Difference of the two coefficients for $r = [0.0001, 0.2]$

In figure (C.4) we placed an upper limit of 10^4 $1/m$ in the values that coefficient $\mathbb{F}_1^{(A)}$ could get. We observe that as $\sigma \to 0$, coefficient $\mathbb{F}_1^{(A)}$ tends to have either large values, i.e. values up to 10^{15} or negative values. Physically meaning, since this coefficient represents the average of the random variable $\frac{1}{h + r_{low}(\beta) + r_{up}(\beta)}$, which is always a positive number, we expect that it is a positive number.One way of proving that the coefficient is not suited for any further simulations, is to calculate its limit while $\sigma \to 0$, which should approach $\frac{1}{h}$. We will also calculate the limits of coefficient $\mathbb{F}_1^{(B)}$, which should also approach $\frac{1}{h}$ and the limits of coefficients $\mathbb{F}_2^{(A)}$ and $\mathbb{F}_2^{(B)}$ which should approach $\frac{1}{h^2}$. The calculated limits are the following

$$\lim_{\sigma \to 0} \mathbb{F}_1^{(A)} = \infty$$

$$\lim_{\sigma \to 0} \mathbb{F}_1^{(A)} = \infty$$

$$\lim_{\sigma \to 0} \mathbb{F}_1^{(B)} = \frac{1}{h}$$

$$\lim_{\sigma \to 0} \mathbb{F}_2^{(B)} = \frac{1}{h^2}$$

Seeing that the coefficients acquired by the Taylor Expansion are in harmony with the limits, meaning that if we set $\sigma = 0$ we get $\frac{1}{h}$ and $\frac{1}{h^2}$, those are the coefficients that we will use in the proposed approach simulations.